ESAIM: M2AN 53 (2019) 1391–1432
https://doi.org/10.1051/m2an/2019032

ESAIM: Mathematical Modelling and Numerical Analysis
www.esaim-m2an.org

A DYNAMIC MULTILAYER SHALLOW WATER MODEL FOR POLYDISPERSE SEDIMENTATION

Raimund Bürger[1], Enrique D. Fernández-Nieto[2] and Víctor Osores[1,*]

Abstract. A multilayer shallow water approach for the approximate description of polydisperse sedimentation in a viscous fluid is presented. The fluid is assumed to carry finely dispersed solid particles that belong to a finite number of species that differ in density and size. These species segregate and form areas of different composition. In addition, the settling of particles influences the motion of the ambient fluid. A distinct feature of the new approach is the particular definition of the average velocity of the mixture. It takes into account the densities of the solid particles and the fluid and allows us to recover the global mass conservation and linear momentum balance laws of the mixture. This definition motivates a modification of the Masliyah–Lockett–Bassoon (MLB) settling velocities of each species. The multilayer shallow water model allows one to determine the spatial distribution of the solid particles, the velocity field, and the evolution of the free surface of the mixture. The final model can be written as a multilayer model with variable density where the unknowns are the average velocities and concentrations in each layer, the transfer terms across each interface, and the total mass. An explicit formula of the transfer terms leads to a reduced form of the system. Finally, an explicit bound of the minimum and maximum eigenvalues of the transport matrix of the system is utilized to design a Harten–Lax–van Leer (HLL)-type path-conservative numerical method. Numerical simulations illustrate the coupled polydisperse sedimentation and flow fields in various scenarios, including sedimentation in a type of basin that is used in practice in mining industry and in a basin whose bottom topography gives rise to recirculations of the fluid and high solids concentrations.

Mathematics Subject Classification. 65N06, 76T20.

Received March 26, 2018. Accepted April 25, 2019.

1. Introduction

1.1. Scope

The process of sedimentation of small particles suspended in a viscous fluid, water or air combined with the flow of the solid-fluid mixture arises in numerous geophysical situations such as settling and convective

Keywords and phrases. Multilayer shallow water model, polydisperse sedimentation, path-conservative method, viscous flow, recirculation.

[1] CI[2]MA and Departamento de Ingeniería Matemática, Facultad de Ciencias Físicas y Matemáticas, Universidad de Concepción, Casilla 160-C, Concepción, Chile.

[2] Departamento de Matemática Aplicada I, ETS Arquitectura, Universidad de Sevilla, Avda. Reina Mercedes No. 2, 41012 Sevilla, Spain.

*Corresponding author: victorosores@udec.cl

sediment transport in rivers and estuaries, gravity currents and debris flows, as well as in clarification tanks, wastewater treatment plants, and thickeners in the mining industry. While for many unit operations in industrial applications a spatially one-dimensional description, usually in one vertical direction aligned with the governing body force (mostly gravity) is sufficient, we are here interested in flows that involve a significant horizontal bulk flow of the mixtures in addition to vertical segregation, and where typically the horizontal dimensions of the domain are much larger than the vertical. In these situations, instead of solving a fully three-dimensional model (such as the three-dimensional Navier–Stokes equations for an incompressible fluid), one prefers a so-called shallow water or Saint-Venant approach that is based on a vertically integrated version of the underlying model. In the presence of large friction coefficients, considerable water depth, wind, and other effects, however, the standard single-layer shallow water approach is considered invalid since the horizontal velocity can hardly be approximated by a vertically constant velocity. In this case so-called multilayer shallow water models are preferred [1, 4, 40]. The multilayer approach consists in subdividing the computational domain into M layers in vertical direction, which leads to a system of Saint-Venant equations (one version of the Saint-Venant system for each layer). If a hydrostatic pressure is assumed then the unknowns are a horizontal velocity for each layer and point of the horizontal computational grid plus the total height of the fluid column at that position, along with the solids concentrations in each layer at that position. The vertical velocity components can be calculated by post-processing the horizontal velocity components no partial differential equations (PDEs) need to be solved.

It is the purpose of this paper to develop a new multilayer shallow water model framework of polydisperse sedimentation with these properties, along with a method for the numerical solution in the important subcase of one horizontal space dimension and neglect of sediment compressibility and viscosity of the mixture. Here polydispersivity means that the solid particles belong to a finite number N of species that differ in size or density, and where particles of different species segregate and form areas of different composition. The solid species and the fluid are described as $N+1$ superimposed continuous phases. The main novelty is the choice of the mass average of the velocities of the $N+1$ phases to describe the movement of the mixture, in contrast to a previous effort [28] where that velocity was defined as a volume average of phase velocities. The advantage of the present approach is that the mass and linear momentum balance of the mixture are recovered, and therefore consistency with a single-phase flow model is recovered. That said, we mention that in [28] the vertical settling velocities of the N solids phases as nonlinear functions of the local composition are determined by the well-known Masliyah–Lockett–Bassoon (MLB) model [32, 34]. This model is also utilized herein but in a modified form.

The final model that is eventually solved can be stated as a system of balance laws of the type

$$\partial_t \boldsymbol{w} + \partial_x \boldsymbol{\mathcal{F}}(\boldsymbol{w}) = \boldsymbol{\mathcal{S}}(\boldsymbol{w}, \partial_x \boldsymbol{w}) + \boldsymbol{\mathcal{G}}(\boldsymbol{w}, \partial_x \boldsymbol{w}), \tag{1.1}$$

where t is time, x is the horizontal space coordinate, the unknown $\boldsymbol{w} = \boldsymbol{w}(t,x)$ is a vector of $(N+1)M+1$ scalar unknown functions that represent the total mass of the mixture, the horizontal velocity component in each of the M layers, and the N solids concentrations in each of the M layers. The flux vector $\boldsymbol{\mathcal{F}}(\boldsymbol{w})$ and the source terms $\boldsymbol{\mathcal{S}}(\boldsymbol{w}, \partial_x \boldsymbol{w})$ and $\boldsymbol{\mathcal{G}}(\boldsymbol{w}, \partial_x \boldsymbol{w})$ arise from reduced versions of the balance equations, as well as from jump conditions across the interfaces between the layers. These ingredients will be specified in later parts of the paper. The particular form (1.1) is suitable for the application of specialized methods for first-order hyperbolic systems with non-conservative terms.

1.2. Related work

General references to models of sedimentation include [6, 33]. Models of polydisperse sedimentation in one space dimension similar to the MLB model, and which give rise to strongly coupled systems of nonlinear conservation laws or possibly degenerate convection-diffusion equations were thoroughly studied in recent years including analyses of hyperbolicity [13, 23], extensions to flocculated suspensions forming compressible sediments [8], construction of entropy solutions [7, 24], development of efficient numerical schemes [10, 14, 15], and applications in geophysics [25], water resource recovery [16], and others (see also references in the cited works). On

the other hand, theoretical and experimental works on polydisperse gravity currents, with which our numerical results could in principle be compared, include [9,21,30].

To put this work further into the proper perspective, we mention that suspended sediment transport in shallow regimes by using a Saint-Venant or shallow water model combined with passive transport equations for the different species is a well-known approach [18,26,27,31,35,43]. These models are obtained by averaging the original three-dimensional equations along the height of the fluid and allow one to simulate sediment transport with a relative small computational cost. The drawback of these models is that they only take into account the mean depth-average concentration of solid particles in suspension. The vertical distribution and settling of the particles suspended within the fluid is not described, which is achieved by the present multilayer Saint-Venant approach [1–4,40]. In fact, numerical simulations by using a multilayer approach allow one to recover interesting properties that are not observed when using just a hydrostatic shallow water model [3]. Moreover, in that paper it is shown that the multilayer approach provides an alternative to the solution of the free-surface Navier–Stokes system, leading to a precise description of the vertical profile of the horizontal velocity while preserving the robustness and the computational efficiency of the usual Saint-Venant system. Similar conclusions have been obtained by applying the multilayer technique to density-stratified flows [5].

To calculate the complete velocity field of the mixture within the approach developed herein, we will use the mass balance equation of the mixture and the mass jump condition in the interfaces between layers to compute the vertical velocity of the mixture. As we will see later, this vertical velocity is linear by layer and it has possibly a jump between adjacent layers given by the jump condition. In [29] the authors introduced this idea for an incompressible fluid. Here in the mixture each species has a constant density but the mixture itself is compressible, and due to this modifications it moves as one phase satisfying laws of conservation of mass and momentum.

The numerical solution of the resulting multilayer model (1.1) is based on recently developed specialized methods for first-order hyperbolic systems with non-conservative products. In [22] the authors propose a formal definition for such products and provide a notion of weak solution for the Riemann problem. Numerical schemes to solve systems of PDEs in non-conservative form are proposed in [20,37,38,42] (this list is not complete). In [19] the authors introduce new first-order finite volume solvers, so-called PVM (polynomial viscosity matrix) methods, to solve Cauchy problems for hyperbolic systems of conservation laws with source terms and/or nonconservative products. This method allows one to compute an approximation of the viscosity matrix by a polynomial evaluation of a Roe matrix, which avoids the necesessity to compute the complete characteristic decomposition of this matrix.

1.3. Outline of the paper

The remainder of the paper is organized as follows. In Section 2 we introduce the governing partial differential equations (PDEs) governing polydisperse sedimentation, starting with the continuity equations (Sect. 2.1) and the linear momentum balances (Sect. 2.2) for the solids and fluid phases and the mixture. The definition of the slip velocity, or solid-fluid relative velocity, for each of the solids phases in terms of the modified form of the MLB model is outlined in Section 2.3. For ease of reference, we summarize in Section 2.4 the governing PDEs to which the multilayer approach is subsequently applied in Section 3. The layers, interfaces, and boundaries arising in the multilayer approach are introduced in Section 3.1, followed by definition of some notation in Section 3.2. The general concept of weak solutions of the governing PDEs in the multilayer setting, based on the appropriate jump conditions across the interface between adjacent layers, is introduced in Section 3.3. For the mass conservation and linear momentum balance equations of Section 2.4 the jump conditions give rise to the mass fluxes across the interlayer interfaces and a relation that in addition to the mass fluxes involves between the extra (or viscous) stress tensors, see Sections 3.4 and 3.5, respectively. In Section 3.6 we show how the vertical velocities for each solids species are defined for each layer. The corresponding vertical velocities of the mixture are derived in Section 3.7. Then, in Section 4 we introduce the assumption of a hydrostatic pressure. The closure of the model is described in Section 5, and the final form of the equations that will actually be solved is developed. In particular, in Section 5.1 the treatment is limited to one horizontal space dimension

and fixed proportionalities of each layer with respect to the total height of the mixture are introduced. The assumptions stated so far lead to the interlayer mass fluxes in closed form and reduce the model to $M(N+1)+1$ scalar PDEs for variables from one may recover the primitive variables, namely the solids concentrations and horizontal velocity components in each layer and the total height of the mixture. This is outlined in Section 5.2. The expression for the total interlayer mass flux is deduced in Appendix A. In Section 6 we present a numerical scheme to solve and simulate numerically the polydisperse sedimentation process. Specifically, we demonstrate in Section 6.1 that the final model takes the form of a first-order system of balance equations, and in Section 6.2 describe the HLL-path-conservative method used for its solution. Section 7 is devoted to the presentation of four numerical examples (after stating some preliminaries, Sect. 7.1), namely for bidisperse sedimentation in solely one vertical space dimension (Test 1), bidisperse sedimentation in a horizontal channel with an inclined bottom (Test 2), sedimentation in a domain whose bottom has a "bump" (Test 3), and cylindrical dam break involving bidisperse sedimentation over a $3D$ paraboloid bottom (Test 4) (see Sects. 7.2–7.5). Some conclusions are collected in Section 8.

In Appendix B, we introduce a bound for the characteristic velocities of the proposed multilayer model formulated in Section 5. In Appendix C we provide details of some of the calculations that lead to the final system of Section 4.

2. Governing equations

2.1. Continuity equations

Let us consider $N \in \mathbb{N}$ species of spherical solid particles dispersed in a viscous fluid. For each solid species j, $j = 1, \ldots, N$, we denote by ϕ_j, ρ_j, and d_j its volumetric concentration, density, and particle diameter, respectively, where we assume that $d_1 \geq d_2 \geq \cdots \geq d_N$. Furthermore, in $d = 3$ space dimensions we denote by $\boldsymbol{v}_j = (u_j, v_j, w_j)^{\mathrm{T}} \in \mathbb{R}^3$ its phase velocity with the horizontal component $(u_j, v_j) \in \mathbb{R}^2$, while in $d = 2$ space dimensions (one horizontal, one vertical) the velocity is $(u_j, w_j) \in \mathbb{R}^2$ with the scalar horizontal component u_j. In both cases, w_j is the vertical velocity component. The same notation is used for the fluid indexed by $j = 0$. The model is based on the continuity and linear momentum balance equations for the N solid species and the fluid. The continuity equations are given by

$$\partial_t(\rho_j \phi_j) + \nabla \cdot (\rho_j \phi_j \boldsymbol{v}_j) = 0, \quad j = 0, \ldots, N. \tag{2.1}$$

Since all densities ρ_j are constant, we may divide the j-th equation in (2.1) by ρ_j, obtaining

$$\partial_t \phi_j + \nabla \cdot (\phi_j \boldsymbol{v}_j) = 0, \quad j = 0, \ldots, N. \tag{2.2}$$

(Here and in the remaining of the paper, partial derivatives of indexed quantities are always understood in the sense $\partial_t \phi_j = \partial_t(\phi_j)$, etc.) Let $\Phi := (\phi_0, \ldots, \phi_N)^{\mathrm{T}}$. We define the density of the mixture

$$\rho := \rho(\Phi) := \rho_0 \phi_0 + \rho_1 \phi_1 + \cdots + \rho_N \phi_N. \tag{2.3}$$

(Notice that while the individual phase densities $\rho_0, \rho_1, \ldots, \rho_N$ are constants, $\rho = \rho(\Phi)$ is variable and depends on the local composition Φ of the mixture. Since the components of Φ are dimensionless volume fractions, the dimension of ρ is again a density). Then summing all equations in (2.1) yields that the mass average velocity of the mixture

$$\boldsymbol{v} := (u, v, w)^{\mathrm{T}} := \frac{1}{\rho} \sum_{m=0}^{N} \rho_m \phi_m \boldsymbol{v}_m = \frac{1}{\rho} \left[\left(\rho - \sum_{j=1}^{N} \rho_j \phi_j \right) \boldsymbol{v}_0 + \sum_{k=1}^{N} \rho_k \phi_k \boldsymbol{v}_k \right] \tag{2.4}$$

satisfies the global mass balance of the mixture

$$\partial_t \rho + \nabla \cdot (\rho \boldsymbol{v}) = 0, \tag{2.5}$$

where we observe that (2.5) has the same form as the continuity equation of a single-phase fluid with variable density ρ and velocity $\boldsymbol{v}$; in fact, the mass average velocity $\boldsymbol{v}$ is introduced precisely for the purpose of achieving this form. Defining the slip velocities $\boldsymbol{u}_i := \boldsymbol{v}_i - \boldsymbol{v}_0$ ($\boldsymbol{u}_0 = 0$) and $\lambda_i := \rho_i\phi_i/\rho$ for $i = 1, \ldots, N$, we now derive the identity

$$\rho_j\phi_j\boldsymbol{v}_j = \rho_j\phi_j\big(\boldsymbol{u}_j + \boldsymbol{v} - (\lambda_1\boldsymbol{u}_1 + \cdots + \lambda_N\boldsymbol{u}_N)\big), \quad j = 1, \ldots, N; \tag{2.6}$$

hence the solids mass balance equations from (2.1) can be rewritten in terms of $\boldsymbol{v}$ and $\boldsymbol{u}_1, \ldots, \boldsymbol{u}_N$ as

$$\partial_t(\rho_j\phi_j) + \nabla\cdot\big(\rho_j\phi_j\big(\boldsymbol{u}_j + \boldsymbol{v} - (\lambda_1\boldsymbol{u}_1 + \cdots + \lambda_N\boldsymbol{u}_N)\big)\big) = 0, \quad j = 1, \ldots N.$$

Summing all these equations plus that of the fluid, we recover, again, the mass balance of the mixture.

Remark 2.1. The main difference between the model that we present here and the one introduced in [29] becomes from the definition of the average velocity $\boldsymbol{v}$ (Eq. (2.4)). In [29] authors consider a multilayer approach of a polydisperse sedimentation model with the classical MLB settling velocity and average velocity

$$\boldsymbol{v} := \sum_{m=0}^{N} \phi_m\boldsymbol{v}_m. \tag{2.7}$$

The usual definition of the average velocity only consider the concentrations of the species and the fluid. The definition of mass average velocity of the mixture (2.4) considers densities and concentrations of each one of the solids species and of the fluid in which the particles are dispersed. This fact gives a superior behavior to the proposed mass average velocity because it allows us to recover global mass and linear momentum balance laws of the mixture. Moreover, using this definition we also propose a modification of the classical MLB model, which now consider the total density of the mixture too (see Sect. 2.3).

2.2. Linear momentum balances

The respective momentum balance equations for the N solids species and the fluid are given by

$$\partial_t(\rho_j\phi_j\boldsymbol{v}_j) + \nabla\cdot(\rho_j\phi_j\boldsymbol{v}_j\otimes\boldsymbol{v}_j) = \nabla\cdot\boldsymbol{T}_j + \rho_j\phi_j\boldsymbol{b} + \boldsymbol{m}_j^{\mathrm{f}} + \boldsymbol{m}_j^{\mathrm{s}}, \quad j = 1, \ldots, N, \tag{2.8}$$

$$\partial_t(\rho_0\phi_0\boldsymbol{v}_0) + \nabla\cdot(\rho_0\phi_0\boldsymbol{v}_0\otimes\boldsymbol{v}_0) = \nabla\cdot\boldsymbol{T}_0 + \rho_0\phi_0\boldsymbol{b} - (\boldsymbol{m}_1^{\mathrm{f}} + \cdots + \boldsymbol{m}_N^{\mathrm{f}}). \tag{2.9}$$

Here $\boldsymbol{T}_j$ denotes the stress tensor of the particle species j, $j = 1, \ldots, N$, $\boldsymbol{T}_0$ that of the fluid, $\boldsymbol{b}$ is the body force, $\boldsymbol{m}_j^{\mathrm{f}}$ and $\boldsymbol{m}_{ji}^{\mathrm{s}}$ are the interaction forces per unit volume between solid species j and the fluid and between the solid species j and i, respectively, and $\boldsymbol{m}_j^{\mathrm{s}} = \boldsymbol{m}_{j1}^{\mathrm{s}} + \cdots + \boldsymbol{m}_{jN}^{\mathrm{s}}$ is the particle-particle interaction terms of species j. In light of considerable experimental and theoretical justification [8], the quantities $\boldsymbol{m}_{ji}$ are neglected at the very low Reynolds numbers considered here.

Summing all equations in (2.8) plus (2.9) and setting $\boldsymbol{T} = \sum_{j=0}^{N}\boldsymbol{T}_j$ yields

$$\partial_t\left(\sum_{j=0}^{N}\rho_j\phi_j\boldsymbol{v}_j\right) + \nabla\cdot\left(\sum_{j=0}^{N}\rho_j\phi_j\boldsymbol{v}_j\otimes\boldsymbol{v}_j\right) = \nabla\cdot\boldsymbol{T} + \rho\boldsymbol{b}.$$

Defining the diffusion velocities $\boldsymbol{u}_j^{\mathrm{d}} := \boldsymbol{v}_j - \boldsymbol{v}$ for $j = 0, \ldots, N$, we may rewrite the above expression as

$$\partial_t(\rho\boldsymbol{v}) + \nabla\cdot(\rho\boldsymbol{v}\otimes\boldsymbol{v}) = \nabla\cdot\left(\boldsymbol{T} - \sum_{j=0}^{N}\rho_j\phi_j\boldsymbol{u}_j^{\mathrm{d}}\otimes\boldsymbol{u}_j^{\mathrm{d}}\right) + \rho\boldsymbol{b}.$$

Finally, the linear momentum balance equation for the mixture is given by

$$\partial_t(\rho\boldsymbol{v}) + \nabla\cdot(\rho\boldsymbol{v}\otimes\boldsymbol{v}) = \nabla\cdot\boldsymbol{\Sigma} + \rho\boldsymbol{b},$$

where $\boldsymbol{\Sigma} := \boldsymbol{T} - \sum_{j=0}^{N} \rho_j \phi_j \boldsymbol{u}_j^{\mathrm{d}} \otimes \boldsymbol{u}_j^{\mathrm{d}}$ denotes the stress tensor of the mixture. (This reduces to $\boldsymbol{\Sigma} = \boldsymbol{T}$ if the fluid and solid velocities are the same.)

We assume here that the stress tensors of the solid and fluid phases can be written as $\boldsymbol{T}_j = -p_j \boldsymbol{I} + \boldsymbol{T}_j^{\mathrm{E}}$ for $j = 1, \ldots, N$ and $\boldsymbol{T}_0 = -p_0 \boldsymbol{I} + \boldsymbol{T}_0^{\mathrm{E}}$, respectively, where $p_j = (\phi_j/\phi)(\phi p + \sigma_{\mathrm{e}}(\phi))$ denotes the phase pressure of particle species j, $p_0 = (1-\phi)p$ that of the fluid. The total concentration of particles is $\phi = \phi_1 + \cdots + \phi_N = 1 - \phi_0$. $\boldsymbol{T}_0^{\mathrm{E}}$ and $\boldsymbol{T}_j^{\mathrm{E}}$ are the viscous stress tensors of the fluid and solid phases respectively, and σ_{e} is the effective solid stress.

The interaction solid-fluid force per unit volume is given by

$$\boldsymbol{m}_j^{\mathrm{f}} = \alpha_j(\Phi)\boldsymbol{u}_j + \beta_j(\Phi)\nabla\phi_j, \tag{2.10}$$

where α_j is the resistance coefficient for the transfer of momentum between the fluid and solid phase species j. Following the arrgument of [8], namely inserting inserting (2.10) into the linear momentum balances, considering the mixture at equilibrium in a settling column so that all slip velocities and the fluid velocity vanish and $\nabla p = -\rho_0 g \boldsymbol{k}$, where $\boldsymbol{k}$ is the upward-pointing unit vector, we obtain that $\beta_1(\Phi) = \cdots = \beta_N(\Phi) = p$. Introducing the continuity equation (2.1) in the momentum equations (2.8) and assuming that gravity is the only body force, *i.e.*, $\boldsymbol{b} = g\boldsymbol{k}$ where $\boldsymbol{k}$ is the downward-pointing unit vector, we obtain the linear momentum balances in the following form:

$$\rho_j \phi_j \mathrm{D}_t \boldsymbol{v}_j = \nabla \cdot \boldsymbol{T}_j^{\mathrm{E}} - \phi_j \nabla p - \rho_j \phi_j g \boldsymbol{k} + \alpha_j(\Phi)\boldsymbol{u}_j + \boldsymbol{m}_j^{\mathrm{s}} - \nabla\left(\frac{\phi_j}{\phi}\sigma_{\mathrm{e}}(\phi)\right), \quad j = 1, \ldots, N, \tag{2.11}$$

$$\rho_0 D_t \boldsymbol{v}_0 = -\nabla p + \frac{1}{1-\phi}\nabla \cdot \boldsymbol{T}_0^{\mathrm{E}} + \rho_0 g \boldsymbol{k} - (\alpha_1 \boldsymbol{u}_1 + \cdots + \alpha_N \boldsymbol{u}_N), \tag{2.12}$$

where we use the standard notation $\mathrm{D}_t \boldsymbol{v} = \partial_t \boldsymbol{v} + (\boldsymbol{v} \cdot \nabla)\boldsymbol{v}$.

2.3. Explicit formula for the slip velocities $\boldsymbol{u_j}$

An explicit expression for the slip velocities $\boldsymbol{u}_j$ is derived in [8] by a dimensional analysis applied to the linear momentum equations for the solid species and the fluid, (2.11) and (2.12), respectively. This procedure yields the explicit form

$$\boldsymbol{u}_j = g\frac{\phi_j}{\alpha_j(\Phi)}\left((\bar{\rho}_j - \bar{\boldsymbol{\rho}}^{\mathrm{T}}\Phi)\boldsymbol{k} + \frac{\sigma_{\mathrm{e}}(\phi)}{g\phi_j}\nabla\left(\frac{\phi_j}{\phi}\right) + \frac{1-\phi}{g\phi}\nabla\sigma_{\mathrm{e}}(\phi)\right), \quad j = 1, \ldots, N, \tag{2.13}$$

where we introduce the reduced densities $\bar{\rho}_j := \rho_j - \rho_0$, $j = 1, \ldots, N$ and the vector $\bar{\boldsymbol{\rho}} := (\bar{\rho}_1, \ldots, \bar{\rho}_N)^{\mathrm{T}}$. Following [8, 32, 34] we choose $\phi_j/\alpha_j(\Phi) = -d_j^2 V(\phi)/18\mu_0$, where μ_0 is the viscosity of the fluid, and the function $V(\phi)$, known as hindered settling factor, that is supposed to satisfy $V(\phi) > 0$ and $V'(\phi) < 0$ for $0 < \phi < \phi_{\max}$. A common choice of this function is the Richardson–Zaki [39] expression

$$V(\phi) = \begin{cases} (1-\phi)^{n_{\mathrm{RZ}}-2} & \text{for } \phi \le 1, \\ 0 & \text{for } \phi > 1, \end{cases} \quad n_{\mathrm{RZ}} > 2. \tag{2.14}$$

Since we are interested in modelling only the sedimentation process we will not consider effects of sediment compressibility, so we assume that the effective solid stress σ_{e} is equal to 0. Therefore the final form of the slip velocities is given by

$$\boldsymbol{u}_j = \mu\delta_j V(\phi)(\bar{\rho}_j - \bar{\boldsymbol{\rho}}^{\mathrm{T}}\Phi)\boldsymbol{k}, \quad j = 1, \ldots, N, \tag{2.15}$$

where we introduce the parameters $\mu := -g d_1^2/(18\mu_0)$ and $\delta_j := d_j^2/d_1^2$, $j = 1, \ldots, N$, where we recall that d_1 is the largest particle diameter.

Inserting (2.15) into (2.6) we get

$$\rho_j\phi_j\boldsymbol{v}_j = \rho_j\phi_j\boldsymbol{v} + \rho_j f_j^{\mathrm{M}}(\Phi)\boldsymbol{k} \quad \text{for } j = 1,\dots,N. \tag{2.16}$$

Note that we use the mass average velocity (2.4) instead of the classical definition given by the volume average velocity (2.7). Then we obtain a modification of MLB model, defined by

$$f_j^{\mathrm{M}}(\Phi) := \phi_j v_j^{\mathrm{MLB}} = \phi_j \mu V(\phi)\left(\delta_j(\bar{\rho}_j - \bar{\boldsymbol{\rho}}^{\mathrm{T}}\Phi) - \sum_{k=1}^{N}\lambda_k\delta_k(\bar{\rho}_k - \bar{\boldsymbol{\rho}}^{\mathrm{T}}\Phi)\right), \quad j = 1,\dots,N. \tag{2.17}$$

Finally, the continuity and momentum equations for the solids can be written as

$$\partial_t\phi_j + \nabla\cdot\left(\phi_j\boldsymbol{v} + f_j^{\mathrm{M}}(\Phi)\boldsymbol{k}\right) = 0, \qquad j = 1,\dots,N, \tag{2.18}$$

$$\rho_j\left(\partial_t(\phi_j\boldsymbol{v}_j) + \nabla\cdot(\phi_j\boldsymbol{v}_j\otimes\boldsymbol{v}_j)\right) = \nabla\cdot\boldsymbol{T}_j^{\mathrm{E}} - \phi_j\nabla p - \rho_j\phi_j g\boldsymbol{k} + \alpha_j(\Phi)\boldsymbol{u}_j, \quad j = 1,\dots,N. \tag{2.19}$$

We remark here that the vertical velocities of particles expressed as combination of the vertical average velocity of the mixture $w = \lambda_0 w_0 + \cdots + \lambda_N w_N$ and the fluxes $f_j^{\mathrm{M}}(\Phi)$ satisfy

$$\rho_j\phi_j w_j = \rho_j\phi_j w + \rho_j f_j^{\mathrm{M}}(\Phi), \tag{2.20}$$

moreover we have the identity

$$\sum_{j=1}^{N}\lambda_j w_j = (1-\lambda_0)w + \frac{1}{\rho}\sum_{j=1}^{N}\rho_j f_j^{\mathrm{M}}$$

that can be rearranged as

$$\lambda_0 w_0 = \lambda_0 w - \frac{1}{\rho}\sum_{j=1}^{N}\rho_j f_j^{\mathrm{M}}.$$

From the above equation we may define a similar relation as (2.15) for the velocity of the fluid

$$\rho_0\phi_0\boldsymbol{v}_0 := \rho_0\phi_0\boldsymbol{v} + \rho_0 f_0^{\mathrm{M}}(\Phi)\boldsymbol{k} = \rho_0\phi_0\boldsymbol{v} - \sum_{j=1}^{N}\rho_j f_j^{\mathrm{M}}(\Phi)\boldsymbol{k}. \tag{2.21}$$

2.4. Final form of the model equations

The final form of the model is given by the mass conservation and linear momentum balance equations for the solids species after introducing (2.13) into (2.19) and the fuid, it can be written as

$$\partial_t(\rho_j\phi_j) + \nabla\cdot(\rho_j\phi_j\boldsymbol{v}_j) = 0, \qquad j = 0,\dots,N, \tag{2.22}$$

$$\rho_j(\partial_t(\phi_j\boldsymbol{v}_j) + \nabla\cdot(\phi_j\boldsymbol{v}_j\otimes\boldsymbol{v}_j)) = \nabla\cdot\boldsymbol{T}_j^{\mathrm{E}} - \phi_j\nabla p - \phi_j\rho g\boldsymbol{k}, \quad j = 0,\dots,N, \tag{2.23}$$

and where the quantities $\rho_j\phi_j\boldsymbol{v}_j$ are given by (2.16). If we sum up from 0 to N the equations (2.23), then we have

$$\partial_t\left(\sum_{j=0}^{N}\rho_j\phi_j\boldsymbol{v}_j\right) + \nabla\cdot\left(\sum_{j=0}^{N}\rho_j\phi_j\boldsymbol{v}_j\otimes\boldsymbol{v}_j\right) = \nabla\cdot\boldsymbol{T} - \rho g\boldsymbol{k}, \tag{2.24}$$

with $\boldsymbol{T} = \sum_{j=0}^{N}\boldsymbol{T}_j = -p\boldsymbol{I} + \boldsymbol{T}^{\mathrm{E}}$.

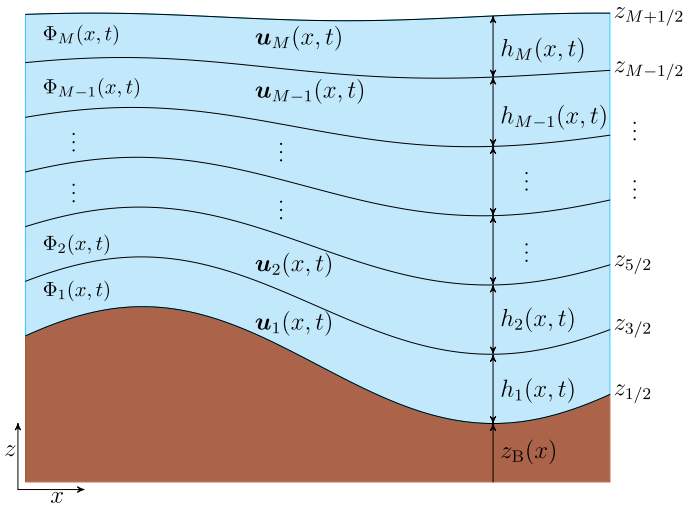

FIGURE 1. Sketch of the multilayer approach.

3. A MULTILAYER APPROACH

3.1. Layers, interfaces, and boundaries

We shall consider a d-dimensional space ($d = 2, 3$). For a given final time $T > 0$ and each time $t \in [0, T]$ we denote by $\Omega_{\mathrm{F}}(t)$ the fluid domain and by $I_{\mathrm{F}}(t)$ its projection onto the horizontal plane. In order to introduce a multilayer system, the fluid domain is divided along the vertical direction into $M \in \mathbb{N}^*$ pre-set layers of thickness $h_\alpha(t, \boldsymbol{x})$ with $M + 1$ interfaces

$$\Gamma_{\alpha+1/2}(t) = \big\{(\boldsymbol{x}, z) \in \mathbb{R}^d : z = z_{\alpha+1/2}(t, \boldsymbol{x}),\ \boldsymbol{x} \in I_{\mathrm{F}}(t)\big\}, \quad \alpha = 0, 1, \ldots, M$$

(see Fig. 1). We assume that the interfaces $\Gamma_{\alpha+1/2}(t)$ are smooth, concretely at least of class C^1 in time and space. We denote by $z_{\mathrm{B}} = z_{1/2}$ and $z_{\mathrm{S}} = z_{M+1/2}$ the equations of the bottom and the free surface interfaces $\Gamma_{\mathrm{B}}(t)$ and $\Gamma_{\mathrm{S}}(t)$, respectively. The thickness of layer α at time t and horizontal position $\boldsymbol{x}$ is

$$h_\alpha = h_\alpha(t, \boldsymbol{x}) = z_{\alpha+1/2}(t, \boldsymbol{x}) - z_{\alpha-1/2}(t, \boldsymbol{x}), \quad \alpha = 1, \ldots, M,$$

such that $z_{\alpha+1/2} = z_{\mathrm{B}} + h_1 + \cdots + h_\alpha$ for $\alpha = 1, \ldots, M$. Then the height of the fluid is $h := z_{\mathrm{S}} - z_{\mathrm{B}} = h_1 + \cdots + h_M$.

The boundary $\partial\Omega_{\mathrm{F}}(t)$ of $\Omega_{\mathrm{F}}(t)$ can be represented as $\partial\Omega_{\mathrm{F}}(t) = \Gamma_{\mathrm{B}}(t) \cup \Gamma_{\mathrm{S}}(t) \cup \Theta(t)$, where $\Theta(t)$ is the inflow/outflow boundary which we assume here to be vertical. The fluid domain is split as $\overline{\Omega_{\mathrm{F}}(t)} = \cup_{\alpha=1}^{M} \overline{\Omega_\alpha(t)}$, where we define the layers and their boundaries as

$$\Omega_\alpha(t) := \big\{(\boldsymbol{x}, z) : \boldsymbol{x} \in I_{\mathrm{F}}(t) \text{ and } z_{\alpha-1/2} < z < z_{\alpha+1/2}\big\},$$

such that

$$\partial\Omega_\alpha(t) := \Gamma_{\alpha-1/2}(t) \cup \Gamma_{\alpha+1/2}(t) \cup \Theta_\alpha(t), \quad \Theta_\alpha(t) := \big\{(\boldsymbol{x}, z) : \boldsymbol{x} \in \partial I_{\mathrm{F}}(t) \text{ and } z_{\alpha-1/2} < z < z_{\alpha+1/2}\big\}.$$

Hence the inflow/outflow boundary is split as $\overline{\Theta(t)} = \cup_{\alpha=1}^{M} \overline{\Theta_\alpha(t)}$.

3.2. Notation

Based in part on the definition of layers above, we introduce the following notation:

(i) For two tensors $\boldsymbol{a}$ and $\boldsymbol{b}$ of sizes (n,m) and (n,p) respectively, we shall denote by $(\boldsymbol{a};\ \boldsymbol{b})$ the tensor of size $(n,m+p)$ which is the concatenation of $\boldsymbol{a}$ and $\boldsymbol{b}$ in this order.

(ii) For $\boldsymbol{x}=(x_1,\dots,x_{d-1})$ and the differential operator $\nabla=(\partial_{x_1},\dots,\partial_{x_{d-1}},\partial_z)$, we define

$$\bar{\nabla}:=(\partial_t;\nabla)=(\partial_t,\partial_{x_1},\dots,\partial_{x_{d-1}},\partial_z),\quad \nabla_{\boldsymbol{x}}:=(\partial_{x_1},\dots,\partial_{x_{d-1}}).$$

(iii) For $\alpha=0,1,\dots,M$ and for a function f, we set

$$f^-_{\alpha+1/2}:=(f|_{\Omega_\alpha(t)})\big|_{\Gamma_{\alpha+1/2}(t)},\quad f^+_{\alpha+1/2}:=(f|_{\Omega_{\alpha+1}(t)})\big|_{\Gamma_{\alpha+1/2}(t)}.$$

If f is continuous across $\Gamma_{\alpha+1/2}(t)$, we simply set $f_{\alpha+1/2}:=f|_{\Gamma_{\alpha+1/2}(t)}$. We shall also use the notation

$$\tilde{f}_{\alpha+1/2}:=\frac{1}{2}\big(f^+_{\alpha+1/2}+f^-_{\alpha+1/2}\big).$$

(iv) We denote by $\boldsymbol{\eta}_{\alpha+1/2}$ the spatial unit normal vector to the interface $\Gamma_{\alpha+1/2}(t)$ outward to the layer $\Omega_\alpha(t)$ for a given time t, that is

$$\boldsymbol{\eta}_{\alpha+1/2}:=\frac{1}{\sqrt{1+|\nabla_{\boldsymbol{x}}z_{\alpha+1/2}|^2}}(\nabla_{\boldsymbol{x}}z_{\alpha+1/2},-1)^{\mathrm{T}},\quad \alpha=0,\dots,M.$$

Furthermore, $\boldsymbol{n}_{t,\alpha+1/2}$ denotes the (space-time) unit normal vector $\Gamma_{\alpha+1/2}(t)$ pointing to $\Omega_{\alpha+1}(t)$, *i.e.*,

$$\boldsymbol{n}_{t,\alpha+1/2}:=\frac{1}{\sqrt{1+|\nabla_{\boldsymbol{x}}z_{\alpha+1/2}|^2+(\partial_t z_{\alpha-1/2})^2}}(\partial_t z_{\alpha+1/2},\nabla_{\boldsymbol{x}}z_{\alpha+1/2},-1)^{\mathrm{T}},\quad \alpha=0,\dots,M.$$

(v) Let $\alpha\in\{1,\dots,M-1\}$, and assume that y is a scalar, vectorial, or tensorial quantity defined in $\Omega_\alpha(t)$ and $\Omega_{\alpha+1}(t)$, such that the one-sided limits of y on either side of $\Gamma_{\alpha+1/2}(t)$, that is

$$y^+_{t,\alpha+1/2}:=\lim_{\substack{z\to z_{\alpha+1/2}\\ z>z_{\alpha+1/2}}} y(\boldsymbol{x},z,t),\quad y^-_{t,\alpha+1/2}:=\lim_{\substack{z\to z_{\alpha+1/2}\\ z<z_{\alpha+1/2}}} y(\boldsymbol{x},z,t),$$

are well defined. Then we denote by $[\![y]\!]_{t,\alpha+1/2}$ the jump of y across $\Gamma_{\alpha+1/2}(t)$, that is,

$$[\![y]\!]_{t,\alpha+1/2}=y^+_{t,\alpha+1/2}-y^-_{t,\alpha+1/2}.$$

If y does not depend on z within each of the layers $\Omega_\alpha(t)$ and $\Omega_{\alpha+1}(t)$, then this implies

$$[\![y]\!]_{t,\alpha+1/2}=(y|_{\Omega_{\alpha+1}(t)}-y|_{\Omega_\alpha(t)})\big|_{\Gamma_{\alpha+1/2}(t)}. \tag{3.1}$$

Remark 3.1. If we add the time variable as one more dimension, then the corresponding domain Ω_T is actually given by $\Omega_T=\{(t,\boldsymbol{x},z):t\in(0,T],(\boldsymbol{x},z)\in\Omega_{\mathrm{F}}(t)\}$ with $\partial\Omega_T=\Lambda_T\cup\Lambda_1\cup\Lambda_2$, where $\Lambda_T=\{(t,\boldsymbol{x},z):t\in(0,T),(\boldsymbol{x},z)\in\partial\Omega_{\mathrm{F}}(t)\}$, $\Lambda_1=\{0\}\times\Omega_{\mathrm{F}}(0)$, and $\Lambda_2=\{T\}\times\Omega_{\mathrm{F}}(T)$. Since we integrate over $\Omega_{\mathrm{F}}(t)$, we retain here the boundary Λ_T for the computations even if it means cancelling the tests functions over the boundaries Λ_1 and Λ_2.

3.3. Weak solution with discontinuities

Let us recall the conditions to be satisfied by a piecewise smooth weak solution $(\boldsymbol{v}_0,\dots,\boldsymbol{v}_N,\phi_0,\dots,\phi_N,p)$ of (2.22)–(2.24), where $\boldsymbol{v}_0$, $\boldsymbol{v}_j$ are defined by (2.16) and (2.21) respectively.

Definition 3.2. Assume that the velocities $\boldsymbol{v}_0,\boldsymbol{v}_1,\dots,\boldsymbol{v}_N$, the pressure p and the volume fractions $\phi_0,\phi_1,\dots,\phi_N$ are smooth in each $\Omega_\alpha(t)$, but possibly discontinuous across the predetermined hypersurfaces $\Gamma_{\alpha+1/2}(t)$ for $\alpha=1,\dots,M-1$. Then

$$\boldsymbol{y}:=(\boldsymbol{v}_0,\dots,\boldsymbol{v}_N,\phi_0,\dots,\phi_N,p):\Omega_T\ni(t,\boldsymbol{x},z)\mapsto\boldsymbol{y}(t,\boldsymbol{x},z)\in\mathbb{R}^{N+1}\times\mathbb{R}^{N+1}\times\mathbb{R}$$

is a *weak solution* of (2.22)–(2.24) if the following conditions hold:

(i) The function $\boldsymbol{y}$ is a standard weak solution of (2.22)–(2.24) in each layer $\Omega_\alpha(t)$, $\alpha = 1, \ldots, M$.
(ii) For each $\alpha = 1, \ldots, M-1$ and $t \in (0, T]$, the following normal flux jump conditions across the interface $\Gamma_{\alpha+1/2}(t)$ are satisfied: for the conservation of mass equations,

$$\left[\!\left[(\rho_j\phi_j; \rho_j\phi_j\boldsymbol{v}_j)\right]\!\right]_{t,\alpha+1/2} \cdot \boldsymbol{n}_{t,\alpha+1/2} = 0 \quad \textit{for all } j = 0, \ldots, N, \tag{3.2}$$

and for the momentum conservation law corresponding to equation (2.24),

$$\left[\!\left[\left(\sum_{m=0}^{N} \rho_m\phi_m\boldsymbol{v}_m; \sum_{m=0}^{N} \rho_m\phi_m\boldsymbol{v}_m \otimes \boldsymbol{v}_m - \boldsymbol{T}\right)\right]\!\right]_{t,\alpha+1/2} \cdot \boldsymbol{n}_{t,\alpha+1/2} = 0, \tag{3.3}$$

where

$$\boldsymbol{T} = -p\boldsymbol{I} + \boldsymbol{T}^{\mathrm{E}} \tag{3.4}$$

is the stress tensor of the mixture.

In order to develop the multilayer model, we assume the layers thicknesses small enough to neglect the dependence of the horizontal velocities and the concentrations on the vertical variable inside each layer. Moreover, we assume that the vertical velocity is piecewise linear in z, and possibly discontinuous. Concretely, for all $\alpha = 1, \ldots, M$ and $j = 0, \ldots, N$ we denote $\boldsymbol{v}_j|_{\Omega_\alpha(t)} := \boldsymbol{v}_{j,\alpha} := (\boldsymbol{u}_\alpha, w_{j,\alpha})^{\mathrm{T}}$, $\phi_{j,\alpha} := \phi_j|_{\Omega_\alpha(t)}$, and for all $\alpha = 1, \ldots, M$, $p_\alpha := p|_{\Omega_\alpha(t)}$, where $\boldsymbol{u}_\alpha$, $\phi_{j,\alpha}w_{j,\alpha} = \phi_{j,\alpha}w_\alpha + f^{\mathrm{M}}_{j,\alpha}$, and $\phi_{j,\alpha}$, respectively, stand for the horizontal and vertical velocities and volumetric concentration of species j in layer α. Let us also denote the average velocity of each layer by

$$\boldsymbol{v}^{\alpha:} = \frac{1}{\rho}\sum_{j=0}^{N} \rho_j\phi_{j,\alpha}\boldsymbol{v}_{j,\alpha} = (\boldsymbol{u}_\alpha, w_\alpha), \quad \alpha = 1, \ldots, M,$$

(where we choose an upper index for α to avoid confusion with the lower index j), and assume that

$$\partial_z\boldsymbol{u}_\alpha = 0, \quad \partial_z\phi_{j,\alpha} = 0, \quad \partial_z w_{j,\alpha} = d_{j,\alpha}(t, \boldsymbol{x}), \quad \partial_z p_\alpha(t, \boldsymbol{x}) = g_\alpha(t, \boldsymbol{x}), \tag{3.5}$$

for some smooth functions $d_{j,\alpha}(t, \boldsymbol{x})$ and $g_\alpha(t, \boldsymbol{x})$. That is, we suppose that the horizontal velocity $\boldsymbol{u}_\alpha$ and the concentration of each of the species $\phi_{j,\alpha}$ do not depend on z inside each layer, and that $w_{j,\alpha}$ and p_α are linear in z inside each layer.

There is no hope for such a particular set $((\boldsymbol{u}_\alpha, w_{1,\alpha})^{\mathrm{T}}, \ldots, (\boldsymbol{u}_\alpha, w_{N,\alpha})^{\mathrm{T}}, \phi_{1,\alpha}, \ldots, \phi_{N,\alpha}, p_\alpha)$ to be a solution of the complete equations in the layer $\Omega_\alpha(t)$. Instead, we shall consider a reduced weak formulation with particular test functions, that we describe in the following sections. Let us also denote $\Phi_\alpha = (\phi_{0,\alpha}, \phi_{1,\alpha}, \ldots, \phi_{N,\alpha})^{\mathrm{T}}$ and

$$\bar{\rho}_\alpha := \rho_0\phi_{0,\alpha} + \rho_1\phi_{1,\alpha} + \cdots + \rho_N\phi_{N,\alpha}. \tag{3.6}$$

3.4. Mass conservation jump conditions

In what follows we analyze the jump conditions (3.2) and (3.3), where we recall that (3.5) implies that

$$\boldsymbol{u}^+_{\alpha-1/2}(t, \boldsymbol{x}) = \boldsymbol{u}^-_{\alpha+1/2}(t, \boldsymbol{x}) = \boldsymbol{u}_\alpha(t, \boldsymbol{x}), \quad \text{and} \quad \phi^+_{j,\alpha-1/2}(t, \boldsymbol{x}) = \phi^-_{j,\alpha+1/2}(t, \boldsymbol{x}) = \phi_{j,\alpha}(t, \boldsymbol{x}), \tag{3.7}$$

so that the jumps $[\![\boldsymbol{u}]\!]_{t,\alpha+1/2}$ and $[\![\phi_j]\!]_{t,\alpha+1/2}$, $j = 0, \ldots, N$, are indeed given by (3.1). The mass conservation jump conditions (3.2) are then satisfied provided that

$$G_{j,\alpha+1/2} := G^-_{j,\alpha+1/2} = G^+_{j,\alpha+1/2}, \quad j = 0, 1, \ldots, N, \tag{3.8}$$

where we define for $j = 0, 1, \dots, N$

$$\begin{aligned} G^+_{j,\alpha+1/2} &:= \rho_j \phi_{j,\alpha+1}\big(\partial_t z_{\alpha+1/2} + \boldsymbol{u}_{\alpha+1} \cdot \nabla_{\boldsymbol{x}} z_{\alpha+1/2} - w^+_{j,\alpha+1/2}\big), \\ G^-_{j,\alpha+1/2} &:= \rho_j \phi_{j,\alpha}\big(\partial_t z_{\alpha+1/2} + \boldsymbol{u}_{\alpha} \cdot \nabla_{\boldsymbol{x}} z_{\alpha+1/2} - w^-_{j,\alpha+1/2}\big). \end{aligned} \tag{3.9}$$

(We remark that $G_{j,\alpha+1/2}$ is the normal mass flux for species j at the interface $\Gamma_{\alpha+1/2}(t)$.) Taking into account the structure of the vertical velocity, let us denote

$$w^\pm_{j,\alpha+1/2} = w^\pm_{\alpha+1/2} + f^\pm_{j,\alpha+1/2}/\phi^\pm_{j,\alpha+1/2}. \tag{3.10}$$

where $f^\pm_{j,\alpha+1/2}$ must satisfy

$$\sum_{j=0}^{N} \rho_j f^+_{j,\alpha+1/2} = \sum_{j=0}^{N} \rho_j f^-_{j,\alpha+1/2} = 0.$$

If we add up in j, it becomes clear that $G_{\alpha+1/2} = G^-_{\alpha+1/2} = G^+_{\alpha+1/2}$, where

$$G_{\alpha+1/2} := \sum_{j=0}^{N} G_{j,\alpha+1/2}$$

and

$$\begin{aligned} G^+_{\alpha+1/2} &= \bar\rho_{\alpha+1}\big(\partial_t z_{\alpha+1/2} + \boldsymbol{u}_{\alpha+1} \cdot \nabla_{\boldsymbol{x}} z_{\alpha+1/2} - w^+_{\alpha+1/2}\big), \\ G^-_{\alpha+1/2} &= \bar\rho_{\alpha}\big(\partial_t z_{\alpha+1/2} + \boldsymbol{u}_{\alpha} \cdot \nabla_{\boldsymbol{x}} z_{\alpha+1/2} - w^-_{\alpha+1/2}\big), \end{aligned} \tag{3.11}$$

which corresponds to the jump condition for (2.5). (The quantity $G_{\alpha+1/2}$ will be referred to as total normal mass flux across the interface $\Gamma_{\alpha+1/2}(t)$.) Then, from (3.9) to (3.11) we obtain

$$G^+_{j,\alpha+1/2} = \frac{\rho_j \phi_{j,\alpha+1}}{\bar\rho_{\alpha+1}} G_{\alpha+1/2} - \rho_j f^+_{j,\alpha+1/2}, \quad G^-_{j,\alpha+1/2} = \frac{\rho_j \phi_{j,\alpha}}{\bar\rho_{\alpha}} G_{\alpha+1/2} - \rho_j f^-_{j,\alpha+1/2},$$

and these two equations allow us to obtain

$$G_{j,\alpha+1/2} = \tilde\phi_{j,\alpha+1/2} G_{\alpha+1/2} - \rho_j \tilde f_{j,\alpha+1/2}, \tag{3.12}$$

where we define the averages

$$\tilde\phi_{j,\alpha+1/2} := \frac{1}{2}\left(\frac{\rho_j \phi_{j,\alpha+1}}{\bar\rho_{\alpha+1}} + \frac{\rho_j \phi_{j,\alpha}}{\bar\rho_{\alpha}}\right), \quad \tilde f_{j,\alpha+1/2} = \frac{1}{2}\big(f^+_{j,\alpha+1/2} + f^-_{j,\alpha+1/2}\big), \quad j = 0, \dots, N. \tag{3.13}$$

Let us also remark that condition (3.8) can be written as

$$f^+_{j,\alpha+1/2} - f^-_{j,\alpha+1/2} = G_{\alpha+1/2}\left(\frac{\phi_{j,\alpha+1}}{\bar\rho_{\alpha+1}} - \frac{\phi_{j,\alpha}}{\bar\rho_{\alpha}}\right). \tag{3.14}$$

Then, from previous equations we obtain

$$f^\pm_{j,\alpha+1/2} = \tilde f_{j,\alpha+1/2} \pm \frac{G_{\alpha+1/2}}{2}\left(\frac{\phi_{j,\alpha+1}}{\bar\rho_{\alpha+1}} - \frac{\phi_{j,\alpha}}{\bar\rho_{\alpha}}\right).$$

3.5. Momentum conservation jump conditions

The momentum jump condition (3.3) is rewritten as

$$[\![\boldsymbol{T}]\!]_{t,\alpha+1/2}\cdot\left(\nabla_{\boldsymbol{x}}z_{\alpha+1/2},-1\right)^{\mathrm{T}}=\sum_{j=0}^{N}\left[\!\left[(\rho_j\phi_j\boldsymbol{v}_j;\rho_j\phi_j\boldsymbol{v}_j\otimes\boldsymbol{v}_j)\right]\!\right]_{t,\alpha+1/2}\cdot\left(\partial_t z_{\alpha+1/2},\nabla_{\boldsymbol{x}}z_{\alpha+1/2},-1\right)^{\mathrm{T}}. \tag{3.15}$$

Moreover, using (3.8), we have

$$\left[\!\left[(\rho_j\phi_j\boldsymbol{v}_j;\rho_j\phi_j\boldsymbol{v}_j\otimes\boldsymbol{v}_j)\right]\!\right]_{t,\alpha+1/2}\cdot\left(\partial_t z_{\alpha+1/2},\nabla_{\boldsymbol{x}}z_{\alpha+1/2},-1\right)^{\mathrm{T}}=G_{j,\alpha+1/2}[\![\boldsymbol{v}_j]\!]_{t,\alpha+1/2},\quad j=0,1,\ldots,N,$$

Inserting this into (3.15) we get

$$[\![\boldsymbol{T}]\!]_{t,\alpha+1/2}\cdot\left(\nabla_{\boldsymbol{x}}z_{\alpha+1/2},-1\right)^{\mathrm{T}}=\sum_{j=0}^{N}G_{j,\alpha+1/2}[\![\boldsymbol{v}_j]\!]_{t,\alpha+1/2}.$$

As a consequence, condition (3.3) can be written as

$$[\![\boldsymbol{T}]\!]_{t,\alpha+1/2}\cdot\boldsymbol{\eta}_{\alpha+1/2}=\frac{1}{\sqrt{1+|\nabla_{\boldsymbol{x}}z_{\alpha+1/2}|^2}}\sum_{j=0}^{N}G_{j,\alpha+1/2}[\![\boldsymbol{v}_j]\!]_{t,\alpha+1/2}. \tag{3.16}$$

For $\alpha=1,\ldots,M-1$, and consistently with (3.4), the total stress is decomposed as

$$\boldsymbol{T}^{\pm}_{\alpha+1/2}=-p_{\alpha+1/2}\boldsymbol{I}+\boldsymbol{T}^{\mathrm{E},\pm}_{\alpha+1/2}, \tag{3.17}$$

where $p_{\alpha+1/2}$ is the kinematic pressure and $\boldsymbol{T}^{\mathrm{E},\pm}_{\alpha+1/2}$ are the limit approximations of $\boldsymbol{T}^{\mathrm{E}}$ at $\Gamma_{\alpha+1/2}$. This means that $\boldsymbol{T}^{\mathrm{E},\pm}_{\alpha+1/2}$ must satisfy

$$[\![\boldsymbol{T}^{\mathrm{E}}]\!]_{t,\alpha+1/2}\cdot\boldsymbol{\eta}_{\alpha+1/2}=\left(\boldsymbol{T}^{\mathrm{E},+}_{\alpha+1/2}-\boldsymbol{T}^{\mathrm{E},-}_{\alpha+1/2}\right)\cdot\boldsymbol{\eta}_{\alpha+1/2}=\frac{1}{\sqrt{1+|\nabla_{\boldsymbol{x}}z_{\alpha+1/2}|^2}}\sum_{j=0}^{N}G_{j,\alpha+1/2}[\![\boldsymbol{v}_j]\!]_{t,\alpha+1/2}, \tag{3.18}$$

where $G_{j,\alpha+1/2}$ is defined by (3.12). Moreover, by consistency, $\boldsymbol{T}^{\mathrm{E},\pm}_{\alpha+1/2}$ should satisfy

$$\frac{1}{2}\left(\boldsymbol{T}^{\mathrm{E},+}_{\alpha+1/2}+\boldsymbol{T}^{\mathrm{E},-}_{\alpha+1/2}\right)=:\tilde{\boldsymbol{T}}^{\mathrm{E}}_{\alpha+1/2}=\begin{bmatrix}\tilde{\boldsymbol{T}}^{\mathrm{E}}_{\mathrm{h},\alpha+1/2} & \tilde{\boldsymbol{T}}^{\mathrm{E}}_{\boldsymbol{x}z,\alpha+1/2}\\ \left(\tilde{\boldsymbol{T}}^{\mathrm{E}}_{\boldsymbol{x}z,\alpha+1/2}\right)^{\mathrm{T}} & \tilde{T}^{\mathrm{E}}_{zz,\alpha+1/2}\end{bmatrix}, \tag{3.19}$$

where $\tilde{\boldsymbol{T}}^{\mathrm{E}}_{\alpha+1/2}$ is an approximation of $\boldsymbol{T}^{\mathrm{E}}|_{\Gamma_{\alpha+1/2}}$, to be defined and $\tilde{\boldsymbol{T}}^{\mathrm{E}}_{\mathrm{h},\alpha+1/2}$, $\tilde{\boldsymbol{T}}^{\mathrm{E}}_{\boldsymbol{x}z,\alpha+1/2}$, and $\tilde{T}^{\mathrm{E}}_{zz,\alpha+1/2}$ denote the horizontal, mixed, and vertical components of $\tilde{\boldsymbol{T}}^{\mathrm{E}}_{\alpha+1/2}$, respectively. Concretely, if we utilize the expression for a viscous-linear fluid,

$$\boldsymbol{T}^{\mathrm{E}}=\boldsymbol{T}^{\mathrm{E}}(\boldsymbol{v})=\mu\boldsymbol{D}(\boldsymbol{v})=\frac{\mu}{2}\left(\nabla\boldsymbol{v}+(\nabla\boldsymbol{v})^{\mathrm{T}}\right),$$

where $\boldsymbol{D}(\boldsymbol{v})=(1/2)(\nabla\boldsymbol{v}+(\nabla\boldsymbol{v})^{\mathrm{T}})$ is the infinitesimal rate of strain, then we define $\tilde{\boldsymbol{T}}^{\mathrm{E}}_{\alpha+1/2}=\mu\tilde{\boldsymbol{D}}_{\alpha+1/2}$, where $\tilde{\boldsymbol{D}}_{\alpha+1/2}$ is an approximation of $\boldsymbol{D}(\boldsymbol{v})$ at the interface $z_{\alpha+1/2}$. Finally, we can solve the system defined by (3.18) and the equation resulting by multiplying scalarly (3.19) by the vector $\boldsymbol{\eta}_{\alpha+1/2}$. This way, we obtain the expression of $\boldsymbol{T}^{\mathrm{E},\pm}_{\alpha+1/2}$ that satisfies the jump condition and the consistency condition on the interface. We can solve it easily and we obtain

$$\boldsymbol{T}^{\mathrm{E},\pm}_{\alpha+1/2}\cdot\boldsymbol{\eta}_{\alpha+1/2}=\tilde{\boldsymbol{T}}^{\mathrm{E}}_{\alpha+1/2}\cdot\boldsymbol{\eta}_{\alpha+1/2}\pm\frac{1}{2}\frac{1}{\sqrt{1+|\nabla_{\boldsymbol{x}}z_{\alpha+1/2}|^2}}\sum_{j=0}^{N}G_{j,\alpha+1/2}[\![\boldsymbol{v}_j]\!]_{t,\alpha+1/2}. \tag{3.20}$$

3.6. Vertical velocity of the solid particles

First, we select $\alpha \in \{1, \dots, M\}$, and integrate vertically the mass balance equations (2.22) over $(z_{\alpha-1/2}, z)$ for $z \in (z_{\alpha-1/2}, z_{\alpha+1/2})$. This yields

$$\int_{z_{\alpha-1/2}}^{z} \big(\partial_t(\rho_j\phi_j) + \nabla\cdot(\rho_j\phi_j\boldsymbol{v}_j)\big)\,\mathrm{d}\zeta = 0, \quad j = 1, \dots, N.$$

Under the assumptions (3.5) and recalling that $\boldsymbol{v}_j = \boldsymbol{v} + f_j^{\mathrm{M}}(\Phi)/\phi_j\boldsymbol{k} = (\boldsymbol{u}, w_j)$ and $w_j = w + f_j^{\mathrm{M}}(\Phi)/\phi_j$, we obtain

$$\partial_t(\rho_j\phi_{j,\alpha})(z - z_{\alpha-1/2}) + \nabla_{\boldsymbol{x}}\cdot(\rho_j\phi_{j,a}\boldsymbol{u}_\alpha)(z - z_{\alpha-1/2}) + \rho_j\phi_{j,\alpha}\big(w_{j,\alpha}(t,\boldsymbol{x},z) - w^+_{j,\alpha-1/2}\big) = 0.$$

This equation implies that the vertical velocity $w_{j,\alpha}$ is given by

$$w_{j,\alpha}(t,\boldsymbol{x},z) = w^+_{j,\alpha-1/2} - \frac{1}{\rho_j\phi_{j,\alpha}}\big(\partial_t(\rho_j\phi_{j,\alpha}) + \nabla_{\boldsymbol{x}}\cdot(\rho_j\phi_{j,\alpha}\boldsymbol{u}_\alpha)\big)(z - z_{\alpha-1/2}), \quad j = 1, \dots, N. \tag{3.21}$$

In addition, from the condition (3.11) at the interfaces, we obtain the quantities

$$\begin{aligned} w^+_{j,\alpha-1/2} = \frac{1}{\rho_j\phi_{j,\alpha}}\big(&(\rho_j\phi_{j,\alpha} - \rho_j\phi_{j,\alpha-1})\partial_t z_{\alpha-1/2} \\ &+ (\rho_j\phi_{j,\alpha}\boldsymbol{u}_\alpha - \rho_j\phi_{j,\alpha-1}\boldsymbol{u}_{\alpha-1})\cdot\nabla_{\boldsymbol{x}} z_{\alpha-1/2} + \rho_j\phi_{j,\alpha-1}w^-_{j,\alpha-1/2}\big), \end{aligned}$$

where

$$w^-_{j,\alpha-1/2} = w^+_{j,\alpha-3/2} - \frac{h_{\alpha-1}}{\rho_j\phi_{j,\alpha-1}}\big(\partial_t(\rho_j\phi_{j,\alpha-1}) + \nabla_{\boldsymbol{x}}\cdot(\rho_j\phi_{j,\alpha-1}\boldsymbol{u}_{\alpha-1})\big).$$

Using the horizontal velocities specified by the model, the average vertical velocities in the layers are computed sucessively from below to above as follows, where $j = 0, \dots, N$. First the quantity $w^+_{j,1/2}$ is determined from the given mass transfer $G_{j,1/2}$, through the bottom condition (3.8) at the bottom by

$$w^+_{j,1/2} = \partial_t z_{\mathrm{B}} + \boldsymbol{u}_1\cdot\nabla_{\boldsymbol{x}} z_{\mathrm{B}} - \frac{G_{1/2}}{\rho_j\phi_{j,1}}.$$

Then, for $\alpha = 1, \dots, M$ and $z \in (z_{\alpha-1/2}, z_{\alpha+1/2})$, we set

$$\begin{aligned} w_{j,\alpha}(t,\boldsymbol{x},z) &= w^+_{j,\alpha-1/2} - \frac{1}{\rho_j\phi_{j,\alpha}}\big(\partial_t(\rho_j\phi_{j,\alpha}) + \nabla_{\boldsymbol{x}}\cdot(\rho_j\phi_{j,a}\boldsymbol{u}_\alpha)\big)(z - z_{\alpha-1/2}) \\ w^-_{j,\alpha+1/2} &= w^+_{\alpha-1/2} - \frac{h_\alpha}{\rho_j\phi_{j,\alpha}}\big(\partial_t(\rho_j\phi_{j,\alpha}) + \nabla_{\boldsymbol{x}}\cdot(\rho_j\phi_{j,a}\boldsymbol{u}_\alpha)\big), \\ w^+_{j,\alpha+1/2} &= \frac{1}{\rho_j\phi_{j,\alpha+1}}\big((\rho_j\phi_{j,\alpha+1} - \rho_j\phi_{j,\alpha})\partial_t z_{\alpha+1/2} \\ &\qquad + (\rho_j\phi_{j,\alpha+1}\boldsymbol{u}_{\alpha+1} - \rho_j\phi_{j,\alpha}\boldsymbol{u}_\alpha)\cdot\nabla_{\boldsymbol{x}} z_{\alpha+1/2} + \rho_j\phi_{j,\alpha}w^-_{j,\alpha+1/2}\big). \end{aligned}$$

3.7. Vertical velocity of the mixture

The vertical velocity of the mixture inside Ω_α is obtained summing from 0 to N the vertical velocity of the species inside this layer, which is given by (3.21). This yields

$$\sum_{j=0}^{N}\rho_j\phi_{j,\alpha}w_{j,\alpha}(t,x,z) = \sum_{j=0}^{N}\Big(\rho_j\phi_{j,\alpha}w^+_{j,\alpha-1/2} - \big(\partial_t(\rho_j\phi_{j,\alpha}) + \nabla_{\boldsymbol{x}}\cdot(\rho_j\phi_{j,\alpha}\boldsymbol{u}_\alpha)\big)(z - z_{\alpha-1/2})\Big). \tag{3.22}$$

This equality implies that

$$w_\alpha(t,\boldsymbol{x},z) = w^+_{\alpha-1/2} - \frac{1}{\bar\rho_\alpha}\big(\partial_t\bar\rho_\alpha + \nabla_{\boldsymbol{x}}\cdot(\bar\rho_\alpha\boldsymbol{u}_\alpha)\big)(z - z_{\alpha-1/2}),$$

and using the mass jump condition (3.11), we obtain

$$w^+_{\alpha-1/2} = \frac{1}{\bar\rho_\alpha}\big((\bar\rho_\alpha - \bar\rho_{\alpha-1})\partial_t z_{\alpha+1/2} + (\bar\rho_\alpha\boldsymbol{u}_\alpha - \bar\rho_{\alpha-1}\boldsymbol{u}_{\alpha-1})\cdot\nabla_{\boldsymbol{x}} z_{\alpha+1/2} + \bar\rho_{\alpha-1}w^-_{\alpha-1/2}\big),$$

where

$$w^-_{\alpha-1/2} = w^+_{\alpha-3/2} - \frac{h_{\alpha-1}}{\bar\rho_{\alpha-1}}\big(\partial_t(\bar\rho_{\alpha-1}) + \nabla_{\boldsymbol{x}}\cdot(\bar\rho_{\alpha-1}\boldsymbol{u}_{\alpha-1})\big).$$

Then the vertical velocities of mixture in the layers can be computed successively from below to above as follows. The quantity $w^+_{1/2}$ is determined, from the given mass transference $G_{1/2}$, through the condition (3.8) at the bottom by

$$w^+_{1/2} = \partial_t z_{\mathrm{B}} + \boldsymbol{u}_1\cdot\nabla_{\boldsymbol{x}} z_{\mathrm{B}} - \frac{G_{1/2}}{\rho_1}.$$

Then, for $\alpha = 1,\dots,M$ and $z\in(z_{\alpha-1/2}, z_{\alpha+1/2})$, we calculate successively

$$\begin{aligned}
w_\alpha(t,\boldsymbol{x},z) &= w^+_{\alpha-1/2} - \frac{1}{\bar\rho_\alpha}\big(\partial_t\bar\rho_\alpha + \nabla_{\boldsymbol{x}}\cdot(\bar\rho_\alpha\boldsymbol{u}_\alpha)\big)(z - z_{\alpha-1/2}),\\
w^-_{\alpha+1/2} &= w^+_{\alpha-1/2} - \frac{h_\alpha}{\bar\rho_\alpha}\big(\partial_t\bar\rho_\alpha + \nabla_{\boldsymbol{x}}\cdot(\bar\rho_\alpha\boldsymbol{u}_\alpha)\big),\\
w^+_{\alpha+1/2} &= \frac{1}{\bar\rho_{\alpha+1}}\big((\bar\rho_{\alpha+1} - \bar\rho_\alpha)\partial_t z_{\alpha+1/2} + (\bar\rho_{\alpha+1}\boldsymbol{u}_{\alpha+1} - \bar\rho_\alpha\boldsymbol{u}_\alpha)\cdot\nabla_{\boldsymbol{x}} z_{\alpha+1/2} + \bar\rho_\alpha w^-_{\alpha+1/2}\big).
\end{aligned}$$

4. A particular weak solution with hydrostatic pressure

The assumption of a hydrostatic pressure means that

$$p_\alpha(t,\boldsymbol{x},z) = p_{\alpha+1/2}(t,\boldsymbol{x}) + \bar\rho_\alpha g(z_{\alpha+1/2} - z), \quad \text{where} \quad p_{\alpha+1/2}(t,\boldsymbol{x}) = p_{\mathrm{S}}(t,\boldsymbol{x}) + g\sum_{\beta=\alpha+1}^{M}\bar\rho_\beta h_\beta(t,\boldsymbol{x}). \tag{4.1}$$

Here, the component $p_{\alpha+1/2}$ is the kinematic pressure at $\Gamma_{\alpha+1/2}(t)$ and p_{S} denotes the pressure at the free surface. Then, the unknowns of the systems are the layer depths and the horizontal velocities.

Since $\boldsymbol{v}_{j,\alpha}$ is a weak solution of (2.22)–(2.24) in $\Omega_\alpha(t)$, where $\boldsymbol{v}_j$ defined by (2.16), let us begin by considering the weak formulation of this system in $\Omega_\alpha(t)$ for $\alpha = 1,\dots,N$. Assume that $\boldsymbol{v}_{j,\alpha}\in L^2(0,T;H^1(\Omega_\alpha(t))^d)$, $\partial_t\boldsymbol{v}_{j,\alpha}\in L^2(0,T;L^2(\Omega_\alpha(t))^d)$, $\phi_{j,\alpha}\in L^2(0,T;H^1(\Omega_\alpha(t)))$, $\partial_t\phi_{j,\alpha}\in L^2(0,T;L^2(\Omega_\alpha(t)))$ and $p_\alpha\in L^2(0,T;L^2(\Omega_\alpha(t)))$. Then a weak solution of the original equations in $\Omega_\alpha(t)$ should satisfy for all $\varphi\in L^2(\Omega_\alpha(t))$ and for all $\boldsymbol{\vartheta}\in H^1(\Omega_\alpha(t))^d$ with $\boldsymbol{\vartheta}|_{\partial I_{\mathrm{F}}} = 0$ the identities

$$\begin{aligned}
&\int_{\Omega_\alpha(t)}\big(\partial_t\phi_{j,\alpha} + \nabla\cdot(\phi_{j,\alpha}\boldsymbol{v}_{j,\alpha})\big)\varphi\,\mathrm{d}\Omega = 0,\\
&\int_{\Omega_\alpha(t)}\left(\sum_{j=0}^{N}\rho_j\partial_t(\phi_{j,\alpha}\boldsymbol{v}_{j\alpha})\right)\cdot\boldsymbol{\vartheta}\,\mathrm{d}\Omega + \int_{\Omega_\alpha(t)}\left(\sum_{j=0}^{N}\rho_j\nabla\cdot(\phi_{j,\alpha}\boldsymbol{v}_{j,\alpha}\otimes\boldsymbol{v}_{j,\alpha})\right)\cdot\boldsymbol{\vartheta}\,\mathrm{d}\Omega\\
&+\int_{\Omega_\alpha(t)}\boldsymbol{T}^{\mathrm{E}}:\nabla\boldsymbol{\vartheta}\,\mathrm{d}\Omega - \int_{\Omega_\alpha(t)}p\nabla\cdot\boldsymbol{\vartheta}\,\mathrm{d}\Omega + \int_{\Gamma_{\alpha+1/2}(t)}(\boldsymbol{T}^-_{\alpha+1/2}\boldsymbol{\vartheta})\cdot\boldsymbol{\eta}_{\alpha+1/2}\,\mathrm{d}\Gamma\\
&-\int_{\Gamma_{\alpha-1/2}(t)}(\boldsymbol{T}^+_{\alpha-1/2}\boldsymbol{\vartheta})\cdot\boldsymbol{\eta}_{\alpha-1/2}\,\mathrm{d}\Gamma = -\int_{\Omega_\alpha(t)}g\bar\rho_\alpha\boldsymbol{k}\cdot\boldsymbol{\vartheta}\,\mathrm{d}\Omega.
\end{aligned} \tag{4.2}$$

We consider velocity-pressure pairs with the structure given by (3.5) that satisfy the previous system with particular weak solutions that satisfy (4.2) for test functions such that $\partial_z \varphi = 0$ and

$$\boldsymbol{\vartheta}(t, \boldsymbol{x}, z) = \big(\boldsymbol{\vartheta}_{\mathrm{h}}(t, \boldsymbol{x}), (z - z_{\mathrm{B}})\mathcal{V}(t, \boldsymbol{x})\big)^{\mathrm{T}}, \tag{4.3}$$

where $\boldsymbol{\vartheta}_{\mathrm{h}}$ and $\mathcal{V}$ are smooth functions that do no depend on z. Now following a similar approach as in [29], after some straightforward calculations (see Appendix B) we get the mass conservation law

$$\partial_t(\rho_j \phi_{j,\alpha} h_\alpha) + \nabla_{\boldsymbol{x}} \cdot (\rho_j \phi_{j,\alpha} h_\alpha \boldsymbol{u}_\alpha) = G_{j,\alpha+1/2} - G_{j,\alpha-1/2}, \quad j = 0, 1, \ldots, N, \quad \alpha = 1, \ldots, M, \tag{4.4}$$

where $G_{j,\alpha+1/2}$ is defined by (3.12). We remark that taking into account (3.6), we get

$$\partial_t(\bar{\rho}_\alpha h_\alpha) + \nabla_{\boldsymbol{x}} \cdot (\bar{\rho}_\alpha h_\alpha \boldsymbol{u}_\alpha) = G_{\alpha+1/2} - G_{\alpha-1/2}, \quad \alpha = 1, \ldots, M. \tag{4.5}$$

The balance of momentum equations now take the form

$$\begin{aligned}
&\partial_t(\bar{\rho}_\alpha h_\alpha \boldsymbol{u}_\alpha) + \nabla_{\boldsymbol{x}} \cdot (\bar{\rho}_\alpha h_\alpha \boldsymbol{u}_\alpha \otimes \boldsymbol{u}_\alpha) + \int_{z_{\alpha-1/2}}^{z_{\alpha+1/2}} \nabla_{\boldsymbol{x}} p_\alpha \,\mathrm{d}z - \nabla_{\boldsymbol{x}} \cdot (h_\alpha \boldsymbol{T}^{\mathrm{E}}_{\mathrm{h}}) \\
&\qquad + \big(\tilde{\boldsymbol{T}}^{\mathrm{E}}_{\mathrm{h},\alpha+1/2}(\nabla_{\boldsymbol{x}} z_{\alpha+1/2})^{\mathrm{T}} - \tilde{\boldsymbol{T}}^{\mathrm{E}}_{\boldsymbol{x}z,\alpha+1/2}\big) - \big(\tilde{\boldsymbol{T}}^{\mathrm{E}}_{\mathrm{h},\alpha-1/2}(\nabla_{\boldsymbol{x}} z_{\alpha-1/2})^{\mathrm{T}} - \tilde{\boldsymbol{T}}^{\mathrm{E}}_{\boldsymbol{x}z,\alpha-1/2}\big) \\
&\qquad = \frac{G_{\alpha+1/2}}{2}(\boldsymbol{u}_{\alpha+1} + \boldsymbol{u}_\alpha) - \frac{G_{\alpha-1/2}}{2}(\boldsymbol{u}_\alpha + \boldsymbol{u}_{\alpha-1}).
\end{aligned} \tag{4.6}$$

Introducing the notation

$$\bar{p}_\alpha := p_{\mathrm{S}} + g \sum_{\beta=\alpha+1}^{M} \bar{\rho}_\beta h_\beta + g\bar{\rho}_\alpha \frac{h_\alpha}{2}, \quad \bar{z}_\alpha := z_{\mathrm{B}} + \sum_{\beta=1}^{\alpha-1} h_\beta + \frac{h_\alpha}{2},$$

we obtain the following system for $\alpha = 1, \ldots, M$:

$$\begin{aligned}
&\partial_t(\rho_j \phi_{j,\alpha} h_\alpha) + \nabla_{\boldsymbol{x}} \cdot (\rho_j \phi_{j,\alpha} h_\alpha \boldsymbol{u}_\alpha) = G_{j,\alpha+1/2} - G_{j,\alpha-1/2}, \quad j = 0, \ldots, N, \\
&\partial_t(\bar{\rho}_\alpha h_\alpha \boldsymbol{u}_\alpha) + \nabla_{\boldsymbol{x}} \cdot (\bar{\rho}_\alpha h_\alpha \boldsymbol{u}_\alpha \otimes \boldsymbol{u}_\alpha) + h_\alpha(\nabla_{\boldsymbol{x}} \bar{p}_\alpha + g\bar{\rho}_\alpha \nabla_{\boldsymbol{x}} \bar{z}_\alpha) \\
&\qquad - \nabla_{\boldsymbol{x}} \cdot (h_\alpha \boldsymbol{T}^{\mathrm{E}}_{\mathrm{h}}) + \big(\tilde{\boldsymbol{T}}^{\mathrm{E}}_{\mathrm{h},\alpha+1/2}(\nabla_{\boldsymbol{x}} z_{\alpha+1/2})^{\mathrm{T}} - \tilde{\boldsymbol{T}}^{\mathrm{E}}_{\boldsymbol{x}z,\alpha+1/2}\big) - \big(\tilde{\boldsymbol{T}}^{\mathrm{E}}_{\mathrm{h},\alpha-1/2}(\nabla_{\boldsymbol{x}} z_{\alpha-1/2})^{\mathrm{T}} - \tilde{\boldsymbol{T}}^{\mathrm{E}}_{\boldsymbol{x}z,\alpha-1/2}\big) \\
&\qquad = \frac{G_{\alpha+1/2}}{2}(\boldsymbol{u}_{\alpha+1} + \boldsymbol{u}_\alpha) - \frac{G_{\alpha-1/2}}{2}(\boldsymbol{u}_\alpha + \boldsymbol{u}_{\alpha-1}),
\end{aligned} \tag{4.7}$$

where $\tilde{\boldsymbol{T}}^{\mathrm{E}}_{\mathrm{h},\alpha+1/2}$ and $\tilde{\boldsymbol{T}}^{\mathrm{E}}_{\boldsymbol{x}z,\alpha+1/2}$ are defined by (3.19).

5. Closure and reformulation of the model

5.1. Closure of the model in one horizontal space dimension

For the sake of simplicity, we assume that from here on that the extra (viscous) stress tensor $\boldsymbol{T}^{\mathrm{E}}$ equals zero, and we limit the treatment to one horizontal space dimension. In the sequel, we shall denote the horizontal velocities $\boldsymbol{u}_\alpha$ merely by u_α, as well as replace $\boldsymbol{x}$ by x, etc. We define layers whose thickness h_α is proportional to the total height h, *i.e.* we assume that $h_\alpha = l_\alpha h$ for $\alpha = 1, \ldots, M$, where with $l_1, \ldots, l_M$ are positive constants satisfying $l_1 + \cdots + l_M = 1$. Furthermore, we define $r_{j,\alpha} := \rho_j \phi_{j,\alpha} h$ for $\alpha = 1, \ldots, M$ and $j = 0, \ldots, N$, and $q_\alpha := \bar{\rho}_\alpha h u_\alpha$ for $\alpha = 1, \ldots, M$. Note that system (4.7) consists of $M(N+2)$ scalar equations for the same number of unknowns, namely $\{h, \{q_\alpha, \{r_{j,\alpha}\}_{j=1}^{N}\}_{\alpha=1}^{M}, \{G_{\alpha+1/2}\}_{\alpha=1}^{M-1}\}$. Finally, we define

$$m_\alpha := \bar{\rho}_\alpha h = \sum_{j=0}^{N} r_{j,\alpha} = \rho_0 h + \sum_{j=1}^{N} \frac{\rho_j - \rho_0}{\rho_j} r_{j,\alpha}. \tag{5.1}$$

(The second equality is proved in Sect. D.1 of Appendix D.) Then, instead of writing (4.7) in terms of $\{\{r_{j,\alpha}\}_{j=0}^{N}\}_{\alpha=1}^{M}$, we utilize $\{m_\alpha, \{r_{j,\alpha}\}_{j=1}^{N}\}_{\alpha=1}^{M}$. Moreover, from (5.1) we can recover the height of the fluid column as

$$h = \frac{1}{\rho_0}\left(m_\alpha - \sum_{j=1}^{N} \frac{\rho_j - \rho_0}{\rho_j} r_{j,\alpha}\right). \tag{5.2}$$

Consequently, by taking into account the definition (3.12) of $G_{j,\alpha+1/2}$, we can write the system (4.7) for $\alpha = 1, \ldots, M$ as follows:

$$\partial_t m_\alpha + \partial_x q_\alpha = \frac{1}{l_\alpha}(G_{\alpha+1/2} - G_{\alpha-1/2}), \tag{5.3}$$

$$\begin{aligned}\partial_t r_{j,\alpha} + \partial_x\left(\frac{r_{j,\alpha} q_\alpha}{m_\alpha}\right) = {} & \frac{1}{l_\alpha}\left(\tilde{\phi}_{j,\alpha+1/2} G_{\alpha+1/2} - \tilde{\phi}_{j,\alpha-1/2} G_{\alpha-1/2}\right) \\ & - \frac{\rho_j}{l_\alpha}(\tilde{f}_{j,\alpha+1/2} - \tilde{f}_{j,\alpha-1/2}),\end{aligned} \qquad j = 1, \ldots, N, \tag{5.4}$$

$$\begin{aligned}\partial_t q_\alpha + \partial_x\left(\frac{q_\alpha^2}{m_\alpha} + h\left(p_{\mathrm{S}} + \frac{g}{2} l_\alpha m_\alpha + g \sum_{\beta=\alpha+1}^{M} l_\beta m_\beta\right)\right) = {} & \left(p_{\mathrm{S}} + g \sum_{\beta=\alpha+1}^{M} l_\beta m_\beta\right)\partial_x h \\ & - g m_\alpha \partial_x z_b - g m_\alpha L_{\alpha-1} \partial_x h + \frac{1}{l_\alpha}\left(\tilde{u}_{\alpha+1/2} G_{\alpha+1/2} - \tilde{u}_{\alpha-1/2} G_{\alpha-1/2}\right),\end{aligned} \tag{5.5}$$

where we define

$$\tilde{u}_{\alpha+1/2} := \frac{1}{2}\left(\frac{q_{\alpha+1}}{m_{\alpha+1}} + \frac{q_\alpha}{m_\alpha}\right)$$

and note that $\tilde{\phi}_{j,\alpha+1/2}$, defined by (3.13), can be written as

$$\tilde{\phi}_{j,\alpha+1/2} = \frac{1}{2}\left(\frac{r_{j,\alpha+1}}{m_{\alpha+1}} + \frac{r_{j,\alpha}}{m_\alpha}\right). \tag{5.6}$$

Finally, we can also compute an explicit expression of the interlayer mass flux $G_{\alpha+1/2}$. The deduction of the explicit expression of these terms are presented in Appendix A. Moreover, if we introduce the notation

$$R_\beta := q_\beta - \sum_{j=1}^{N} r_{j\beta} u_\beta \frac{\rho_j - \rho_0}{\rho_j}, \quad \bar{R} := \sum_{\beta=1}^{M} l_\beta R_\beta,$$

we can compute the following difference for the transfer terms (see Eq. (A.5)), which allows us to define them recursively:

$$\frac{\rho_0(\bar{\rho}_{\alpha+1} + \bar{\rho}_\alpha)}{\bar{\rho}_\alpha \bar{\rho}_{\alpha+1}} G_{\alpha+1/2} - \frac{\rho_0(\bar{\rho}_\alpha + \bar{\rho}_{\alpha-1})}{\bar{\rho}_\alpha \bar{\rho}_{\alpha-1}} G_{\alpha-1/2} = l_\alpha \partial_x (R_\alpha - \bar{R}) + \rho_0 \sum_{j=0}^{N} (\tilde{f}_{j,\alpha+1/2} - \tilde{f}_{j,\alpha-1/2}). \tag{5.7}$$

5.2. Recovery of primitive variables

Finally, we can deduce the definition of $G_{\alpha+1/2}$ from previous equations, in terms of the other unknowns of the problem. As a result we obtain a reduced system with $M(N+1)+1$ equations. The system can be defined

by the MN equation (5.4), the M equation (5.5) and the sum of the M equation (5.3). This last equation can be written as

$$\partial_t \bar{m} + \partial_x \left(\sum_{\beta=1}^{M} l_\beta q_\beta \right) = G_{M+1/2} - G_{1/2}, \quad \text{where} \quad \bar{m} := h \sum_{\beta=1}^{M} \bar{\rho}_\beta l_\beta = \sum_{\beta=1}^{M} l_\beta m_\beta. \tag{5.8}$$

Then, once the total mass fluxes $G_{\alpha+1/2}$, $\alpha = 1, \dots, M-1$ are specified (see Sect. A), the unknowns of the system defined by equations (5.4), (5.5) and (5.8) are $\{\bar{m}, \{q_\alpha, \{r_{j,\alpha}\}_{j=1}^{N}\}_{\alpha=1}^{M}\}$. From these unknowns we can recover primitive variables as follows:

$$\begin{aligned}
h &= \frac{1}{\rho_0}\left(\bar{m} - \sum_{\beta=1}^{M} \sum_{j=1}^{N} r_{j,\beta} l_\beta \frac{\rho_j - \rho_0}{\rho_j} \right), \\
m_\alpha &= \rho_0 h + \sum_{j=1}^{N} r_{j,\alpha} \frac{\rho_j - \rho_0}{\rho_j} = \bar{m} + \sum_{\beta=1}^{M} \sum_{j=1}^{N} (r_{j,\alpha} - r_{j,\beta}) l_\beta \frac{\rho_j - \rho_0}{\rho_j}, \\
\bar{\rho}_\alpha &= m_\alpha / h, \\
u_\alpha &= q_\alpha / m_\alpha.
\end{aligned} \tag{5.9}$$

6. Numerical schemes

6.1. First-order system of balance equations

In this section we present a numerical scheme to solve the full system composed by (5.4), (5.5) and (5.8). If we denote the vector of unknowns as

$$\boldsymbol{w} = (\bar{m}, q_1, \dots, q_M, r_{1,1}, \dots, r_{N,1}, \dots, r_{1,\alpha}, \dots, r_{N,\alpha}, \dots, r_{1,M}, \dots, r_{N,M})^{\mathrm{T}}, \tag{6.1}$$

the system can be written as (1.1) in terms of a conservative flux and source terms containing non-conservative products. The flux function $\boldsymbol{\mathcal{F}}(\boldsymbol{w})$ and the source terms $\boldsymbol{\mathcal{S}}(\boldsymbol{w}, \partial_x \boldsymbol{w})$ and $\boldsymbol{\mathcal{G}}(\boldsymbol{w}, \partial_x \boldsymbol{w})$ are vectors of dimension $M(N+1)+1$, defined respectively as follows:

$$\boldsymbol{\mathcal{F}}(\boldsymbol{w}) = \begin{pmatrix} \sum_{\beta=1}^{M} l_\beta \mathcal{F}^{m_\beta} \\ \boldsymbol{\mathcal{F}}^{q} \\ \boldsymbol{\mathcal{F}}^{r,1} \\ \vdots \\ \boldsymbol{\mathcal{F}}^{r,M} \end{pmatrix}, \quad \boldsymbol{\mathcal{S}}(\boldsymbol{w}, \partial_x \boldsymbol{w}) = \begin{pmatrix} 0 \\ \boldsymbol{s} \\ \boldsymbol{0} \\ \vdots \\ \boldsymbol{0} \end{pmatrix}, \quad \boldsymbol{\mathcal{G}}(\boldsymbol{w}, \partial_x \boldsymbol{w}) = \begin{pmatrix} 0 \\ \boldsymbol{\mathcal{G}}^{q} \\ \boldsymbol{\mathcal{G}}^{r,1} \\ \vdots \\ \boldsymbol{\mathcal{G}}^{r,M} \end{pmatrix}.$$

The components of these vectors are defined in what follows. The first component of $\boldsymbol{\mathcal{F}}(\boldsymbol{w})$ is defined via $\mathcal{F}^{m_\alpha} = q_\alpha$ for $\alpha = 1, \dots, M$; moreover, $\boldsymbol{\mathcal{F}}^{q} = (\mathcal{F}^{q_1}, \dots, \mathcal{F}^{q_M})^{\mathrm{T}}$, where $\mathcal{F}^{q_\alpha} = q_\alpha^2 / m_\alpha$ for $\alpha = 1, \dots, M$ and

$$\boldsymbol{\mathcal{F}}^{r,\alpha} := \frac{q_\alpha}{m_\alpha} \begin{pmatrix} r_{1,\alpha} \\ \vdots \\ r_{N,\alpha} \end{pmatrix}, \quad \alpha = 1, \dots, M.$$

The components of $\boldsymbol{s} = (s_1, \dots, s_M)^{\mathrm{T}}$ defining the vector $\boldsymbol{\mathcal{S}}$ are given by

$$s_\alpha := g m_\alpha \partial_x (z_b + h) + g h^2 \left(\left(\frac{l_\alpha}{2} + \sum_{\beta=\alpha+1}^{M} l_\beta \right) \partial_x \bar{\rho}_\alpha + \partial_x \left(\sum_{\beta=\alpha+1}^{M} l_\beta (\bar{\rho}_\beta - \bar{\rho}_\alpha) \right) \right), \quad \alpha = 1, \dots, M,$$

where h and $\bar{\rho}_\alpha$ are computed as described in (5.2) and (5.9), respectively. Finally, the sub-vectors of $\boldsymbol{\mathcal{G}}$ are defined by $\boldsymbol{\mathcal{G}}^q = (\mathcal{G}^{q_1}, \ldots, \mathcal{G}^{q_M}))^{\mathrm{T}}$ with $\mathcal{G}^{q_\alpha} = (\tilde{u}_{\alpha+1/2} G_{\alpha+1/2} - \tilde{u}_{\alpha-1/2} G_{\alpha-1/2})/l_\alpha$ for $\alpha = 1, \ldots, M$ and

$$\boldsymbol{\mathcal{G}}^{r,\alpha} := \frac{1}{l_\alpha} \left(G_{\alpha+1/2} \tilde{\Phi}_{\alpha+1/2} - G_{\alpha-1/2} \tilde{\Phi}_{\alpha-1/2} - \begin{pmatrix} \rho_1 (\tilde{f}_{1,\alpha+1/2} - \tilde{f}_{1,\alpha-1/2}) \\ \vdots \\ \rho_N (\tilde{f}_{N,\alpha+1/2} - \tilde{f}_{N,\alpha-1/2}) \end{pmatrix} \right), \quad \alpha = 1, \ldots, M,$$

where $\tilde{\Phi}_{\alpha+1/2} = (\tilde{\phi}_{1,\alpha+1/2}, \ldots, \tilde{\phi}_{N,\alpha+1/2})$.

Since we will use the flux function of the unknowns m_α to compute the flux function for the unknown $\bar{m}$, we also consider the part of the source term related to the unknowns m_α, which is defined by

$$\mathcal{G}^{m_\alpha} := (G_{\alpha+1/2} - G_{\alpha-1/2})/l_\alpha, \quad \alpha = 1, \ldots, M.$$

(see (5.3)). At this point we introduce the following notation which will be used later. We denote

$$\boldsymbol{w}_\alpha = \begin{pmatrix} m_\alpha \\ q_\alpha \end{pmatrix}, \quad \boldsymbol{\mathcal{F}}_\alpha := \begin{pmatrix} \mathcal{F}^{m_\alpha} \\ \mathcal{F}^{q_\alpha} \end{pmatrix}, \quad \boldsymbol{\mathcal{S}}_\alpha := \begin{pmatrix} 0 \\ s_\alpha \end{pmatrix}, \quad \boldsymbol{\mathcal{G}}_\alpha := \begin{pmatrix} \mathcal{G}^{m_\alpha} \\ \mathcal{G}^{q_\alpha} \end{pmatrix}, \quad \alpha = 1, \ldots, M. \tag{6.2}$$

Note that using this notation, from the definition of the global system we obtain

$$\partial_t \boldsymbol{w}_\alpha + \partial_x \boldsymbol{\mathcal{F}}_\alpha(\boldsymbol{w}_\alpha) = \boldsymbol{\mathcal{S}}_\alpha + \boldsymbol{\mathcal{G}}_\alpha, \quad \alpha = 1, \ldots, M.$$

6.2. Path-conservative method

We consider an HLL-path-conservative method where we set the path as segments (PVM-1U method, see [19]). Nevertheless, in what follows we describe the definition of the method in a form that allows us to avoid the computation of the transport matrix of the system. Moreover, this formulation takes into account that the flux associated with the unknown $\bar{m}$ can be written as the average of the fluxes associated with m_α. A second or higher order extentions of the method can be done following [17]. We discretize the spatial domain into cells $\mathcal{C}_i := [x_{i-1/2}, x_{i+1/2}]$ of width Δx centered at $x_i = (i-1/2)\Delta x$, $i \in \mathbb{Z}$, and discretize time via $t_n = n\Delta t$, $n \in \mathbb{N}_0$. We denote by $\boldsymbol{w}^n_{\alpha,i}$ the approximate value of $\boldsymbol{w}(x, t_n)$ for layer α; similar notation is used for other quantities.

The HLL-PVM-1U method is defined by the following two coefficients,

$$\alpha^n_{0,i+1/2} = (S^n_{\mathrm{R},i+1/2} |S^n_{\mathrm{L},i+1/2}| - S^n_{\mathrm{L},i+1/2} |S^n_{\mathrm{R},i+1/2}|)/(S^n_{\mathrm{R},i+1/2} - S^n_{\mathrm{L},i+1/2}),$$
$$\alpha^n_{1,i+1/2} = (|S^n_{\mathrm{R},i+1/2}| - |S^n_{\mathrm{L},i+1/2}|)/(S^n_{\mathrm{R},i+1/2} - S^n_{\mathrm{L},i+1/2}).$$

Here the characteristic velocities $S^n_{\mathrm{L},i+1/2}$ and $S^n_{\mathrm{R},i+1/2}$ are global approximations (they are the same for each layer) of the minimum and maximum wave speed. Taking into account Theorem B.1 (see Appendix B) we set the following definition of $S^n_{\mathrm{L},i+1/2}$ and $S^n_{\mathrm{R},i+1/2}$,

$$S^n_{\mathrm{L},i+1/2} = \bar{u}^n_{i+1/2} - \Psi^n_{i+1/2}, \qquad S^n_{\mathrm{R},i+1/2} = \bar{u}^n_{i+1/2} + \Psi^n_{i+1/2}, \tag{6.3}$$

where

$$\bar{u}^n_{i+1/2} := \frac{1}{M} \sum_{\beta=1}^{M} u^n_{\beta,i+1/2},$$

$$\Psi^n_{i+1/2} := \frac{2M-1}{\sqrt{2M(2M-1)}} \left(2 \sum_{\beta=1}^{M} (\bar{u}^n_{i+1/2} - u^n_{i+1/2})^2 + \frac{g h^n_{i+1/2}}{\rho_0} \left(\rho_0 + \frac{1}{M} \sum_{\beta=1}^{M} (2\beta - 1) \bar{\rho}^n_{\beta,i+1/2} \right) \right)^{1/2},$$

where M is the number of layers. The HLL-PVM-1U method proposed can be written as

$$\boldsymbol{w}_{\alpha,i}^{n+1} = \boldsymbol{w}_{\alpha,i}^{n} - \frac{\Delta t}{\Delta x}\big(\tilde{\boldsymbol{\mathcal{F}}}_{\alpha,i+1/2}^{n} - \tilde{\boldsymbol{\mathcal{F}}}_{\alpha,i-1/2}^{n}\big) + \Delta t \boldsymbol{\mathcal{S}}_{\alpha,i}^{n} + \Delta t \boldsymbol{\mathcal{G}}_{\alpha,i}^{n},$$

where here the numerical flux $\tilde{\boldsymbol{\mathcal{F}}}_{\alpha,i+1/2}^{n} = (\tilde{\mathcal{F}}_{i+1/2}^{m_\alpha,n}, \tilde{\mathcal{F}}_{i+1/2}^{q_\alpha,n})^{\mathrm{T}}$ is given by

$$\begin{aligned}\tilde{\boldsymbol{\mathcal{F}}}_{\alpha,i+1/2}^{n} := \frac{1}{2}\Big(\boldsymbol{\mathcal{F}}_\alpha\big(\boldsymbol{w}_{\alpha,i+1}^{n}\big) + \boldsymbol{\mathcal{F}}_\alpha\big(\boldsymbol{w}_{\alpha,i}^{n}\big)\Big) - \frac{1}{2}\Big(&\alpha_{0,i+1/2}^{n}\big(\boldsymbol{w}_{\alpha,i+1}^{n} - \boldsymbol{w}_{\alpha,i}^{n} + \boldsymbol{\mathcal{C}}_{\alpha,i+1/2}^{n} + \boldsymbol{S}_{\alpha,i+1/2}^{n}\big)\\ &+ \alpha_{1,i+1/2}^{n}\big(\boldsymbol{\mathcal{F}}_\alpha(\boldsymbol{w}_{\alpha,i+1}^{n}) - \boldsymbol{\mathcal{F}}_\alpha\big(\boldsymbol{w}_{\alpha,i}^{n}\big) + \boldsymbol{S}_{\alpha,i+1/2}^{n}\big)\Big),\end{aligned}$$

where

$$\boldsymbol{\mathcal{C}}_{\alpha,i+1/2}^{n} = \begin{pmatrix}\dfrac{\bar\rho_{\alpha,i+1}^{n} + \bar\rho_{\alpha,i}^{n}}{2}(z_{i+1} - z_i)\\ 0\end{pmatrix}, \quad \boldsymbol{\mathcal{S}}_{\alpha,i}^{n} = \frac{1}{2}\big(\boldsymbol{S}_{\alpha,i+1/2}^{n} + \boldsymbol{S}_{\alpha,i-1/2}^{n}\big), \quad \boldsymbol{S}_{\alpha,i+1/2}^{n} = g\begin{pmatrix}0\\ s_{\alpha,i+1/2}^{n}\end{pmatrix},$$

$$\begin{aligned}s_{\alpha,i+1/2}^{n} = \frac{1}{2}\Bigg(&(m_{i+1}^{n} + m_i^{n})(\eta_{i+1}^{n} - \eta_i^{n}) + (h_{i+1}^{2,n} + h_i^{2,n})\Bigg(\frac{l_\alpha}{2} + \sum_{\beta=\alpha+1}^{M} l_\beta\Bigg)(\bar\rho_{\alpha,i+1}^{n} - \bar\rho_{\alpha,i}^{n})\\ &+ (h_{i+1}^{n} + h_i^{n})\sum_{\beta=\alpha+1}^{M} l_\beta\big((\bar\rho_{\beta,i+1}^{n} - \bar\rho_{\alpha,i+1}^{n})h_{i+1}^{n} - (\bar\rho_{\beta,i}^{n} - \bar\rho_{\alpha,i}^{n})h_i^{n}\big)\Bigg),\end{aligned}$$

and

$$\boldsymbol{\mathcal{G}}_{\alpha,i}^{n} = \begin{pmatrix}\mathcal{G}_i^{m_\alpha,n}\\ \mathcal{G}_i^{q_\alpha,n}\end{pmatrix}.$$

To compute $\mathcal{G}_i^{m_\alpha,n}$ and $\mathcal{G}_i^{q_\alpha,n}$ we approximate the transfer term $G_{\alpha+1/2}$ by setting

$$G_{\alpha+1/2,i}^{n} := \frac{1}{2}\big(G_{\alpha+1/2,i+1/2}^{n} + G_{\alpha+1/2,i-1/2}^{n}\big),$$

where $G_{\alpha+1/2,i+1/2}^{n}$ is an approximation at $x = x_{i+1/2}$. By using the recursivity equality (5.7), we approximate the transfer term by

$$\begin{aligned}\rho_0\frac{\hat\rho_{\alpha+1}^{n} + \hat\rho_\alpha^{n}}{\hat\rho_{\alpha+1}^{n}\hat\rho_\alpha^{n}}G_{\alpha+1/2,i+1/2}^{n} = \rho_0\frac{\hat\rho_\alpha^{n} + \hat\rho_{\alpha-1}^{n}}{\hat\rho_\alpha^{n}\hat\rho_{\alpha-1}^{n}}G_{\alpha-1/2,i+1/2}^{n} + \frac{l_\alpha}{\Delta x}\big(R_{\alpha,i+1}^{n} - \bar R_{i+1}^{n} - R_{\alpha,i}^{n} + \bar R_i^{n}\big)\\ + \sum_{j=1}^{N}\big(\hat f_{j,\alpha+1/2,i+1/2}^{n} - \hat f_{j,\alpha-1/2,i+1/2}^{n}\big)(\rho_j - \rho_0),\end{aligned}$$

with

$$\begin{aligned}\hat\rho_\alpha^{n} &:= \frac{1}{2}\big(\bar\rho_{\alpha,i+1}^{n} + \bar\rho_{\alpha,i}^{n}\big), \quad \alpha = 1,\dots,M;\\ \hat f_{j,\alpha+1/2,i+1/2}^{n} &:= \frac{1}{2}\big(f_{j,\alpha+1/2,i+1}^{n} + f_{j,\alpha+1/2,i}^{n}\big), \quad \alpha = 1,\dots,M, \quad j = 1,\dots,N,\end{aligned}$$

where $f_{j,\alpha+1/2,i}^{n}$ is the numerical approximation of the vertical flux $\tilde f_{j,\alpha+1/2}$ given by

$$\begin{aligned}f_{j,\alpha+1/2}^{n} = \frac{1}{2}\big(\phi_{j,\alpha}v_j^{\mathrm{MLB}}(\Phi_\alpha) + \phi_{j,\alpha+1}v_j^{\mathrm{MLB}}(\Phi_{\alpha+1})\big) - \frac{E_{\alpha+1}}{2}(\phi_{j,\alpha+1} - \phi_{j,\alpha})\\ - \frac{\phi_{j,\alpha}}{2}\big|v_j^{\mathrm{MLB}}(\Phi_{\alpha+1}) - v_j^{\mathrm{MLB}}(\Phi_\alpha)\big|\mathrm{sgn}(\phi_{j,\alpha+1} - \phi_{j,\alpha}),\end{aligned}$$

based on Scheme 8 from [12] and where $\Phi_\alpha := (\phi_{1,\alpha},\dots,\phi_{N,\alpha})^{\mathrm{T}}$ and $E_\alpha := \max_{j=1,\dots,N} |v_j^{\mathrm{MLB}}(\Phi_\alpha)|$, where v_j^{MLB} is the hindered settling velocity given by (2.17). Then we have

$$\begin{aligned}
\mathcal{G}_i^{m_\alpha,n} &= \big(G^n_{\alpha+1/2,i} - G^n_{\alpha-1/2,i}\big)/l_\alpha,\\
\mathcal{G}_i^{q_\alpha,n} &= \big(\bar{u}^n_{\alpha+1/2,i}G^n_{\alpha+1/2,i} - \bar{u}^n_{\alpha-1/2,i}G^n_{\alpha-1/2,i}\big)/l_\alpha,\\
\bar{u}^n_{\alpha+1/2,i} &= \frac{1}{2}\left(\frac{u^n_{\alpha+1,i+1}+u^n_{\alpha,i+1}}{2} + \frac{u^n_{\alpha+1,i}+u^n_{\alpha,i}}{2}\right).
\end{aligned}$$

Moreover, since the solid concentrations are passive scalars in the system, *i.e.* $\mathcal{F}^{r_{j,\alpha}} = (r_{j,\alpha}/m_\alpha)\mathcal{F}^{m_\alpha}$, we use the following upwinding formula to compute the numerical flux relative to $r^n_{j,\alpha}$:

$$\tilde{\mathcal{F}}^{r_{j,\alpha},n}_{i+1/2} = \begin{cases} (r^n_{j,\alpha,i}/m^n_{\alpha,i})\tilde{\mathcal{F}}^{m_\alpha,n}_{i+1/2} & \text{if } \tilde{\mathcal{F}}^{m_\alpha,n}_{i+1/2} > 0,\\ (r^n_{j,\alpha,i+1}/m^n_{\alpha,i+1})\tilde{\mathcal{F}}^{m_\alpha,n}_{i+1/2} & \text{otherwise,}\end{cases} \qquad j = 1,\dots,N.$$

Finally, the numerical scheme to approximate the unknowns of the problem is defined as follows:

$$\begin{aligned}
\bar{m}_i^{n+1} &= \bar{m}_i^n - \frac{\Delta t}{\Delta x}\sum_{\beta=1}^{M} l_\beta \tilde{\mathcal{F}}^{m_\beta,n}_{i+1/2},\\
q^{n+1}_{\alpha,i} &= q^n_{\alpha,i} - \frac{\Delta t}{\Delta x}\big(\tilde{\mathcal{F}}^{q_\alpha,n}_{i+1/2} - \tilde{\mathcal{F}}^{q_\alpha,n}_{i-1/2}\big) + \frac{\Delta t}{2}\big(s^n_{\alpha,i+1/2} + s^n_{\alpha,i-1/2}\big) + \Delta t\mathcal{G}_i^{q_\alpha,n},\\
r^{n+1}_{j,\alpha,i} &= r^n_{j,\alpha,i} - \frac{\Delta t}{\Delta x}\big(\tilde{\mathcal{F}}^{r_{j,\alpha},n}_{i+1/2} - \tilde{\mathcal{F}}^{r_{j,\alpha},n}_{i-1/2}\big) + \Delta t\mathcal{G}_i^{r_{j,\alpha},n},
\end{aligned}$$

with

$$\begin{aligned}
\mathcal{G}_i^{r_{j,\alpha},n} &= \frac{1}{l_\alpha}\big(\bar{\phi}^n_{j,\alpha+1/2,i}G^n_{\alpha+1/2,i} - \bar{\phi}^n_{j,\alpha-1/2,i}G^n_{\alpha-1/2,i}\big) - \frac{\rho_j}{l_\alpha}\big(\hat{f}^n_{j,\alpha+1/2,i+1/2} - \hat{f}^n_{j,\alpha-1/2,i+1/2}\big),\\
\bar{\phi}^n_{j,\alpha+1/2,i} &= \frac{1}{2}\left(\frac{1}{2}\left(\frac{r^n_{j,\alpha+1,i+1}}{m^n_{\alpha+1,i+1}} + \frac{r^n_{j,\alpha,i+1}}{m^n_{\alpha,i+1}}\right) + \frac{1}{2}\left(\frac{r^n_{j,\alpha+1,i}}{m^n_{\alpha+1,i}} + \frac{r^n_{j,\alpha,i}}{m^n_{\alpha,i}}\right)\right).
\end{aligned}$$

7. Numerical tests

7.1. Preliminaries

In all tests we use the global constants $g = 9.8\,\mathrm{m/s^2}$ (acceleration of gravity), $\phi_{\max} = 0.68$ ((nominal) maximal total solids concentration, a dimensionless volume fraction), and employ the Richardson–Zaki hindered settling factor (2.14) with $n_{\mathrm{RZ}} = 4.7$. The viscosity and density of the pure fluid are $\mu_0 = 0.02416\,\mathrm{Pa\,s}$ and $\rho_0 = 1208\,\mathrm{kg/m^3}$, respectively. In all tests the particles are assumed to have the same density $\rho_1 = \cdots = \rho_N = 2790\,\mathrm{kg/m^3}$. These parameters correspond to an experiment by Schneider *et al.* [41].

We limit the computation of numerical solutions to four tests. Firstly, one case of zero horizontal but one vertical direction (Test 1), and two cases of one horizontal and one vertical direction (Tests 2 and 3) . In the latter tree cases, the (horizontal) x-interval $[0, L]$ is subdivided into C subintervals $[x_{i-1/2}, x_{i+1/2}] = [(i-1)\Delta x, i\Delta x]$ of length $\Delta x = L/C$, centered at $x_i = (i-1/2)\Delta x$, $i = 1,\dots,C$. In what follows, we use the following CFL condition to determine Δt in each iteration:

$$\frac{\Delta t}{\Delta x}\max_{1\le i\le C}\max\{|S_{\mathrm{R},i+1/2}|, |S_{\mathrm{L},i+1/2}|\} = \mathrm{CFL},$$

where $S_{\mathrm{R},i+1/2}$ and $S_{\mathrm{L},i+1/2}$ are the bounds of the eigenvalues defined in (6.3) and $\mathrm{CFL} = 0.5$. Furthermore, for Test 3 we compute an approximate L^1 error at a fixed end time $t = t_{\mathrm{end}}$ of a scalar component g_i of the numerical

solution by means of a reference solution based on a number of C_{ref} cells. Precisely, let us denote by $\{g_i(t_{\text{end}})\}_{i=1}^{C}$ and $\{g_i^{\text{ref}}(t_{\text{end}})\}_{i=1}^{C_{\text{ref}}}$ the numerical solution at time t_{end} calculated with C and C_{ref} cells, respectively, where we assume that $\nu := C_{\text{ref}}/C \in \mathbb{N}$. Then we compute the projected reference solution $\{\tilde{g}_i^{\text{ref}}(t_{\text{end}})\}_{i=1}^{C}$ using

$$\tilde{g}_i^{\text{ref}}(t_{\text{end}}) = \frac{1}{\nu}\sum_{k=1}^{\nu} g_{\nu(i-1)+k}^{\text{ref}}(t_{\text{end}}), \quad i = 1, \dots, C.$$

Then, we define the approximate L^1 error of the numerical solution $\{g_i(t_{\text{end}})\}_{i=1}^{C}$ at time $t = t_{\text{end}}$ as

$$e_{C,C_{\text{ref}}}(t_{\text{end}}) := \frac{1}{C}\sum_{j=1}^{C} \left|\tilde{g}_i^{\text{ref}}(t_{\text{end}}) - g_i(t_{\text{end}})\right|. \tag{7.1}$$

Finally, a 3D simulation (Test 4) is presented. With the purpose of brevity we do not give the details in the paper of the model and the numerical method. For the implementation of the numerical method we consider a rectangular grid in the horizontal 2D domain and the usual application of a 1D finite volume method at each edge of the cell.

7.2. Test 1: One-dimensional vertical sedimentation

In the first numerical test we consider $N = 3$ solid species dispersed in a viscous fluid. The solid particle diameters are $d_1 = 4.96 \times 10^{-4}$ m, $d_2 = 3.25 \times 10^{-4}$ m and $d_3 = 1.0 \times 10^{-4}$ m.

We consider a vertical domain of height $h = 0.3$ m discretized into $M = 50$ layers (z_i nodes), with initial solid concentrations $\phi_1(t = 0) = 0.1$, $\phi_2(t = 0) = 0.05$ and $\phi_3(t = 0) = 0.09$ constant in all the domain. Figure 2 displays simulated concentration profiles at different times. Comparing the simulated behaviour of the modified MLB model (defined by (2.17)) with that of the original MLB model (that is recovered if we set $\lambda_1 = \cdots = \lambda_N = 1$ in (2.17)), we can see that the modified MLB velocities predict that the solid particles settle slightly more slowly than when the classical MLB velocities are used. That said, we remark that the 1D vertical modified MLB model coincides with the proposed multilayer approximation only if the transfer term $G_{\alpha+1/2}$ is set to zero. In other words, if we block the transfer of mass term across the interface in the multilayer approach, we recover the classical one-dimensional numerical method for polydisperse sedimentation [12] but with the new MLB velocity.

The 1D vertical model corresponds to solving the following system of ODEs that represent a semi-discretization of the spatio-temporal model:

$$\partial_t \phi_{j,\alpha} = -\frac{1}{h l_\alpha}(f_{j,\alpha+1/2} - f_{j,\alpha-1/2}), \quad j = 1, \dots, N, \quad \alpha = 1, \dots, M,$$

where $f_{j,\alpha+1/2}$ is the numerical approximation of the vertical flux function $f_j = \phi_j v_j^{\text{MLB}}$.

The mass transfer is not equal to zero in this new multilayer model even though the horizontal velocities are equal zero. In this case, from the definition (A.5) of $G_{\alpha+1/2}$ we deduce the transfer term

$$G_{\alpha+1/2} = \rho_0 \sum_{j=0}^{N} \tilde{f}_{j,\alpha+1/2}.$$

Since within the classical MLB model, the average velocity does not take into account the densities of the particles, it can be deduced that

$$\sum_{j=0}^{N} \tilde{f}_{j,\alpha+1/2} = 0.$$

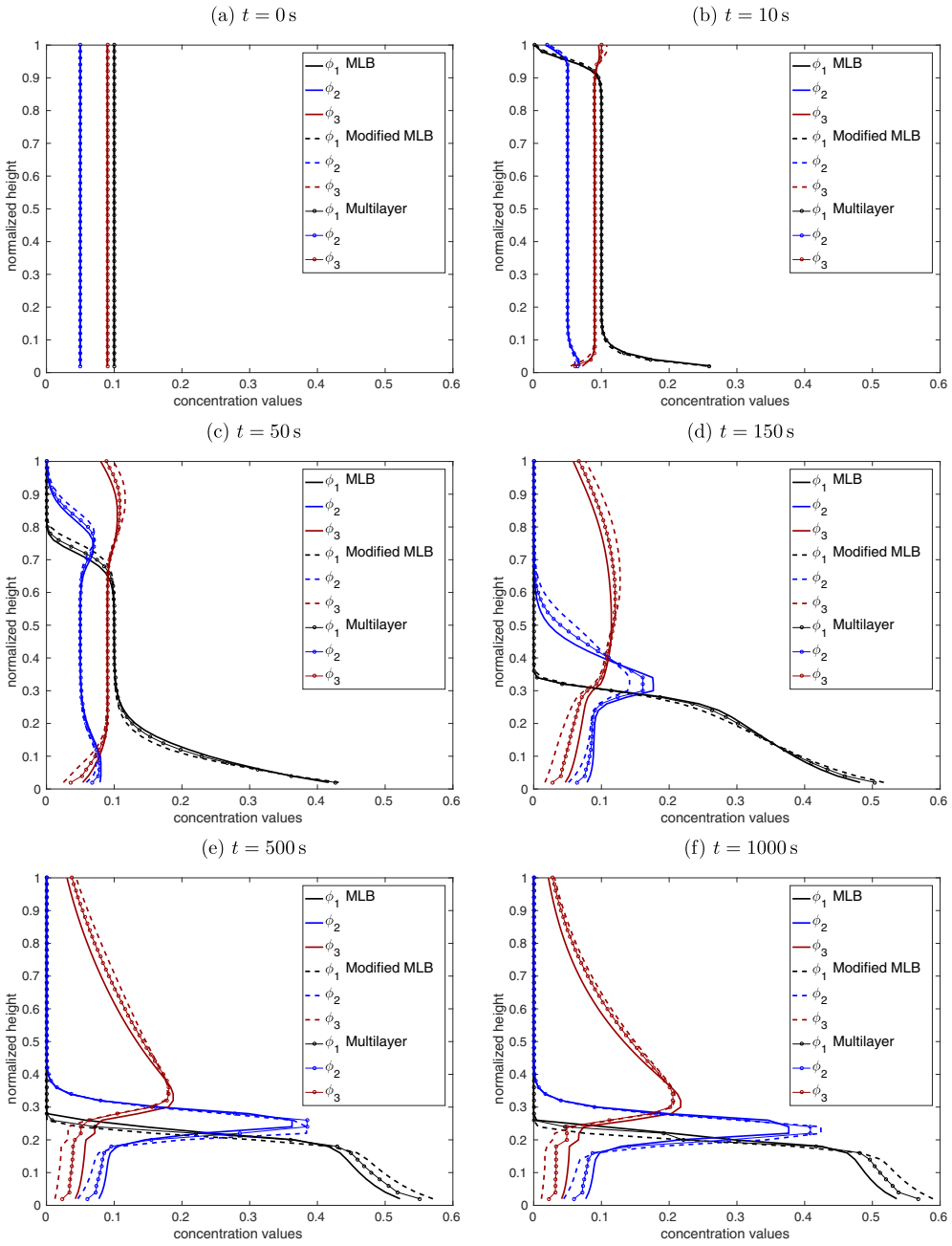

FIGURE 2. Test 1: Concentrations of the solid species with respect the normalized height at times $t = 0$, 10, 50, 150, 500, and 1000 s.

Then $G_{\alpha+1/2} = 0$. With the proposed modification of MLB model, $G_{\alpha+1/2} \neq 0$ because this term takes into account the exact mass conservation, which implies that

$$\sum_{j=0}^{N} \rho_j \tilde{f}_{j,\alpha+1/2} = 0.$$

As a consequence, the proposed model is able to reproduce a vertical velocity of the fluid generated by the vertical movement of the solid particles. However, the three models predict fairly similar sedimentation behaviour of the three models. The larger species settle faster than those with smaller size, and the smaller particles float (that is, move upward) when the biggest particles settle. This behavior is expected. At $t = 500\,\mathrm{s}$ the solution is almost stationary. In Figure 2 a very small variation in the concentration of the smallest particles can be observed if we compare the figures corresponding to $t = 500$ and $t = 1000\,\mathrm{s}$.

7.3. Test 2: Sedimentation with imposed velocity

In this numerical test we simulate bidisperse sedimentation in a horizontal channel, with an inclined bottom, of length $L = 1\,\mathrm{m}$. Here and in Test 3 we use $C = 150$ subintervals and $M = 10$ layers in the horizontal and vertical discretization, respectively, and in both tests we use $N = 2$ solids species of diameters $d_1 = 4.96\times10^{-4}\,\mathrm{m}$ and $d_2 = 1.25 \times 10^{-4}\,\mathrm{m}$, respectively (these are the original particle sizes used in [41]). The bottom elevation is given by $z_{\mathrm{B}}(x) = -0.1x + 0.1\,\mathrm{m}$ for $x \in [0, L]$. We here assume the initial condition

$$\phi_{1,\alpha}(0,x) = 0, \quad \phi_{2,\alpha}(0,x) = 0 \quad u_\alpha(0,x) = 0 \quad \text{for all } \alpha = 1,\dots,M, \text{ for all } x \in [0,L],$$

and for the height $h(t = 0) = 0.3 - z_{\mathrm{B}}$. Furthermore, as boundary condition we impose at $x = 0$ a linear horizontal velocity $u(z)_{|x=0} = 0.133z + 0.128\,\mathrm{m/s}$, whose average value is $0.15\,\mathrm{m/s}$. A uniform distribution of the sediment concentrations is set at the left boundary, *i.e.*,

$$\phi_{1,\alpha|x=0} = \frac{1}{M}\sum_{\beta=1}^{M} \phi_{1,\beta|x=0}, \quad \phi_{2,\alpha|x=0} = \frac{1}{M}\sum_{\beta=1}^{M} \phi_{2,\beta|x=0} \quad \text{for all } \alpha = 1,\dots,M$$

with $\sum_{\beta=1}^{M} \phi_{1,\beta|x=0} = 0.05$ and $\sum_{\beta=1}^{M} \phi_{2,\beta|x=0} = 0.025$. At the right boundary a homogeneous Neumann condition is imposed.

Here, we are interested in seeing how the particles, besides settling due to the force of gravity, are transported horizontally when horizontal velocities are imposed on the left boundary. In Test 1 we have seen that some particles, depending on their size, move downward or upward, and the bigger particles settler faster than smaller particles (in the same environment). The difference here is that we impose linear horizontal velocities by layers and fixed concentrations over the left boundary and we want to see the behavior of the particles (horizontal movement, sedimentation and suspension of some particles). In Figures 3 and 4 for the first species we can see both phenomena, namely settling and horizontal transport of the particles due to the imposed horizontal velocity at the fluid. We see for example in Figures 4a and 4c and more clearly in Figure 4e and correspondingly Figures 3a, 3c and 3e that the particles of bigger size are deposited rapidly over the bottom, furthermore we see how the concentration goes from initial condition ($\phi_{1,\alpha} = 0$) to high concentration in the first layer, decreasing from the bottom to the free surface. In all the domain the concentration in the first layer always is greater than in the upper layers, due to the size of species 1. Furthermore this behavior its present at all times from $t = 0$ to $t = 100\,\mathrm{s}$.

If we make reference to the applications (water recovery for example), we can say that in the free surface close to the right boundary we obtain fluid free of particles of species 1 but yet with particles of species 2 at smaller concentration, as we see in Figures 3 and 4 in lines of concentration by layers and concentration by color, respectively. On the other hand, we can observe the horizontal movement of both solid species from the left to the right boundary, see Figures 3 and 4. Clearly, the concentration of each solid species $\phi_{1,\alpha}$ and $\phi_{2,\alpha}$

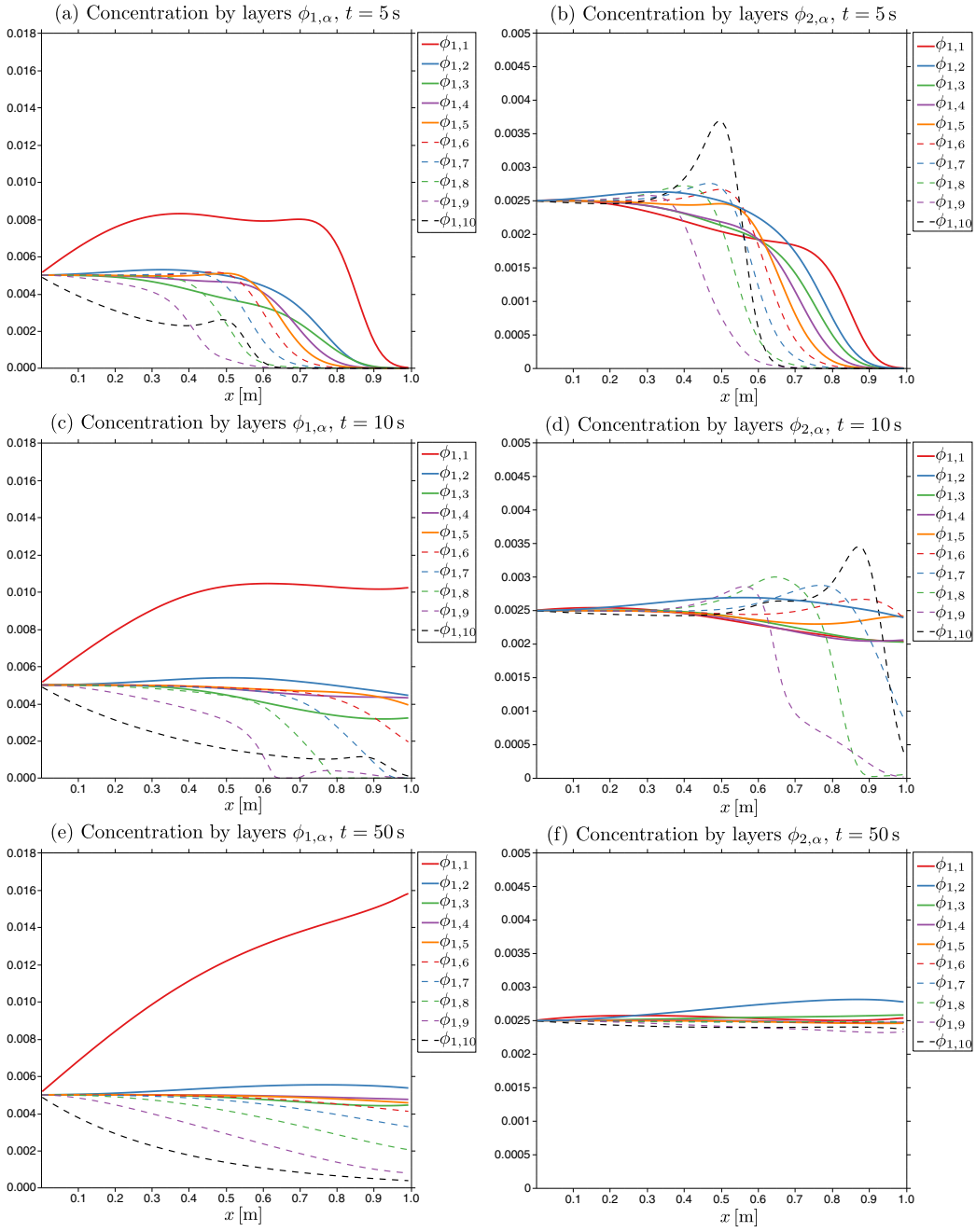

FIGURE 3. Test 2: Concentration of solid species ϕ_1, ϕ_2 by layer.

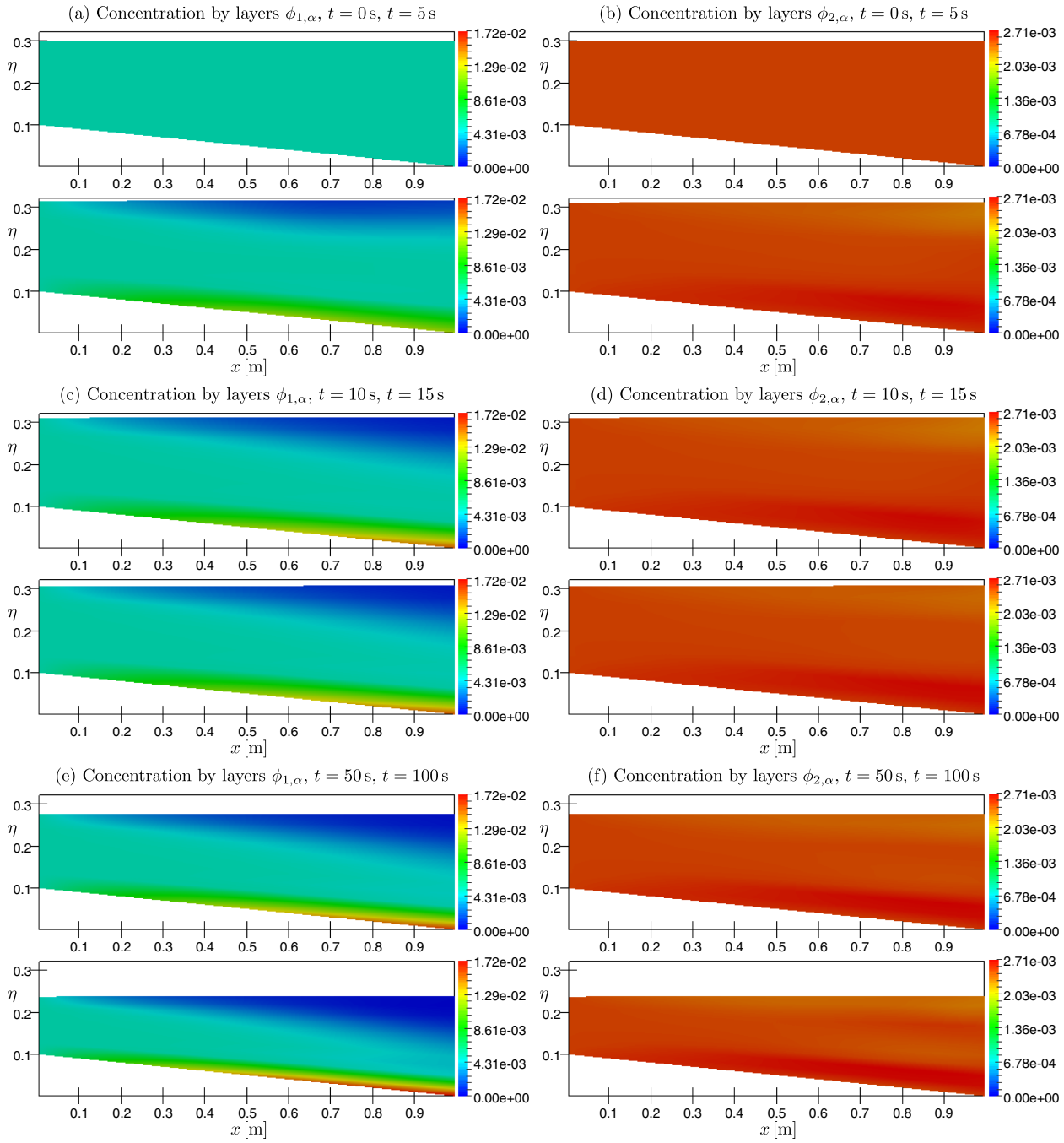

FIGURE 4. Test 2: Concentration of solid species ϕ_1, ϕ_2 by colors, $\eta(x) = z_{\mathrm{B}}(x) + h(x)\,\mathrm{m}$.

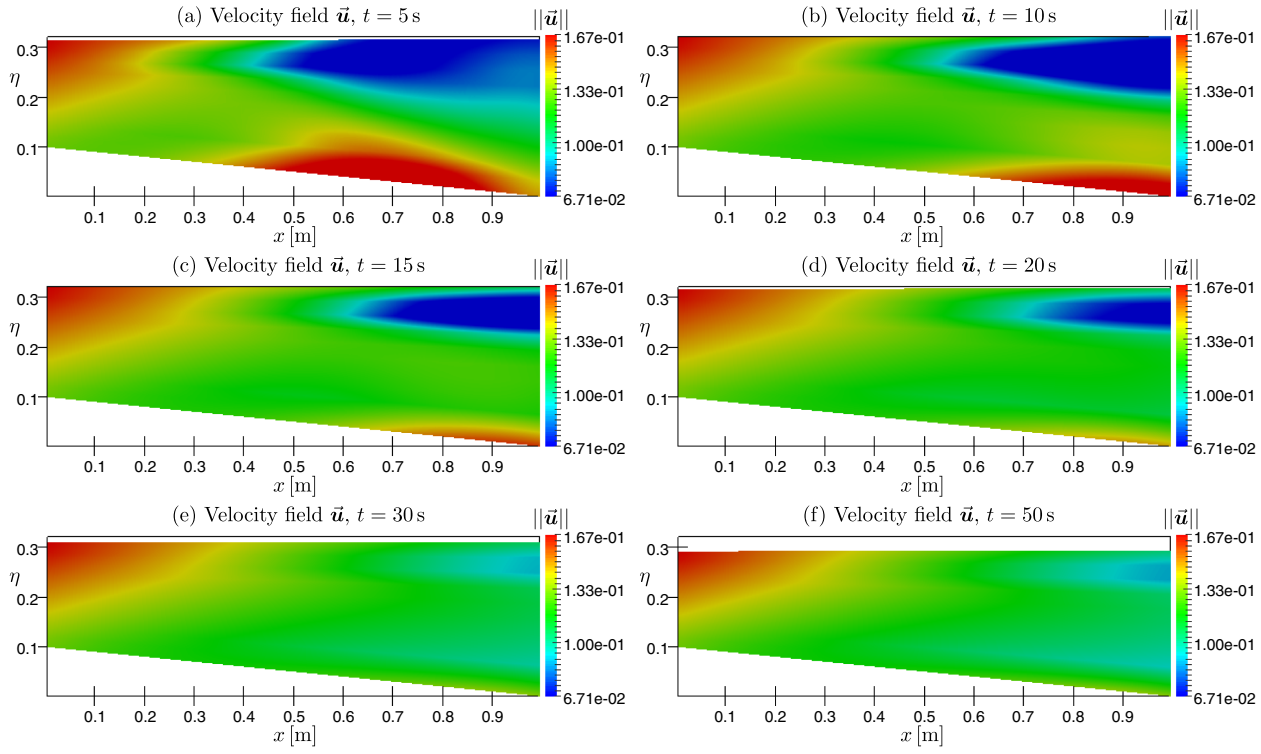

FIGURE 5. Test 2: Magnitude of the velocity field $\boldsymbol{u}$ and free surface, $\eta(x) = z_{\mathrm{B}}(x) + h(x)\,\mathrm{m}$.

TABLE 1. Test 3: Approximate L^1 errors for (*top*) $r_{1,\alpha}$, (*middle*) $r_{2,\alpha}$ and (*bottom*) $\bar{m}$ and q_α, in each case for $\alpha = 2, 4, 6, 8, 10$ at time $t = 1\,\mathrm{s}$.

C	L^1 error $r_{1,2}$	L^1 error $r_{1,4}$	L^1 error $r_{1,6}$	L^1 error $r_{1,8}$	L^1 error $r_{1,10}$
40	7.33e-04	8.93e-05	1.18e-04	7.71e-05	6.76e-05
80	5.45e-04	6.13e-05	8.50e-05	6.56e-05	4.99e-05
160	3.89e-04	4.24e-05	5.87e-05	5.37e-05	3.51e-05
320	2.44e-04	2.73e-05	3.87e-05	3.92e-05	2.35e-05

C	L^1 error $r_{2,2}$	L^1 error $r_{2,4}$	L^1 error $r_{2,6}$	L^1 error $r_{2,8}$	L^1 error $r_{2,10}$
40	3.73e-04	4.53e-05	5.94e-05	5.01e-05	3.79e-05
80	2.78e-04	3.12e-05	4.26e-05	3.98e-05	3.03e-05
160	1.98e-04	2.16e-05	2.94e-05	3.15e-05	2.22e-05
320	1.24e-04	1.39e-05	1.94e-05	2.25e-05	1.53e-05

C	L^1 error $\bar{m}$	L^1 error q_2	L^1 error q_4	L^1 error q_6	L^1 error q_8	L^1 error q_{10}	cpu time (s)
40	1.27e-04	8.90e-04	3.86e-04	4.80e-04	6.18e-04	3.73e-04	0.16882100
80	3.72e-05	7.42e-04	2.76e-04	3.55e-04	4.65e-04	2.46e-04	0.57736800
160	1.34e-05	5.47e-04	1.81e-04	2.42e-04	3.18e-04	1.47e-04	2.14343400
320	6.92e-06	3.44e-04	1.10e-04	1.51e-04	2.00e-04	8.02e-05	8.82513300

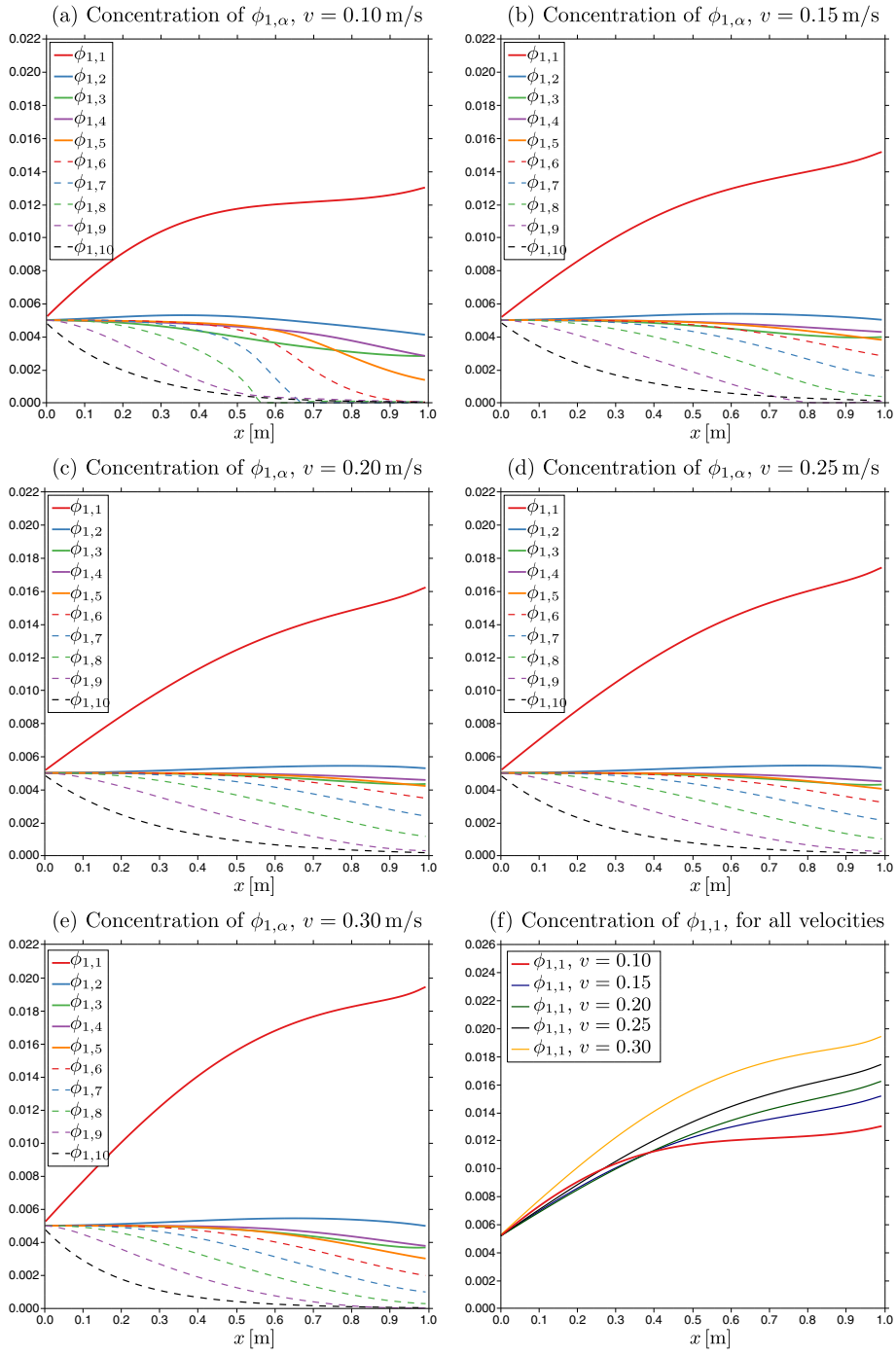

FIGURE 6. Test 2: Concentration for different constant velocities imposed in the left boundary in $t = 100\,\mathrm{s}$.

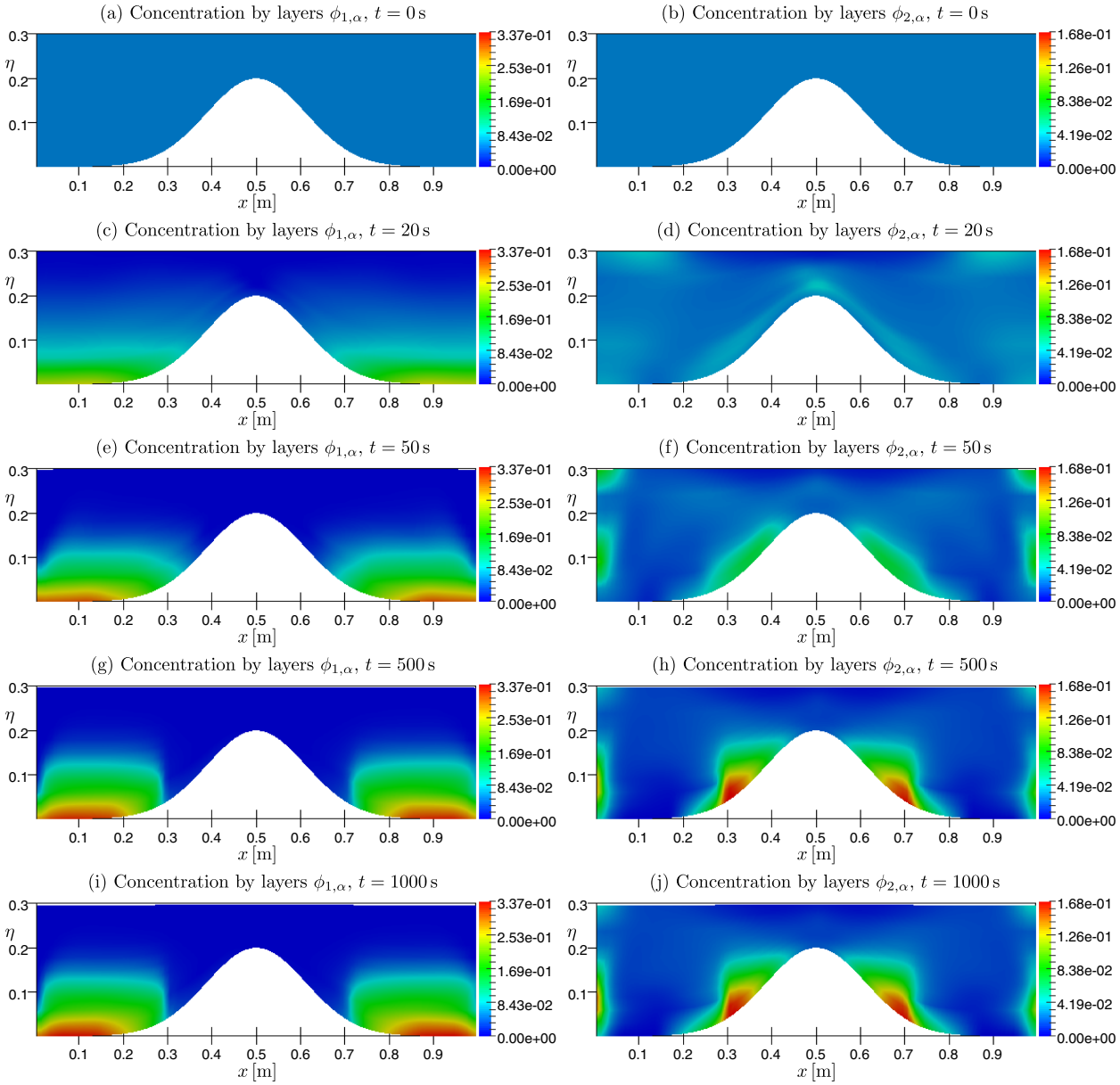

FIGURE 7. Test 3: Concentration of ϕ_1 and ϕ_2 by color in a domain with a bump, $\eta(x) = z_{\mathrm{B}}(x) + h(x)\,\mathrm{m}$.

increases from zero to positive values in all layers. The behaviour of the smaller particles is more difficult to predict due to the suspension phenomena that to appear when the bigger particles settle faster. For this reason, we can see how the concentration of these particles decreases more slowly than that of species 1. The particles of species 2 are in suspension for more time, in other words the sedimentation process for this species is slower. We can see in Figures 4b and 4d for times $t = 0, 5, 10, 15\,\mathrm{s}$ that the concentration of the upper layers begins to increase in the middle of the domain, this means that in this place the particles of species 2 are clearly in

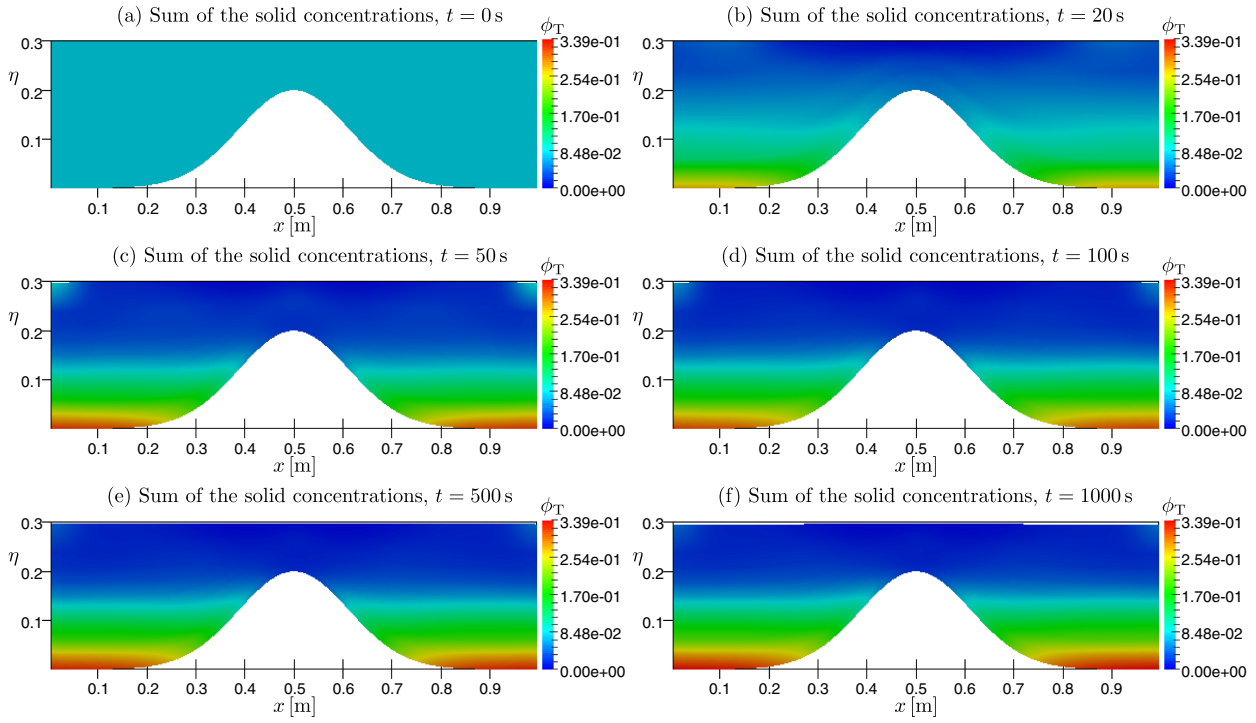

FIGURE 8. Test 3: Concentration by color by $\phi_T = \phi_1 + \phi_2$, $\eta(x) = z_B(x) + h(x)$ m.

suspension near to the free surface. In the following times, in Figures 4e and 4f, we see that some particles begin to settle and the concentration in the second layer increases. We note here that the concentrations in the first layer for species 2 is small because the larger particles have occupied the space, as we have also seen in Figures 2e and 2f in Test 1. In Figure 5 the evolution of the velocity of the fluid is presented, where we have colored the magnitude of the velocity field.

Finally, to see the influence of the velocity magnitude imposed as boundary conditions we have considered the following values: $v = 0.10,\ 0.15,\ 0.20,\ 0.25,\ 0.30\,\mathrm{m/s}$ respectively, constant in all layers as boundary condition in the left and we have kept the same initial condition and we have simulated the sedimentation process with the same diameters and solid densities for the particles. In Figure 6, for simplicity we only show concentrations for species 1 at time $t = 100\,\mathrm{s}$ for the different horizontal velocities. We can see how for a bigger velocity the concentration of species 1 increases in the first layer due to a higher velocity, greater flow and therefore there is a higher influx of particles, which accumulate rapidly at the bottom of the domain. In Figure 6f we see the difference in the concentration of species 1 in the first layer for different horizontal velocities.

7.4. Test 3: Sedimentation in a domain with a bump

In this numerical test we simulate bidisperse sedimentation process over a horizontal channel with a bump of length $L = 1\,\mathrm{m}$. We use $N = 2$ solids species dispersed in a viscous fluid; the particle sizes and densities are the same as in Test 2. The bottom elevation is given by $z_B(x) = 0.2\exp(-40(x-0.5)^2)\,\mathrm{m}$ for $x \in [0, L]$, the initial condition for the height is $h(t=0) = 0.3 - z_B$, and for the concentration of each species

$$\phi_{1,\alpha} = \frac{1}{M}\sum_{\beta=1}^{M}\phi_{1,\beta}(0,x),\ \phi_{2,\alpha} = \frac{1}{M}\sum_{\beta=1}^{M}\phi_{2,\beta}(0,x),\ u_\alpha(0,x) = 0 \quad \text{for all } \alpha = 1,\dots,M \text{ and all } x \in [0,L],$$

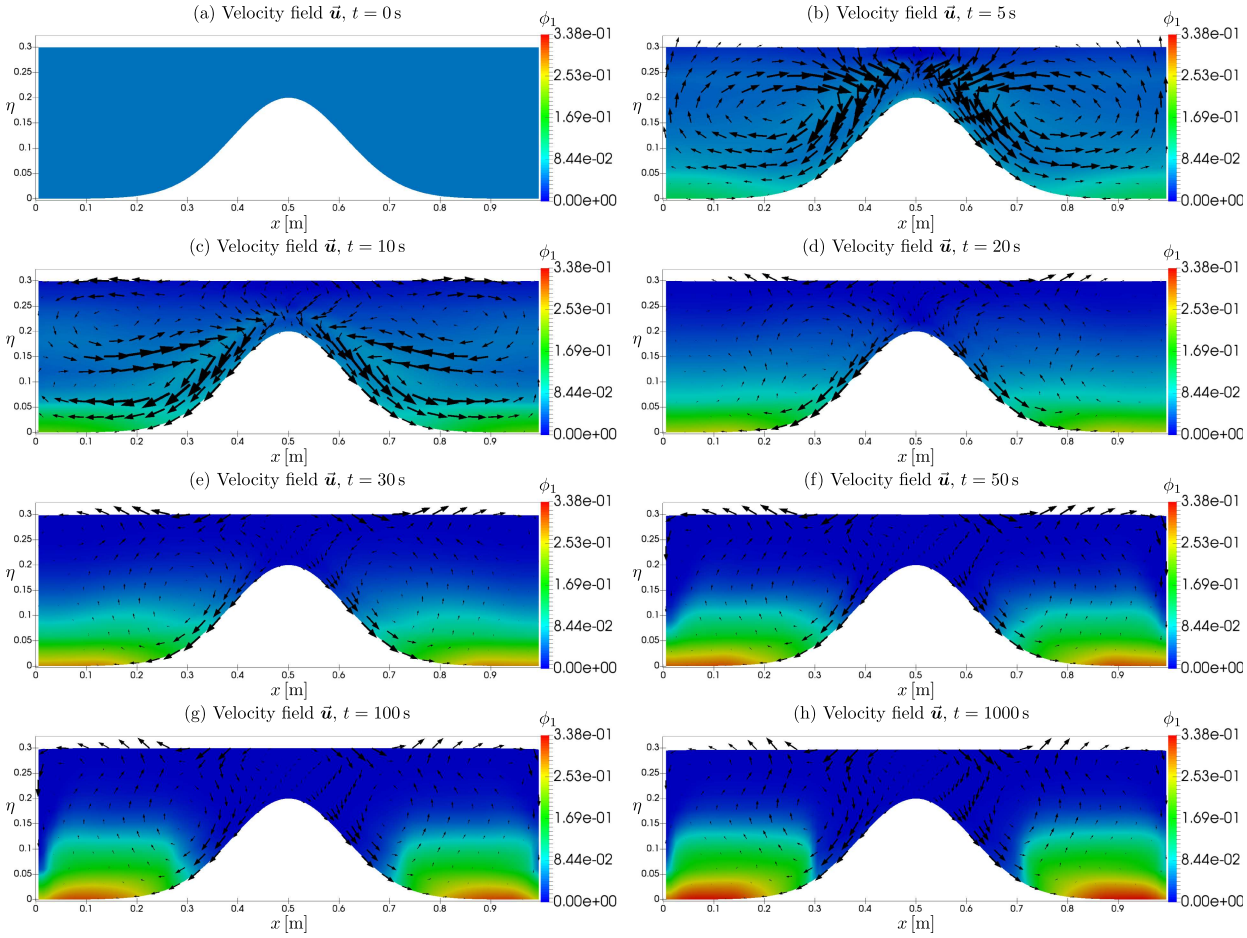

FIGURE 9. Test 3: Velocity field $\boldsymbol{u}$ over concentration ϕ_1, $\eta(x) = z_{\mathrm{B}}(x) + h(x)$.

with $\sum_{\beta=1}^{M} \phi_{1,\beta}(0,x) = 0.05$, $\sum_{\beta=1}^{M} \phi_{2,\beta}(0,x) = 0.025$. The sediment concentrations are vertically uniformly distributed at each point x. As boundary condition we impose a closed basin.

In Figure 7 we present the simulated concentrations of species 1 (ϕ_1) to the right and species 2 (ϕ_2) to the left. We can see the behavior of the particles of the different species when there is a bump in the domain. The bigger particles are deposited rapidly over the bottom, in this case to both sides of the bump, where we can find high concentration of species 1, as we can see in Figures 7a, 7c, 7e, 7g and 7i. The smaller particles initially remain in suspension, but at larger simulated times these particles begin to settle and occupy where the concentration of species 1 is small (see Figs. 7f, 7h and 7j). To see the global behavior of all particles dispersed in the fluid we display in Figure 8 the sum of the concentrations of the all species and we can see how these are deposited in the bottom on both side of the bump and also as some particles of species 2 are kept in suspension. In Figures 9 and 10 we show the velocity field of the fluid and its magnitude respectively, which is a consequence of the particles movement, and we can see how recirculations appear to both sides of the bump. In the first times high velocities appear avoiding that some particles settle rapidly. We see in Figures 7c and 9c how some particles are in suspension because they are inside of an eddy. At larger times the velocity decreases and the particles settle.

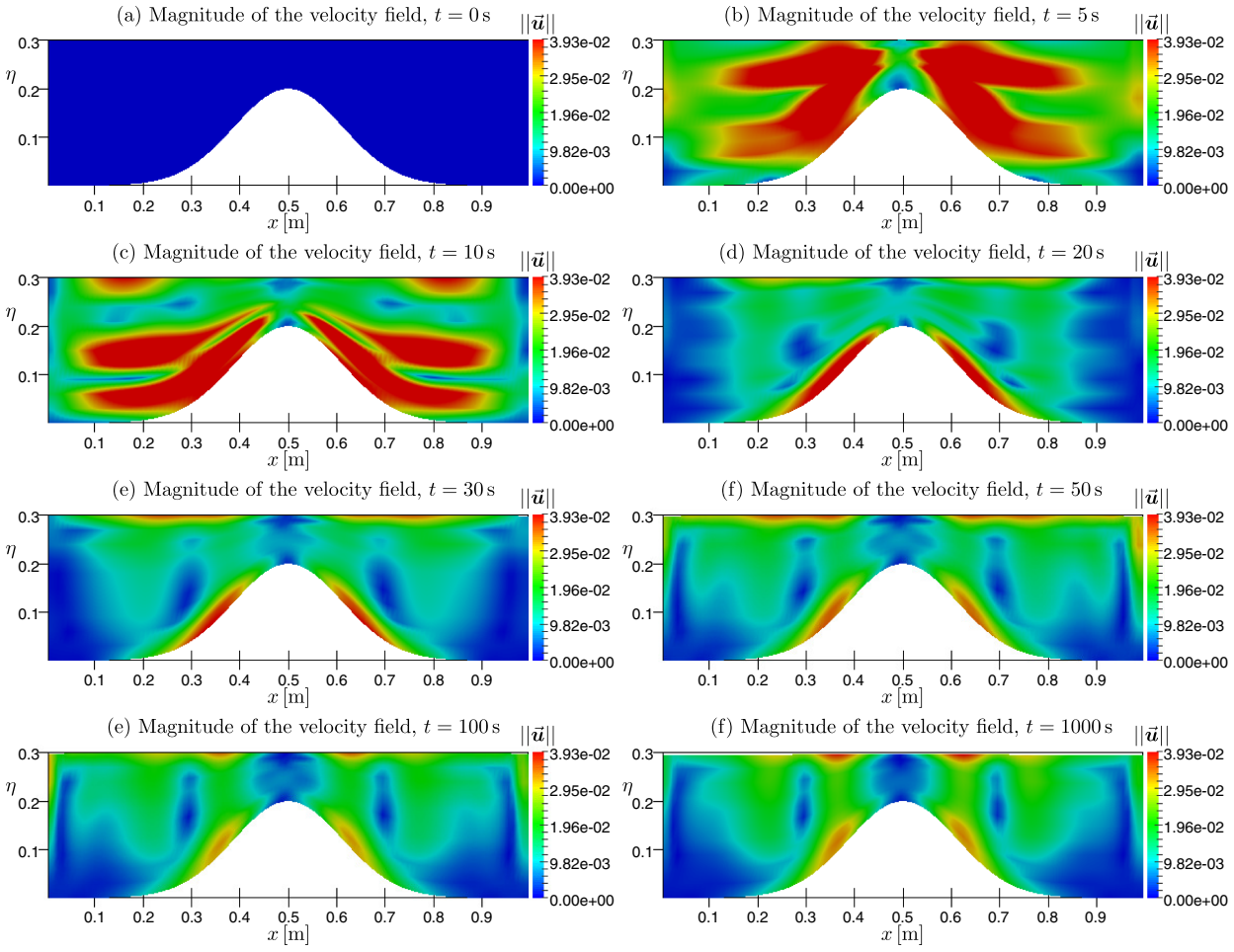

FIGURE 10. Test 3: Magnitude of the velocity field $\boldsymbol{u}$, $\eta(x) = z_{\mathrm{B}}(x) + h(x)$.

Finally in Table 1 we show the numerical error computed with (7.1) at time $t = 1\,\mathrm{s}$ using a reference solution with $C_{\mathrm{ref}} = 5120$. Only the error of some numerical solution are presented due to the big quantities of them. CPU times are also presented in Table 1, corresponding to a Laptop with Intel Core I5 (2.20 Ghz $\times$ 4) and 8GB of RAM.

7.5. Test 4: Sedimentation in a 3D domain

The last numerical test simulates a cylindrical dam break involving bidisperse sedimentation over a 3D paraboloid bottom given by

$$z(x,y) = \begin{cases} 0.71((x-0.5)^2 + (y-0.5)^2) & \text{for } (x-0.5)^2 + (y-0.5)^2 \le 0.21, \\ 0.15 & \text{otherwise,} \end{cases} \qquad (x,y) \in [0,1]^2. \tag{7.2}$$

The diameters of the solid particles are as in Test 2. Here we use a rectangular grid of 100×100 cells in the horizontal directions and $M = 10$ layers in the vertical direction. For all $\alpha = 1, \ldots, M$ the initial condition is

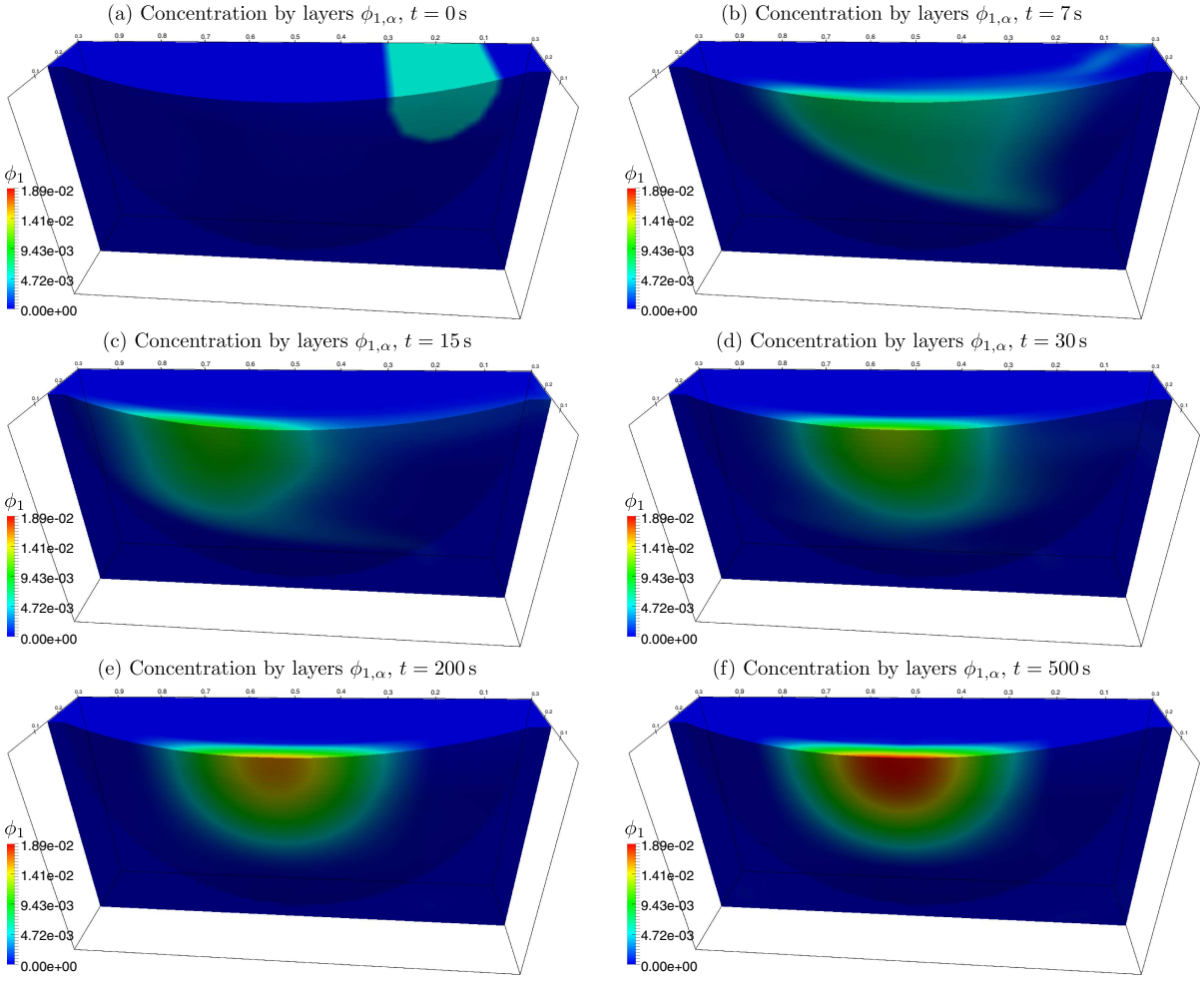

FIGURE 11. Test 4: Concentration of ϕ_1 by color in a 3D domain, $\eta(\boldsymbol{x}) = z_{\mathrm{B}}(\boldsymbol{x}) + h(\boldsymbol{x})\,\mathrm{m}$.

given by

$$\phi_{1,\alpha}(0,\boldsymbol{x}) = \begin{cases} 0.05 & \text{for } (x-0.2)^2 + (y-0.5)^2 \le 0.1, \\ 0 & \text{otherwise,} \end{cases} \qquad \boldsymbol{u}_\alpha(0,\boldsymbol{x}) = 0,$$

$$\phi_{2,\alpha}(0,\boldsymbol{x}) = \begin{cases} 0.025 & \text{for } (x-0.2)^2 + (y-0.5)^2 \le 0.1, \\ 0 & \text{otherwise,} \end{cases}$$

along with the height $h(t=0) = 0.3 - z_{\mathrm{B}}$. Figures 11 and 12 show the concentrations ϕ_1 of the big particles and ϕ_2 of the small particles, respectively, inside the fluid domain and as a vertical cut in the middle of the domain, all seen from below. We show the solution at times $t = 0, 7, 15, 30\,\mathrm{s}$ because at these times the movement of the mixture exhibits interesting features. At short times we can see how both species of particles oscillate from right to left and back until the particles lose velocity and settle. In Figure 11 we see that the bigger particles move faster than the small ones and Figures 12 and 14 illustrate how the small particles are carried to the right wall (from this point of view of the solution) due to the recirculation of the mixture produced. Due to the small size of the particles of species 2 (ϕ_2), the movement of the mixture moves these particles to point of the domain

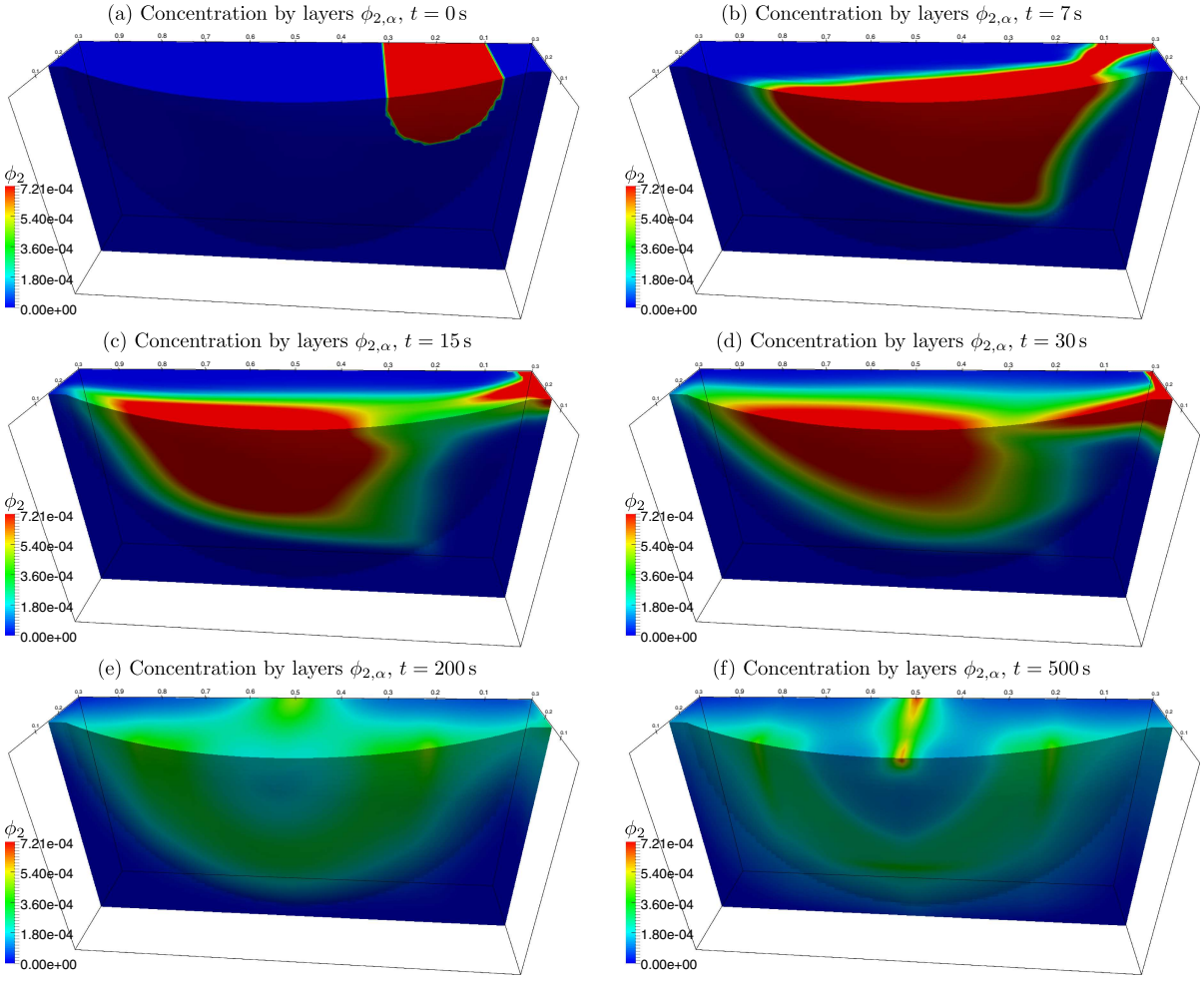

FIGURE 12. Test 4: Concentration of ϕ_2 by color in a 3D domain, $\eta(\boldsymbol{x}) = z_{\mathrm{B}}(\boldsymbol{x}) + h(\boldsymbol{x})$ m.

where the concentration of the big particles is small. (This phenomenon can be seen in Test 3.) At large times all particles settle and we observe a stratification of the sediment as illustrated in Test 1. In Figure 13 we show the total concentration $\phi_{\mathrm{T}} = \phi_1 + \phi_2$. Figure 14 displays the evolution of the velocity of the mixture. In Figure 14a (for $t = 1$s) two circulations can be observed, one at each side of the dam break. At the next instant we see how the velocity changes its direction in an oscillating manner. Finally, we remark that the velocity decreases in time; in Figure 14f (corresponding to $t = 50$s) it is already small. The computational time to compute the solution for $t = 500$s was four days and six hours. However, these times do not worry because this code can easily be parallelized to attain shorter CPU times.

8. Conclusions

We have formulated a multilayer shallow water model framework for polydispere sedimentation that can be used for simulations in industrial applications such as clarification tanks, wastewater treatment, and thickeners in the mining industry, but which is especially suitable for the description of natural geophysical process such as sediment transport and polydisperse sedimentation in rivers and estuaries. This model provides the velocity

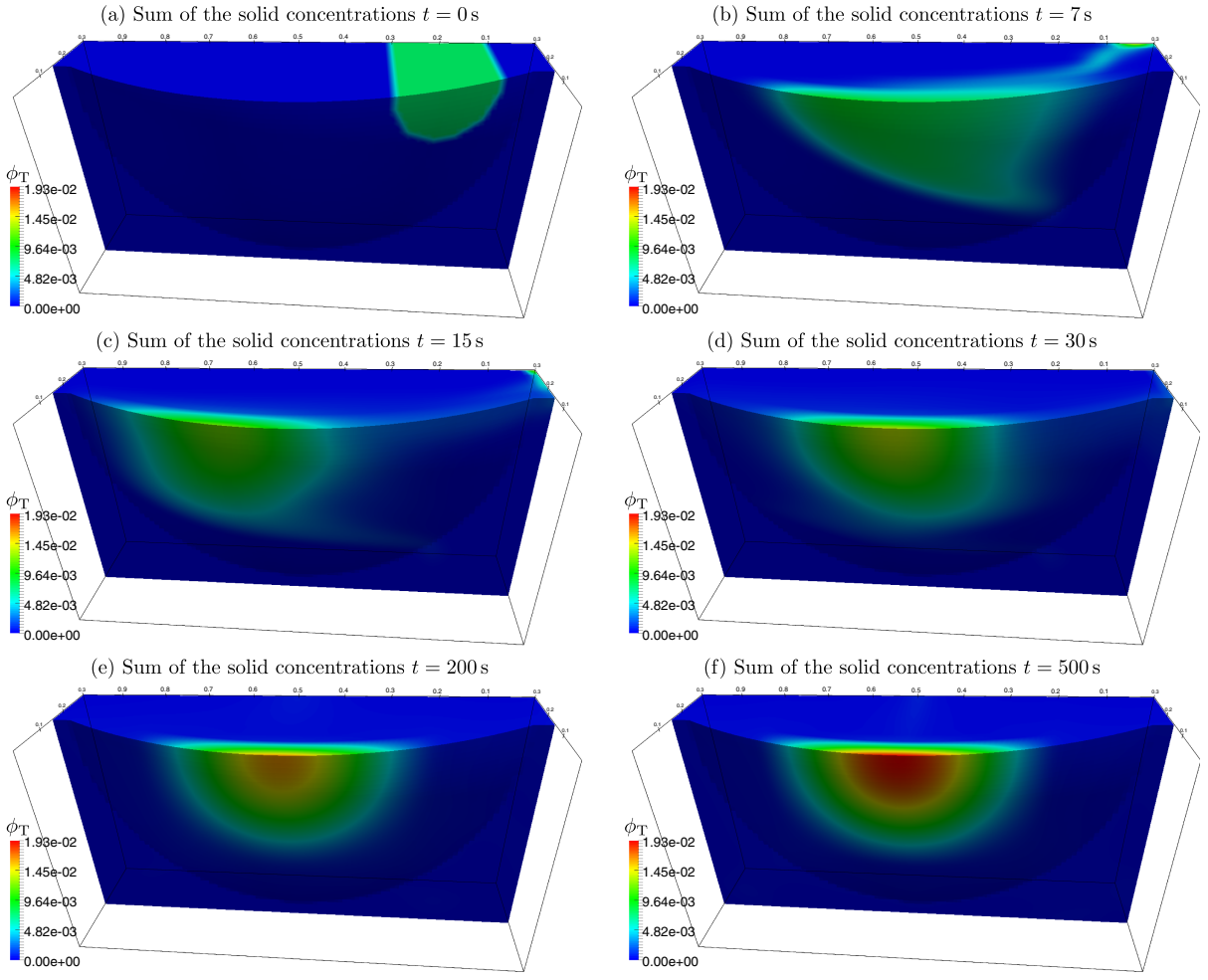

FIGURE 13. Test 4: Concentration by color by $\phi_\mathrm{T} = \phi_1 + \phi_2$, $\eta(\boldsymbol{x}) = z_\mathrm{B}(\boldsymbol{x}) + h(\boldsymbol{x})\,\mathrm{m}$.

field of the mixture, the concentrations of the each solid species, and the evolution of the free surface. We recall that the description of the movement of the mixture in terms of the mass-average velocity $\boldsymbol{v}$ has the advantage that the mass and linear momentum balance of the mixture is recovered. This contrasts with earlier treatments [8, 11, 28] that are based on the volume-average velocity that is divergence free, and therefore constant in one space dimension. The latter property is an advantage especially for the description of unit operations with controllable volume flow rates, but it does not allow for a straightforward derivation of the momentum balance of the mixture [11].

Clearly, the model framework outlined in Sections 2–4 is more general than the cases treated in the numerical tests. We are currently implementing an extension of the scheme to two horizontal space dimensions by including viscous and compression terms. These results will be presented in separate work. On the other hand, still within the reduced horizontally one-dimensional setting of the present work, there is interest in simulating further scenarios such as gravity currents akin to those studied in [9, 21, 30, 43].

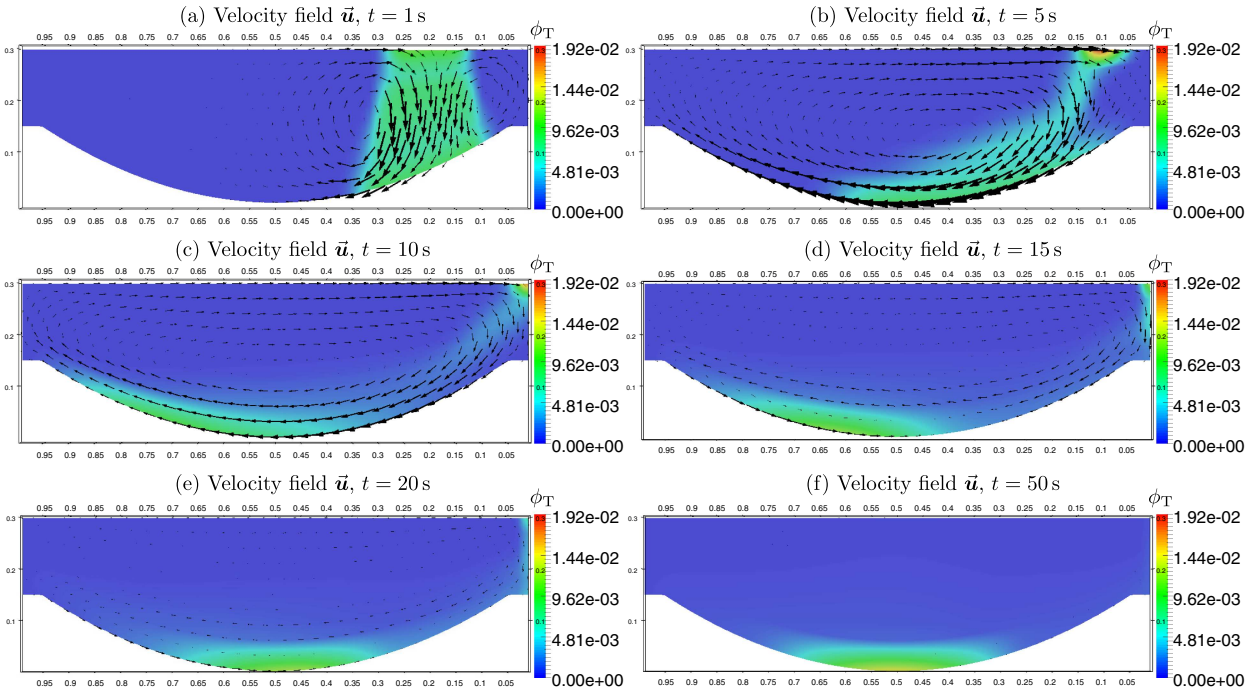

FIGURE 14. Test 4: Velocity field $\boldsymbol{u}$ over concentration $\phi_T = \phi_1 + \phi_2$, $\eta(\boldsymbol{x}) = z_B(\boldsymbol{x}) + h(\boldsymbol{x})$ m.

APPENDIX A. EXPLICIT FORMULA OF THE TOTAL INTERLAYER MASS FLUXES

For the case of a single density of all phases the definition of $G_{\alpha+1/2}$ can be easily deduced, as is shown in [4]. On the other hand, for a multilayer model with variable density proposed in [5] the computation of $G_{\alpha+1/2}$ is done numerically as the solution of a non-linear implicit system. In this subsection we show that although the model proposed in this paper can be seen as a multilayer model with variable density akin to that of [5], we can deduce an explicit definition of $G_{\alpha+1/2}$ in terms of the other unknowns of the problem. To this end, for a fixed layer α we consider the sums of the equations (5.3) from layer 1 to layer α and from layer $\alpha+1$ to layer M, respectively. This yields the equations

$$\sum_{\beta=1}^{\alpha} l_\beta(\partial_t m_\beta + \partial_x q_\beta) = G_{\alpha+1/2} - G_{1/2}, \qquad \sum_{\gamma=\alpha+1}^{M} l_\gamma(\partial_t m_\gamma + \partial_x q_\gamma) = G_{M+1/2} - G_{\alpha+1/2}.$$

By using (5.1) we can write m_α in terms of h and $r_{j,\alpha}$. Then the above equations can be rewritten as

$$L_\alpha \partial_t(\rho_0 h) + \sum_{\beta=1}^{\alpha}\sum_{j=1}^{N} l_\beta \partial_t r_{j,\beta}\frac{\rho_j - \rho_0}{\rho_j} + \sum_{\beta=1}^{\alpha} l_\beta \partial_x q_\beta = G_{\alpha+1/2} - G_{1/2}, \tag{A.1}$$

$$(1 - L_\alpha)\partial_t(\rho_0 h) + \sum_{\gamma=\alpha+1}^{M}\sum_{j=1}^{N} l_\gamma \partial_t r_{j,\gamma}\frac{\rho_j - \rho_0}{\rho_j} + \sum_{\gamma=\alpha+1}^{M} l_\gamma \partial_x q_\gamma = G_{M+1/2} - G_{\alpha+1/2}. \tag{A.2}$$

Now we can combine previous equations to eliminate the dependence on $\partial_t(\rho_0 h)$. We subtract equation (A.1) multiplied by $(1-L_\alpha)$ from equation (A.2) multiplied by L_α. As a result we obtain

$$\begin{aligned}&(1-L_\alpha)\sum_{\beta=1}^{\alpha}\sum_{j=1}^{N} l_\beta \partial_t r_{j,\beta}\frac{\rho_j-\rho_0}{\rho_j} - L_\alpha \sum_{\gamma=\alpha+1}^{M}\sum_{j=1}^{N} l_\gamma \partial_t r_{j,\gamma}\frac{\rho_j-\rho_0}{\rho_j}\\ &= G_{\alpha+1/2} - (1-L_\alpha)\sum_{\beta=1}^{\alpha} l_\beta \partial_x q_\beta + L_\alpha \sum_{\gamma=\alpha+1}^{M} l_\gamma \partial_x q_\gamma - (1-L_\alpha)G_{1/2} - L_\alpha G_{M+1/2}.\end{aligned}$$

Utilizing (5.4) to substitute $\partial_t r_{j,\beta}$ and $\partial_t r_{j,\gamma}$ in the previous equation we get

$$\begin{aligned}&\big(G_{\alpha+1/2} - (1-L_\alpha)G_{1/2} - L_\alpha G_{M+1/2}\big)\left(1 - \sum_{j=1}^{N}\frac{\rho_j-\rho_0}{\rho_j}\tilde{\phi}_{j,\alpha+1/2}\right)\\ &= (1-L_\alpha)\sum_{\beta=1}^{\alpha} l_\beta\left(\partial_x q_\beta - \sum_{j=1}^{N}\partial_x(r_{j,\beta}u_\beta)\frac{\rho_j-\rho_0}{\rho_j}\right) - L_\alpha\sum_{\gamma=\alpha+1}^{M} l_\gamma\left(\partial_x q_\gamma - \sum_{j=1}^{N}\partial_x(r_{j,\gamma}u_\gamma)\frac{\rho_j-\rho_0}{\rho_j}\right)\\ &\quad - \sum_{j=1}^{N}\big(\tilde{f}_{j,\alpha+1/2} - (1-L_\alpha)\tilde{f}_{j,1/2} - L_\alpha\tilde{f}_{j,M+1/2}\big)(\rho_j-\rho_0).\end{aligned}$$

Moreover, in view the definition of $\tilde{\phi}_{j,\alpha+1/2}$ given by (3.13) or (5.6), the number that multiplies $G_{\alpha+1/2}$ is always positive. In fact, we obtain

$$1 - \sum_{j=1}^{N}\frac{\rho_j-\rho_0}{\rho_j}\tilde{\phi}_{j,\alpha+1/2} = \frac{1}{2}\left(\frac{\rho_0}{\bar{\rho}_{\alpha+1}} + \frac{\rho_0}{\bar{\rho}_\alpha}\right) = \frac{\rho_0(\bar{\rho}_{\alpha+1}+\bar{\rho}_\alpha)}{2\bar{\rho}_\alpha\bar{\rho}_{\alpha+1}}. \tag{A.3}$$

Furthermore, we can use that

$$\sum_{j=0}^{N}\rho_j\tilde{f}_{j,\alpha+1/2} = 0 \Leftrightarrow \sum_{j=1}^{N}\rho_j\tilde{f}_{j,\alpha+1/2} = -\rho_0\tilde{f}_{0,\alpha+1/2}. \tag{A.4}$$

Introducing (A.3), (A.4), and the fact that $\tilde{f}_{j,1/2} = \tilde{f}_{j,M+1/2} = 0$, we get the equality

$$\begin{aligned}G_{\alpha+1/2} &= (1-L_\alpha)G_{1/2} + L_\alpha G_{M+1/2}\\ &\quad + \frac{2\bar{\rho}_\alpha\bar{\rho}_{\alpha+1}}{\rho_0(\bar{\rho}_{\alpha+1}+\bar{\rho}_\alpha)}\left((1-L_\alpha)\sum_{\beta=1}^{\alpha} l_\beta\left(\partial_x q_\beta - \sum_{j=1}^{N}\partial_x(r_{j,\beta}u_\beta)\frac{\rho_j-\rho_0}{\rho_j}\right)\right.\\ &\quad \left. - L_\alpha\sum_{\gamma=\alpha+1}^{M} l_\gamma\left(\partial_x q_\gamma - \sum_{j=1}^{N}\partial_x(r_{j,\gamma}u_\gamma)\frac{\rho_j-\rho_0}{\rho_j}\right) + \rho_0\sum_{j=0}^{N}\tilde{f}_{j,\alpha+1/2}\right).\end{aligned} \tag{A.5}$$

Appendix B. A bound of the characteristic velocities

In order to find a bound of the characteristic velocities of the proposed multilayer model (5.3)–(5.5), we rewrite the model in the form $\partial_t\tilde{\boldsymbol{w}} + \boldsymbol{\mathcal{A}}(\tilde{\boldsymbol{w}})\partial_x\tilde{\boldsymbol{w}} = \boldsymbol{b}$ with

$$\tilde{\boldsymbol{w}} = (m_1,\dots,m_M,,q_1,\dots,q_M,r_{1,1},\dots,r_{N,1},\dots,r_{1,M},\dots,r_{N,M})^{\mathrm{T}}.$$

An explicit bound of the minimum and maximum eigenvalues of $\boldsymbol{\mathcal{A}}$ in dependence of the all horizontal velocities and all densities by layer is provided in the following theorem.

Theorem B.1. *If λ_k for $k = 1, \dots, 2M + NM$ denote the eigenvalues of $\boldsymbol{\mathcal{A}}$ and these are real, then*

$$\bar{u} - \Psi \leq \lambda_k \leq \bar{u} + \Psi \quad \text{for all } k = 1, \dots, 2M + NM, \tag{B.1}$$

where

$$\bar{u} := \frac{1}{M} \sum_{\beta=1}^{M} u_\beta,$$

M is the number of the layers, N is the number of solid particle species and the quantity Ψ is defined as

$$\Psi := \sqrt{\frac{2M-1}{2M}} \left(2 \sum_{i=1}^{M} (\bar{u} - u_i)^2 + gh\rho_0^{-1} \left(\rho_0 + \frac{1}{M} \sum_{\beta=1}^{M} (2\beta - 1)\bar{\rho}_\beta \right) \right)^{1/2}.$$

Since $\sqrt{(2M-1)/(2M)} \leq 1$, another bound can be defined by considering only the second factor of ψ. To prove Theorem B.1 it is sufficient to apply the result presented in [36] to the characteristic polynomial of matrix $\boldsymbol{\mathcal{A}}$. This result states that if all the roots x of a polynomial of degree n, that is, solutions x of

$$a_n x^n + a_{n-1} x^{n-1} + \ldots + a_0 = 0,$$

are real, then they lie in the range bounded by

$$-\frac{a_{n-1}}{n a_n} \pm (n-1) \left(\frac{a_{n-1}^2}{n^2 a_n^2} - \frac{2a_{n-2}}{n(n-1)a_n} \right)^{1/2}.$$

Appendix C. A particular weak solution with hydrostatic pressure: deduction of equations

We detail here the calculations needed to obtain the system (4.7), starting with the equations of mass conservation. We choose a scalar test function $\varphi = \varphi(t, \boldsymbol{x})$ that is independent of z. Then, in general for a weak solution $\boldsymbol{v}_j$ the mass conservation equation (2.22) yields for all $\alpha = 0, \dots, M$ and $j = 0, 1, \dots, N$:

$$\begin{aligned}
0 &= \int_{\Omega_\alpha(t)} (\partial_t(\rho_j \phi_j) + \nabla_{\boldsymbol{x}} \cdot (\rho_j \phi_j \boldsymbol{v}_j)) \varphi \, \mathrm{d}\Omega \\
&= \int_{I_{\mathrm{F}}(t)} \varphi(t, \boldsymbol{x}) \left(\int_{z_{\alpha-1/2}}^{z_{\alpha+1/2}} \left(\partial_t(\rho_j \phi_j) + \nabla_{\boldsymbol{x}} \cdot (\rho_j \phi_j \boldsymbol{u}) + \partial_z(\rho_j \phi_j w_j) \right) \mathrm{d}z \right) \mathrm{d}\boldsymbol{x} \\
&= \int_{I_{\mathrm{F}}(t)} \varphi(t, \boldsymbol{x}) \left(\partial_t \left(\int_{z_{\alpha-1/2}}^{z_{\alpha+1/2}} \rho_j \phi_j \, \mathrm{d}z \right) + \nabla_{\boldsymbol{x}} \cdot \left(\int_{z_{\alpha-1/2}}^{z_{\alpha+1/2}} (\rho_j \phi_j \boldsymbol{u}) \, \mathrm{d}z \right) - \rho_j \phi_{j,\alpha} \partial_t z_{\alpha+1/2} \right. \\
&\quad - \rho_j \phi_{j,\alpha} \boldsymbol{u}^-_{\alpha+1/2} \cdot \nabla_{\boldsymbol{x}} z_{\alpha+1/2} + \rho_j \phi_{j,\alpha} w^-_{j,\alpha+1/2} + \rho_j \phi_{j,\alpha} \partial_t z_{\alpha-1/2} \\
&\quad \left. + \rho_j \phi_{j,\alpha} \boldsymbol{u}^+_{\alpha-1/2} \cdot \nabla_{\boldsymbol{x}} z_{\alpha-1/2} - \rho_j \phi_{j,\alpha} w^+_{j,\alpha-1/2} \right) \mathrm{d}\boldsymbol{x}.
\end{aligned}$$

Moreover, noticing that $\partial_t h_\alpha = \partial_t z_{\alpha+1/2} - \partial_t z_{\alpha-1/2}$, we obtain that for all $\varphi(t, .) \in L^2(I_{\mathrm{F}}(t))$,

$$\begin{aligned}
0 = \int_{I_{\mathrm{F}}(t)} \varphi(t, \boldsymbol{x}) \big(&\partial_t(\rho_j \phi_{j,\alpha} h_\alpha) + \nabla_{\boldsymbol{x}} \cdot (\rho_j \phi_{j,\alpha} h_\alpha \, \boldsymbol{u}_\alpha) - \rho_j \phi_{j,\alpha} \partial_t z_{\alpha+1/2} - \rho_j \phi_{j,\alpha} \boldsymbol{u}^-_{\alpha+1/2} \cdot \nabla_{\boldsymbol{x}} z_{\alpha+1/2} \\
&+ \rho_j \phi_{j,\alpha} w^-_{j,\alpha+1/2} + \rho_j \phi_{j,\alpha} \partial_t z_{\alpha-1/2} + \rho_j \phi_{j,\alpha} \boldsymbol{u}^+_{\alpha-1/2} \cdot \nabla_{\boldsymbol{x}} z_{\alpha-1/2} - \rho_j \phi_{j,\alpha} w^+_{j,\alpha-1/2} \big) \, \mathrm{d}\boldsymbol{x}.
\end{aligned} \tag{C.1}$$

Introducing $\boldsymbol{u}_\alpha$ with assumptions (3.5) in the equation (C.1), and taking into account (3.8) and (3.9), we obtain the mass conservation laws (4.4):

$$\partial_t(\rho_j\phi_{j,\alpha}h_\alpha) + \nabla_{\boldsymbol{x}}\cdot(\rho_j\phi_{j,\alpha}h_\alpha\boldsymbol{u}_\alpha) = G_{j,\alpha+1/2} - G_{j,\alpha-1/2}. \tag{C.2}$$

As for the momentum balance equations, we consider test functions $\boldsymbol{\vartheta}\in H^1(\Omega_\alpha)$ that satisfy (4.3). The weak formulation (4.2) follows taking into account the structure of $\boldsymbol{v}$, integrating (2.24) with respect to the variable z and identifying each of the two components of the vector test functions. However, due to the hydrostatic pressure framework the equations that correspond to the vertical component can be omitted. This is equivalent to identifying the weak formulation for test functions in the form $(\boldsymbol{\vartheta}_\mathrm{h},0)^\mathrm{T}$, with $\boldsymbol{\vartheta}_\mathrm{h}=\boldsymbol{\vartheta}_\mathrm{h}(t,\boldsymbol{x})$ independently of z, with $\boldsymbol{\vartheta}_\mathrm{h}|_{\partial I_\mathrm{F}}=0$. Then, from (4.2) and using these test functions, we obtain for the horizontal momentum conservation equation

$$\begin{aligned}
&\int_{\Omega_\alpha(t)}\left(\sum_{j=0}^N\rho_j\partial_t(\phi_{j,\alpha}\boldsymbol{u}_\alpha)\cdot\boldsymbol{\vartheta}_\mathrm{h}\right)\mathrm{d}\Omega+\int_{\Omega_\alpha(t)}\left(\sum_{j=0}^N\rho_j\nabla_{\boldsymbol{x}}\cdot\left(\phi_{j,\alpha}\boldsymbol{u}_\alpha\otimes\boldsymbol{u}_\alpha\right)\cdot\boldsymbol{\vartheta}_\mathrm{h}\right)\mathrm{d}\Omega\\
&\quad+\int_{\Omega_\alpha(t)}\left(\sum_{j=0}^N\rho_j\partial_z(\phi_{j,\alpha}w_{j,\alpha}\boldsymbol{u}_\alpha)\cdot\boldsymbol{\vartheta}_\mathrm{h}\right)\mathrm{d}\Omega+\int_{\Omega_\alpha(t)}\boldsymbol{T}^\mathrm{E}_{\mathrm{h},\alpha}:\nabla_{\boldsymbol{x}}\boldsymbol{\vartheta}\,\mathrm{d}\Omega-\int_{\Omega_\alpha(t)}p_\alpha\nabla_{\boldsymbol{x}}\cdot\boldsymbol{\vartheta}_\mathrm{h}\,\mathrm{d}\Omega\\
&\quad+\int_{\Gamma_{\alpha+1/2}(t)}\left(\boldsymbol{T}^-_{\alpha+1/2}(\boldsymbol{\vartheta}_\mathrm{h},0)^\mathrm{T}\right)\cdot\boldsymbol{\eta}_{\alpha+1/2}\,\mathrm{d}\Gamma-\int_{\Gamma_{\alpha-1/2}(t)}\left(\boldsymbol{T}^+_{\alpha-1/2}(\boldsymbol{\vartheta}_\mathrm{h},0)^\mathrm{T}\right)\cdot\boldsymbol{\eta}_{\alpha-1/2}\,\mathrm{d}\Gamma=0
\end{aligned}\tag{C.3}$$

for all $\alpha=1,\dots,M$, where $\boldsymbol{T}^\mathrm{E}_{\mathrm{h},\alpha}=\boldsymbol{T}^\mathrm{E}_\mathrm{h}(\boldsymbol{v}_\alpha)$. Taking into account the definition of $\Omega_\alpha(t)$ in Section 3.1 and the assumption on the independence of z of $\boldsymbol{u}_\alpha$ and $\boldsymbol{\vartheta}_\mathrm{h}$ and writing (C.3) as $\mathcal{I}_1+\cdots+\mathcal{I}_7=0$, where $\mathcal{I}_1,\dots,\mathcal{I}_7$ stand for each of the signed integrals in the left-hand side of (C.3), we obtain

$$\begin{aligned}
\mathcal{I}_1&=\int_{I_\mathrm{F}}\left(\int_{z_{\alpha-1/2}}^{z_{\alpha+1/2}}\partial_t\left(\rho(\Phi_\alpha)\boldsymbol{u}_\alpha\right)\cdot\boldsymbol{\vartheta}_\mathrm{h}\,\mathrm{d}\boldsymbol{x}\right)\mathrm{d}z=\int_{I_\mathrm{F}}h_\alpha\partial_t(\rho(\Phi_\alpha)\boldsymbol{u}_\alpha)\cdot\boldsymbol{\vartheta}_\mathrm{h}\,\mathrm{d}\boldsymbol{x},\\
\mathcal{I}_2&=\int_{I_\mathrm{F}}h_\alpha\nabla_{\boldsymbol{x}}\cdot\left(\rho(\Phi_\alpha)\boldsymbol{u}_\alpha\otimes\boldsymbol{u}_\alpha\right)\cdot\boldsymbol{\vartheta}_\mathrm{h}\,\mathrm{d}\boldsymbol{x},\\
\mathcal{I}_3&=\sum_{j=0}^N\int_{I_\mathrm{F}}\int_{z_{\alpha-1/2}}^{z_{\alpha+1/2}}\rho_j\partial_z(\phi_{j,\alpha}w_{j,\alpha}\boldsymbol{u}_\alpha)\cdot\boldsymbol{\vartheta}_\mathrm{h}\,\mathrm{d}z\,\mathrm{d}\boldsymbol{x}=\sum_{j=0}^N\int_{I_\mathrm{F}}\rho_j\phi_{j,\alpha}\left(w^-_{j,\alpha+1/2}-w^+_{j,\alpha-1/2}\right)\boldsymbol{u}_\alpha\cdot\boldsymbol{\vartheta}_\mathrm{h}\,\mathrm{d}\boldsymbol{x},\\
\mathcal{I}_4&=\int_{I_\mathrm{F}}\left(\int_{z_{\alpha-1/2}}^{z_{\alpha+1/2}}\boldsymbol{T}^\mathrm{E}_{\mathrm{h},\alpha}:\nabla_{\boldsymbol{x}}\boldsymbol{\vartheta}_\mathrm{h}\,\mathrm{d}z\right)\mathrm{d}\boldsymbol{x}=\int_{I_\mathrm{F}}h_\alpha\boldsymbol{T}^\mathrm{E}_{\mathrm{h},\alpha}:\nabla_{\boldsymbol{x}}\boldsymbol{\vartheta}_\mathrm{h}\,\mathrm{d}\boldsymbol{x}=-\int_{I_\mathrm{F}}\nabla_{\boldsymbol{x}}\cdot(h_\alpha\boldsymbol{T}^\mathrm{E}_{\mathrm{h},\alpha})\cdot\boldsymbol{\vartheta}_\mathrm{h}\,\mathrm{d}\boldsymbol{x},\\
\mathcal{I}_5&=-\int_{I_\mathrm{F}}\left(\int_{z_{\alpha-1/2}}^{z_{\alpha+1/2}}p_\alpha\,\mathrm{d}z\right)\nabla\cdot\boldsymbol{\vartheta}_\mathrm{h}\,\mathrm{d}\boldsymbol{x}=\int_{I_\mathrm{F}}\boldsymbol{\vartheta}_\mathrm{h}\cdot\nabla_{\boldsymbol{x}}\left(\int_{z_{\alpha-1/2}}^{z_{\alpha+1/2}}p_\alpha\,\mathrm{d}z\right)\mathrm{d}\boldsymbol{x}\\
&=\int_{I_\mathrm{F}}\boldsymbol{\vartheta}_\mathrm{h}\cdot\left(\int_{z_{\alpha-1/2}}^{z_{\alpha+1/2}}\nabla_{\boldsymbol{x}}p_\alpha\,\mathrm{d}z+p_{\alpha+1/2}\nabla_{\boldsymbol{x}}z_{\alpha+1/2}-p_{\alpha-1/2}\nabla_{\boldsymbol{x}}z_{\alpha-1/2}\right)\mathrm{d}\boldsymbol{x}\\
&=\int_{I_\mathrm{F}}\boldsymbol{\vartheta}_\mathrm{h}\cdot\left(\int_{z_{\alpha-1/2}}^{z_{\alpha+1/2}}\nabla_{\boldsymbol{x}}p_\alpha\,\mathrm{d}z\right)\mathrm{d}\boldsymbol{x}+\int_{I_\mathrm{F}}p_{\alpha+1/2}(\boldsymbol{\vartheta}_\mathrm{h},0)^\mathrm{T}\cdot\boldsymbol{\eta}_{\alpha+1/2}\sqrt{1+|\nabla_{\boldsymbol{x}}z_{\alpha+1/2}|^2}\,\mathrm{d}\boldsymbol{x}\\
&\quad-\int_{I_\mathrm{F}}p_{\alpha-1/2}(\boldsymbol{\vartheta}_\mathrm{h},0)^\mathrm{T}\cdot\boldsymbol{\eta}_{\alpha-1/2}\sqrt{1+|\nabla_{\boldsymbol{x}}z_{\alpha-1/2}|^2}\,\mathrm{d}\boldsymbol{x}=:\mathcal{I}_{5\mathrm{a}}+\mathcal{I}_{5\mathrm{b}}+\mathcal{I}_{5\mathrm{c}},\\
\mathcal{I}_6&=\int_{I_\mathrm{F}}\left(\boldsymbol{T}^-_{\alpha+1/2}(\boldsymbol{\vartheta}_\mathrm{h},0)^\mathrm{T}\right)\cdot\boldsymbol{\eta}_{\alpha+1/2}\sqrt{1+|\nabla_{\boldsymbol{x}}z_{\alpha+1/2}|^2}\,\mathrm{d}\boldsymbol{x},
\end{aligned}$$

and where $\mathcal{I}_7$ is handled analogously to $\mathcal{I}_6$. Moreover, by (3.17), we can simplify

$$\mathcal{I}_6+\mathcal{I}_{5\mathrm{b}}=\int_{I_{\mathrm{F}}}\big(\boldsymbol{T}^{\mathrm{E},-}_{\alpha+1/2}(\boldsymbol{\vartheta}_{\mathrm{h}},0)^{\mathrm{T}}\big)\cdot(\nabla_{\boldsymbol{x}}z_{\alpha+1/2},-1)^{\mathrm{T}}\mathrm{d}\boldsymbol{x}=\int_{I_{\mathrm{F}}}\big(\boldsymbol{T}^{\mathrm{E},-}_{\mathrm{h},\alpha+1/2}(\nabla_{\boldsymbol{x}}z_{\alpha+1/2})^{\mathrm{T}}-\boldsymbol{T}^{\mathrm{E},-}_{\boldsymbol{x}z,\alpha+1/2}\big)\cdot\boldsymbol{\vartheta}_{\mathrm{h}}\,\mathrm{d}\boldsymbol{x}.$$

Furthermore, since $\boldsymbol{T}^{\mathrm{E},-}_{\alpha+1/2}$ is a symmetric matrix, we have that

$$\big(\boldsymbol{T}^{\mathrm{E},-}_{\alpha+1/2}(\boldsymbol{\vartheta}_{\mathrm{h}},0)^{\mathrm{T}}\big)\cdot(\nabla_{\boldsymbol{x}}z_{\alpha+1/2},-1)^{\mathrm{T}}=\big(\boldsymbol{T}^{\mathrm{E},-}_{\alpha+1/2}(\nabla_{\boldsymbol{x}}z_{\alpha+1/2},-1)^{\mathrm{T}}\big)\cdot\big(\boldsymbol{\vartheta}_{\mathrm{h}},0\big)^{\mathrm{T}}.$$

The sum $\mathcal{I}_7+\mathcal{I}_{5\mathrm{c}}$ can be simplified in a similar way. Then the weak formulation (C.3), corresponding to the horizontal momentum equation for this set of test functions, can be written as follows:

$$\begin{aligned}\int_{I_{\mathrm{F}}}\boldsymbol{\vartheta}_{\mathrm{h}}\cdot\Bigg(&h_\alpha\partial_t(\rho(\Phi_\alpha)\boldsymbol{u}_\alpha)+h_\alpha\nabla_{\boldsymbol{x}}\cdot\big(\rho(\Phi_\alpha)\boldsymbol{u}_\alpha\otimes\boldsymbol{u}_\alpha\big)+\sum_{j=0}^{N}\rho_j\phi_{j,\alpha}(w^-_{j,\alpha+1/2}-w^+_{j,\alpha-1/2})\boldsymbol{u}_\alpha\\&+\int_{z_{\alpha-1/2}}^{z_{\alpha+1/2}}\nabla_{\boldsymbol{x}}p_\alpha\,\mathrm{d}z-\nabla_{\boldsymbol{x}}\cdot\big(h_\alpha\boldsymbol{T}^{\mathrm{E}}_{\mathrm{h}}\big)+\big(\boldsymbol{T}^{\mathrm{E},-}_{\mathrm{h},\alpha+1/2}(\nabla_{\boldsymbol{x}}z_{\alpha+1/2})^{\mathrm{T}}-\boldsymbol{T}^{\mathrm{E},-}_{\boldsymbol{x}z,\alpha+1/2}\big)\\&-\big(\boldsymbol{T}^{\mathrm{E},+}_{\mathrm{h},\alpha-1/2}(\nabla_{\boldsymbol{x}}z_{\alpha-1/2})^{\mathrm{T}}-\boldsymbol{T}^{\mathrm{E},+}_{\boldsymbol{x}z,\alpha-1/2}\big)\Bigg)\mathrm{d}\boldsymbol{x}=0,\qquad\forall\,\boldsymbol{\vartheta}_{\mathrm{h}}.\end{aligned}\tag{C.4}$$

Taking into account (3.20) we deduce

$$\begin{aligned}&h_\alpha\partial_t\big(\rho(\Phi_\alpha)\boldsymbol{u}_\alpha\big)+h_\alpha\nabla_{\boldsymbol{x}}\cdot\big(\rho(\Phi_\alpha)\boldsymbol{u}_\alpha\otimes\boldsymbol{u}_\alpha\big)+\sum_{j=0}^{N}\rho_j\phi_{j,\alpha}\big(w^-_{j,\alpha+1/2}-w^+_{j,\alpha-1/2}\big)\boldsymbol{u}_\alpha+\int_{z_{\alpha-1/2}}^{z_{\alpha+1/2}}\nabla_{\boldsymbol{x}}p_\alpha\,\mathrm{d}z\\&\quad-\nabla_{\boldsymbol{x}}\cdot\big(h_\alpha\boldsymbol{T}^{\mathrm{E}}_{\mathrm{h}}\big)+\big(\tilde{\boldsymbol{T}}^{\mathrm{E}}_{\mathrm{h},\alpha+1/2}(\nabla_{\boldsymbol{x}}z_{\alpha+1/2})^{\mathrm{T}}-\tilde{\boldsymbol{T}}^{\mathrm{E}}_{\boldsymbol{x}z,\alpha+1/2}\big)-\big(\tilde{\boldsymbol{T}}^{\mathrm{E}}_{\mathrm{h},\alpha-1/2}(\nabla_{\boldsymbol{x}}z_{\alpha-1/2})^{\mathrm{T}}-\tilde{\boldsymbol{T}}^{\mathrm{E}}_{\boldsymbol{x}z,\alpha-1/2}\big)\\&=\frac{G_{\alpha+1/2}}{2}(\boldsymbol{u}_{\alpha+1}-\boldsymbol{u}_\alpha)+\frac{G_{\alpha-1/2}}{2}(\boldsymbol{u}_\alpha-\boldsymbol{u}_{\alpha-1}).\end{aligned}\tag{C.5}$$

Using (3.22) evaluated at $z=z_{\alpha+1/2}$ and multiplied by $\boldsymbol{u}_\alpha$, we may write (C.5) in the form

$$\begin{aligned}&h_\alpha\rho(\Phi_\alpha)\partial_t\boldsymbol{u}_\alpha+h_\alpha\rho(\Phi_\alpha)\boldsymbol{u}_\alpha\cdot\nabla_{\boldsymbol{x}}\boldsymbol{u}_\alpha+\int_{z_{\alpha-1/2}}^{z_{\alpha+1/2}}\nabla_{\boldsymbol{x}}p_\alpha\,\mathrm{d}z-\nabla_{\boldsymbol{x}}\cdot\big(h_\alpha\boldsymbol{T}^{\mathrm{E}}_{\mathrm{h}}\big)\\&\quad+\big(\tilde{\boldsymbol{T}}^{\mathrm{E}}_{\mathrm{h},\alpha+1/2}(\nabla_{\boldsymbol{x}}z_{\alpha+1/2})^{\mathrm{T}}-\tilde{\boldsymbol{T}}^{\mathrm{E}}_{\boldsymbol{x}z,\alpha+1/2}\big)-\big(\tilde{\boldsymbol{T}}^{\mathrm{E}}_{\mathrm{h},\alpha-1/2}(\nabla_{\boldsymbol{x}}z_{\alpha-1/2})^{\mathrm{T}}-\tilde{\boldsymbol{T}}^{\mathrm{E}}_{\boldsymbol{x}z,\alpha-1/2}\big)\\&=\frac{G_{\alpha+1/2}}{2}(\boldsymbol{u}_{\alpha+1}-\boldsymbol{u}_\alpha)+\frac{G_{\alpha-1/2}}{2}(\boldsymbol{u}_\alpha-\boldsymbol{u}_{\alpha-1}).\end{aligned}\tag{C.6}$$

On the other hand, combining the equation (C.6) with (4.5) multiplied by $\boldsymbol{u}_\alpha$, we obtain the evolution equation for the momentum (4.6):

$$\begin{aligned}&\partial_t\big(\rho(\Phi_\alpha)h_\alpha\boldsymbol{u}_\alpha\big)+\nabla_{\boldsymbol{x}}\cdot\big(h_\alpha\rho(\Phi_\alpha)\boldsymbol{u}_\alpha\otimes\boldsymbol{u}_\alpha\big)+\int_{z_{\alpha-1/2}}^{z_{\alpha+1/2}}\nabla_{\boldsymbol{x}}p_\alpha\,\mathrm{d}z-\nabla_{\boldsymbol{x}}\cdot\big(h_\alpha\boldsymbol{T}^{\mathrm{E}}_{\mathrm{h}}\big)\\&+\big(\tilde{\boldsymbol{T}}^{\mathrm{E}}_{\mathrm{h},\alpha+1/2}(\nabla_{\boldsymbol{x}}z_{\alpha+1/2})^{\mathrm{T}}-\tilde{\boldsymbol{T}}^{\mathrm{E}}_{\boldsymbol{x}z,\alpha+1/2}\big)-\big(\tilde{\boldsymbol{T}}^{\mathrm{E}}_{\mathrm{h},\alpha-1/2}(\nabla_{\boldsymbol{x}}z_{\alpha-1/2})^{\mathrm{T}}-\tilde{\boldsymbol{T}}^{\mathrm{E}}_{\boldsymbol{x}z,\alpha-1/2}\big)\\&=\frac{G_{\alpha+1/2}}{2}(\boldsymbol{u}_{\alpha+1}+\boldsymbol{u}_\alpha)-\frac{G_{\alpha-1/2}}{2}(\boldsymbol{u}_\alpha+\boldsymbol{u}_{\alpha-1}),\end{aligned}\tag{C.7}$$

where, by (4.1), we obtain

$$\begin{aligned}\int_{z_{\alpha-1/2}}^{z_{\alpha+1/2}}\nabla_{\boldsymbol{x}}p_\alpha\,\mathrm{d}z&=h_\alpha\Bigg(\nabla_{\boldsymbol{x}}\Bigg(p_{\mathrm{S}}+g\sum_{\beta=\alpha+1}^{M}\rho(\Phi_\beta)h_\beta+g\rho(\Phi_\alpha)\frac{h_\alpha}{2}\Bigg)+g\rho(\Phi_\alpha)\nabla_{\boldsymbol{x}}\Bigg(z_b+\sum_{\beta=1}^{\alpha-1}h_b+\frac{h_\alpha}{2}\Bigg)\Bigg)\\&=h_\alpha\big(\nabla_{\boldsymbol{x}}\overline{p}_\alpha+g\rho(\Phi_\alpha)\nabla_{\boldsymbol{x}}\bar{z}_\alpha\big).\end{aligned}\tag{C.8}$$

Finally, introducing (C.8) in equation (C.7) and adding the equations (C.2) we obtain the system (4.7).

Appendix D. Miscellaneous technical results

D.1. Proof of 5.1

To see demonstrate that the second equality of (5.1) is correct, we recall that $1-\phi_0 = \phi = \phi_1 + \cdots + \phi_N$ (see Sect. 2.2). In other words, the total volumetric fraction satisfies $\phi_0 + \phi_1 + \cdots + \phi_N = 1$. Then we have

$$\begin{aligned} m_\alpha = \bar{\rho}_\alpha h &= \sum_{j=0}^{N} \rho_j \phi_{j,\alpha} h = \rho_0 \phi_{0,\alpha} h + \sum_{j=1}^{N} r_{j,\alpha} = \rho_0 h \left(1 - \sum_{j=1}^{N} \phi_{j,\alpha}\right) + \sum_{j=1}^{N} r_{j,\alpha} \\ &= \rho_0 h - \sum_{j=1}^{N} \rho_0 \phi_{j,\alpha} h + \sum_{j=1}^{N} r_{j,\alpha} = \rho_0 h - \sum_{j=1}^{N} \rho_0 \frac{\rho_j}{\rho_j} \phi_{j,\alpha} h + \sum_{j=1}^{N} \frac{\rho_j}{\rho_j} r_{j,\alpha} \\ &= \rho_0 h - \sum_{j=1}^{N} \frac{\rho_0}{\rho_j} r_{j,\alpha} + \sum_{j=1}^{N} \frac{\rho_j}{\rho_j} r_{j,\alpha} = \rho_0 h + \sum_{j=1}^{N} \frac{\rho_j - \rho_0}{\rho_j} r_{j,\alpha}. \end{aligned}$$

D.2. Proof of 3.15

The momentum jump condition (3.3) is given by

$$\begin{aligned} 0 &= \left[\!\!\left[\left(\sum_{j=0}^{N} \rho_j \phi_j \boldsymbol{v}_j ; \sum_{j=0}^{N} \rho_j \phi_j \boldsymbol{v}_j \otimes \boldsymbol{v}_j - \boldsymbol{T} \right) \right]\!\!\right]_{t,\alpha+1/2} \cdot \boldsymbol{n}_{t,\alpha+1/2} \\ &= \left[\!\!\left[\left(\sum_{j=0}^{N} \rho_j \phi_j \boldsymbol{v}_j ; \sum_{j=0}^{N} \rho_j \phi_j \boldsymbol{v}_j \otimes \boldsymbol{v}_j - \boldsymbol{T} \right) \right]\!\!\right]_{t,\alpha+1/2} \cdot \left(\partial_t z_{\alpha+1/2}, \nabla_{\boldsymbol{x}} z_{\alpha+1/2}, -1\right)^{\mathrm{T}} \\ &= \sum_{j=0}^{N} \left[\!\left[\left(\rho_j \phi_j \boldsymbol{v}_j ; \rho_j \phi_j \boldsymbol{v}_j \otimes \boldsymbol{v}_j\right) \right]\!\right]_{t,\alpha+1/2} \cdot \left(\partial_t z_{\alpha+1/2}, \nabla_{\boldsymbol{x}} z_{\alpha+1/2}, -1\right)^{\mathrm{T}} - \left[\!\left[\boldsymbol{T} \right]\!\right]_{t,\alpha+1/2} \cdot \left(\nabla_{\boldsymbol{x}} z_{\alpha+1/2}, -1\right)^{\mathrm{T}}. \end{aligned}$$

Finally we get

$$\left[\!\left[\boldsymbol{T} \right]\!\right]_{t,\alpha+1/2} \cdot \left(\nabla_{\boldsymbol{x}} z_{\alpha+1/2}, -1\right)^{\mathrm{T}} = \sum_{j=0}^{N} \left[\!\left[\left(\rho_j \phi_j \boldsymbol{v}_j ; \rho_j \phi_j \boldsymbol{v}_j \otimes \boldsymbol{v}_j\right) \right]\!\right]_{t,\alpha+1/2} \cdot \left(\partial_t z_{\alpha+1/2}, \nabla_{\boldsymbol{x}} z_{\alpha+1/2}, -1\right)^{\mathrm{T}}.$$

Remark: The object inside of the jump operator is a matrix of order 3×4, $\rho_j \phi_j \boldsymbol{v}_j$ is a column of size 3 and $\rho_j \phi_j \boldsymbol{v}_j \otimes \boldsymbol{v}_j$ is a matrix of order 3×3.

Acknowledgements. RB is supported by Fondecyt project 1170473; CRHIAM, project CONICYT/Fondap/15130015; and CONICYT/PIA/Concurso Apoyo a Centros Científicos y Tecnológicos de Excelencia con Financiamiento Basal AFB170001. EDFN is supported by the Spanish Government and FEDER through the Research project MTM 2015-70490-C2-2-R. VO is supported by CONICYT scholarship.

References

[1] E. Audusse, A multilayer Saint-Venant model: derivation and numerical validation. *Discrete Contin. Dyn. Syst. Ser. B* **5** (2005) 189–214.

[2] E. Audusse and M.-O. Bristeau, Finite-volume solvers for a multilayer Saint-Venant system. *Int. J. Appl. Math. Comput. Sci.* **17** (2007) 311–319.

[3] E. Audusse, M.O. Bristeau and A. Decoene, Numerical simulations of 3D free surface flows by a multilayer Saint-Venant model. *Int. J. Numer. Methods Fluids* **56** (2008) 331–350.

[4] E. Audusse, M. Bristeau, B. Perthame and J. Sainte-Marie, A multilayer Saint-Venant system with mass exchanges for shallow water flows. Derivation and numerical validation. *ESAIM: M2AN* **45** (2011) 169–200.

[5] E. Audusse, M.-O. Bristeau, M. Pelanti and J. Sainte-Marie, Approximation of the hydrostatic Navier–Stokes system for density stratified flows by a multilayer model: kinetic interpretation and numerical solution. *J. Comput. Phys.* **230** (2011) 3453–3478.

[6] E. Barsky, Critical regimes of two-phase flows with a polydisperse solid phase. In: Fluid Mechanics and Its Applications. Springer, Dordrecht (2010).

[7] D.K. Basson, S. Berres and R. Bürger, On models of polydisperse sedimentation with particle-size-specific hindered-settling factors. *Appl. Math. Model.* **33** (2009) 1815–1835.

[8] S. Berres, R. Bürger, K.H. Karlsen and E.M. Tory, Strongly degenerate parabolic-hyperbolic systems modeling polydisperse sedimentation with compression. *SIAM J. Appl. Math.* **64** (2003) 41–80.

[9] R.T. Bonnecaze, H.E. Huppert and J.R. Lister, Patterns of sedimentation from polydispersed turbidity currents. *Proc. Roy. Soc. Lond. A* **452** (1996) 2247–2261.

[10] S. Boscarino, R. Bürger, P. Mulet, G. Russo and L.M. Villada, Linearly implicit IMEX Runge–Kutta methods for a class of degenerate convection-diffusion problems. *SIAM J. Sci. Comput.* **37** (2015) B305–B331.

[11] R. Bürger, W.L. Wendland and F. Concha, Model equations for gravitational sedimentation-consolidation processes. *ZAMM Z. Angew. Math. Mech.* **80** (2000) 79–92.

[12] R. Bürger, A. García, K.H. Karlsen and J.D. Towers, A family of numerical schemes for kinematic flows with discontinuous flux. *J. Eng. Math.* **60** (2009) 387–425.

[13] R. Bürger, R. Donat, P. Mulet and C.A. Vega, Hyperbolicity analysis of polydisperse sedimentation models via a secular equation for the flux Jacobian. *SIAM J. Appl. Math.* **70** (2010) 2186–2213.

[14] R. Bürger, R. Donat, P. Mulet and C.A. Vega, On the implementation of WENO schemes for a class of polydisperse sedimentation models. *J. Comput. Phys.* **230** (2011) 2322–2344.

[15] R. Bürger, C. Chalons and L.M. Villada, Antidiffusive Lagrangian-remap schemes for models of polydisperse sedimentation. *Numer. Methods Partial Differ. Equ.* **32** (2016) 1109–1136.

[16] R. Bürger, S. Diehl, M.C. Martí, P. Mulet, I. Nopens, E. Torfs and P.A. Vanrolleghem, Numerical solution of a multi-class model for batch settling in water resource recovery facilities. *Appl. Math. Model.* **49** (2017) 415–436.

[17] M.J. Castro Díaz, J. Gallardo and C. Parés, High order finite volume schemes based on reconstruction of states for solving hyperbolic systems with nonconservative products. applications to shallow-water systems. *Math. Comput.* **75** (2006) 1103–1134.

[18] M.J. Castro Díaz, E.D. Fernández-Nieto, A.M. Ferreiro and C. Parés, Two-dimensional sediment transport models in shallow water equations. A second order finite volume approach on unstructured meshes. *Comput. Methods Appl. Mech. Eng.* **198** (2009) 2520–2538.

[19] M.J. Castro Díaz and E. Fernández-Nieto, A class of computationally fast first order finite volume solvers: PVM methods. *SIAM J. Sci. Comput.* **34** (2012) A2173–A2196.

[20] M.J. Castro Díaz, E.D. Fernández-Nieto, T. Morales de Luna, G. Narbona-Reina and C. Parés, A HLLC scheme for nonconservative hyperbolic problems. Application to turbidity currents with sediment transport. *ESAIM M2AN* **47** (2013) 1–32.

[21] C.M. Choux and T.H. Druitt, Analogue study of particle segregation in pyroclastic density currents, with implications for the emplacement mechanisms of large ignimbrites. *Sedimentology* **49** (2002) 907–928.

[22] G. Dal Maso, P.G. Lefloch and F. Murat, Definition and weak stability of nonconservative products. *J. Math. Pures Appl.* **74** (1995) 483–548.

[23] R. Donat and P. Mulet, A secular equation for the Jacobian matrix of certain multispecies kinematic flow models. *Numer. Methods Partial Differ. Equ.* **26** (2010) 159–175.

[24] R. Dorrell and A.J. Hogg, Sedimentation of bidisperse suspensions. *Int. J. Multiphase Flow* **36** (2010) 481–490.

[25] R. Dorrell, A.J. Hogg, E. Sumner and P. Talling, The structure of the deposit produced by sedimentation of polydisperse suspensions. *J. Geophys. Res.* **116** (2011) F01024.

[26] E.D. Fernández-Nieto, Modelling and numerical simulation of submarine sediment shallow flows: transport and avalanches. *Bol. Soc. Esp. Mat. Apl. SeMA* **49** (2009) 83–103.

[27] E.D. Fernández-Nieto and G. Narbona-Reina, Extension of WAF type methods to non-homogeneous shallow water equations with pollutant. *J. Sci. Comput.* **36** (2008) 193–217.

[28] E.D. Fernández-Nieto, E.H. Koné, T. Morales de Luna and R. Bürger, A multilayer shallow water system for polydisperse sedimentation. *J. Comput. Phys.* **238** (2013) 281–314.

[29] E.D. Fernández-Nieto, E.H. Koné and T. Chacón Rebollo, A multilayer method for the hydrostatic Navier–Stokes equations: a particular weak solution. *J. Sci. Comput.* **60** (2014) 408–437.

[30] T.C. Harris, A.J. Hogg and H.E. Huppert, Polydisperse particle-driven gravity currents. *J. Fluid Mech.* **472** (2002) 333–371.

[31] G.V. Kozyrakis, A.I. Delis, G. Alexandrakis and N.A. Kampanis, Numerical modeling of sediment transport applied to coastal morphodynamics. *Appl. Numer. Math.* **104** (2016) 30–46.

[32] M.J. Lockett and K.S. Bassoon, Sedimentation of binary particle mixtures. *Powder Technol.* **24** (1979) 1–7.

[33] D.L. Marchisio and R.O. Fox, Computational models for polydisperse particulate and multiphase systems. *Cambridge Series in Chemical Engineering*. Cambridge University Press, Cambridge (2013).

[34] J.H. Masliyah, Hindered settling in a multiple-species particle system. *Chem. Eng. Sci.* **34** (1979) 1166–1168.

[35] T. Morales de Luna, M.J. Castro Díaz, C. Parés Madroñal and E.D. Fernández Nieto, On a shallow water model for the simulation of turbidity currents. *Commun. Comput. Phys.* **6** (2009) 848–882.

[36] R.W.D. Nickalls, A new bound for polynomials when all the roots are real. *Math. Gazette* **95** (2011) 520–526.

[37] C. Parés, Numerical methods for nonconservative hyperbolic systems: a theoretical framework. *SIAM J. Numer. Anal.* **44** (2006) 300–321 (electronic).

[38] C. Parés and M. Castro, On the well-balance property of Roe's method for nonconservative hyperbolic systems. Applications to shallow-water systems. *ESAIM: M2AN* **38** (2004) 821–852.

[39] J.F. Richardson and W.N. Zaki, Sedimentation and fluidisation: Part I. *Trans. Inst. Chem. Eng. (London)* **32** (1954) 34–53.

[40] J. Sainte-Marie, Vertically averaged models for the free surface non-hydrostatic Euler system: derivation and kinetic interpretation. *Math. Models Methods Appl. Sci.* **21** (2011) 459–490.

[41] W. Schneider, G. Anestis and U. Schaflinger, Sediment composition due to settling of particles of different sizes. *Int. J. Multiphase Flow* **11** (1985) 419–423.

[42] I. Toumi, A weak formulation of Roe's approximate Riemann solver. *J. Comput. Phys.* **102** (1992) 360–373.

[43] M. Ungarish, An Introduction to Gravity Currents and Intrusions. CRC Press, Boca Raton, FL (2009).